Journal for ImmunoTherapy of Cancer

Trojan-horse silk fibroin nanocarriers loaded with a re-call antigen to redirect immunity against cancer

Elia Bari ,[1] Francesca Ferrera,[2] Tiziana Altosole,[2] Sara Perteghella,[3,4] Pierluigi Mauri,[5] Rossana Rossi,[5] Giulia Passignani,[5] Luca Mastracci,[6,7] Martina Galati,[2] Giuseppina Iliana Astone ,[2] Maddalena Mastrogiacomo,[2] Patrizio Castagnola,[8] Daniela Fenoglio,[2,8] Dario Di Silvestre,[5] Maria Luisa Torre ,[1,4] Gilberto Filaci [2,8]

To cite: Bari E, Ferrera F, Altosole T, *et al*. Trojan-horse silk fibroin nanocarriers loaded with a re-call antigen to redirect immunity against cancer. *Journal for ImmunoTherapy of Cancer* 2023;**11**:e005916. doi:10.1136/jitc-2022-005916

► Additional supplemental material is published online only. To view, please visit the journal online (http://dx.doi.org/10.1136/jitc-2022-005916).

EB, FF and TA contributed equally.
DDS, MLT and GF contributed equally.

Accepted 23 December 2022

For numbered affiliations see end of article.

Correspondence to
Professor Gilberto Filaci; gfilaci@unige.it

ABSTRACT

Background The current challenge for immunotherapies is to generate effective antitumor immunity. Since tumor immune escape mechanisms do not impact pre-existing and consolidated immune responses, we tested the hypothesis of redirecting a pregenerated immunity to cancer: to recall a non-tumor antigen response against the tumor, silk fibroin nanoparticles (SFNs) have been selected as 'Trojan-horse' carriers, promoting the antigen uptake by the tumor cells.

Methods SFNs have been loaded with either ovalbumin (OVA) or CpG oligonucleotide (CpG) as antigen or adjuvant, respectively. In vitro uptake of SFNs by tumor (B16/F10 melanoma and MB49 bladder cancer) or dendritic cells, as well as the presence of OVA-specific T cells in splenic and tumor-infiltrating lymphocytes, were assessed by cytometric analyses. Proof-of-concept of in vivo efficacy was achieved in an OVA-hyperimmune B16/F10 murine melanoma model: SFNs-OVA or SFNs-CpG were injected, separately or in association, into the subcutaneous peritumoral area. Cancer dimensions/survival time were monitored, while, at the molecular level, system biology approaches based on graph theory and experimental proteomic data were performed.

Results SFNs were efficiently in vitro uptaken by cancer and dendritic cells. In vivo peritumor administration of SFNs-OVA redirected OVA-specific cytotoxic T cells intratumorally. Proteomics and systems biology showed that peritumoral treatment with either SFNs-OVA or SFNs-CpG dramatically modified tumor microenvironment with respect to the control (CTR), mainly involving functional modules and hubs related to angiogenesis, inflammatory mediators, immune function, T complex and serpins expression, redox homeostasis, and energetic metabolism. Both SFNs-OVA and SFNs-CpG significantly delayed melanoma growth/survival time, and their effect was additive.

Conclusions Both SFNs-OVA and SFNs-CpG induce effective anticancer response through complementary mechanisms and show the efficacy of an innovative active immunotherapy approach based on the redirection of pre-existing immunity against cancer cells. This approach could be universally applied for solid cancer treatments if translated into the clinic using re-call antigens of childhood vaccination.

WHAT IS ALREADY KNOWN ON THIS TOPIC

⇒ The current challenge for cancer vaccines is to generate effective immune responses against cancer, overcoming the several cancer immune escape mechanisms that hamper tumor antigen-directed immune responses.

WHAT THIS STUDY ADDS

⇒ Our innovative approach redirects an already existing, robust, consolidated immune response against cancer. It exploits a 'Trojan-horse' strategy using silk fibroin nanoparticles as a vehicle of both an antigen and an adjuvant within the tumor.

HOW THIS STUDY MIGHT AFFECT RESEARCH, PRACTICE OR POLICY

⇒ This strategy, translated into clinics, could be universally applied to any cancer and any patient, using, as the immunogen, a re-call antigen: possible objectives consist both in eradication (i.e., in non-metastatic tumors like glioblastoma) and palliation (i.e., treatment of surgically unresectable tumor masses of any nature).

INTRODUCTION

Cancer vaccines should induce effector cancer-specific immune responses. However, although several cancer vaccines have been generated and tested in clinical trials, their general clinical efficacy rate was very poor,[1] and only one cancer vaccine, sipuleucel-T, received approval for clinical use.[2] The main reasons for the failure of vaccination strategy in cancer treatment are the low immunogenicity of tumor-associated antigens and the tumor capacity to downregulate their expression and generate a tolerogenic tumor microenvironment (TME).[3] Cancer vaccines based on tumor neoantigens originating from tumor-specific gene mutations[4] present some drawbacks since they are generally not shared among patients and are poorly presented

by (human leukocyte antigen) HLA molecules.[5] Moreover, they require complex and expensive technologies that dramatically impact therapy costs. Hence, there is an urgent need to imagine new approaches of cancer vaccination to overcome the current difficulties. Clinical evidence teaches that tumor immune suppression does not significantly impact pre-existing, consolidated immune responses, like those induced early in life by pediatric vaccinations.[6] Hence, a new perspective for cancer vaccination could be redirecting pre-existing immunity against tumor. This innovative strategy requires a vector able to vehicle the antigen target of the pre-existing immunity within tumor cells in association with a potent adjuvant able to subvert the immune suppressive milieu present in TME.

In this regard, nanoparticles are a promising tool in cancer immunotherapy.[7 8] They allow optimal delivery of antigens and adjuvants in TME. They may accumulate passively due to the enhanced permeability and retention effect or through specific active targeting.[9] In addition, the fact that nanoparticles may be internalized by both tumor cells and dendritic cells (DCs) allows the delivery of antigens in both cell types, thus facilitating the onset and development of an immune response. In particular, silk fibroin (SF) nanoparticles are of great interest since they are biocompatible, biodegradable, and have adequate mechanical properties for stable delivery and optimal in situ retention of drugs or antigens.[10–12]

Based on the above, we explored the efficacy of a 'Trojan-horse' model of cancer immunotherapy to recall a pre-existing immunity toward the tumor. To this aim, we used silk fibroin nanoparticles (SFNs) as a vehicle for both the antigen, ovalbumin (OVA), and the adjuvant, CpG, in OVA pre-immunized mice. Injectable formulations of SFNs loaded with OVA or CpG were designed, their in vitro internalization by cancer and DCs was determined, and their protecting efficacy against tumor growth was evaluated in a murine model. Application of high-throughput proteomics and systems biology approaches based on protein–protein interaction (PPI) network models[13] allowed the definition of functional modules and hubs involved in their activity.

MATERIALS AND METHODS

Preparation of injectable formulations of SFNs

SF was extracted and solubilized according to a previously reported procedure described in the online supplemental material. SFNs were then prepared by exploiting the fibroin desolvation in acetone.[10 12] Briefly, for SFNs preparation, SF (1.5% w/v) was added dropwise to acetone; for SFNs-OVA, a solution of SF (1% w/v) and OVA (Merck, Darmstadt, Germany) (0.5% w/v) was prepared and then added dropwise to acetone; for SFNs-CpG, a solution of SF (1.5% w/v) and CpG (TIB Molbiol, Genoa, Italy) (0.1% w/v) was prepared and then added dropwise to acetone. The fibroin/acetone volume ratio was 1:5 in all cases. The nanoparticle suspension was further processed and freeze-dried as reported in the online supplemental material. Final formulations were stored at 4°C until use (maximum of 3 months). In addition, a physical mixture of SFNs-OVA and SFNs-CpG was prepared by mixing the freeze-dried formulations of SFNs-OVA and SFNs-CpG in a 1:1 ratio.

Characterization of SFNs injectable formulations

As reported in the online supplemental material, OVA loading in SFNs-OVA was evaluated by size exclusion chromatography, quantifying the residual presence of unbound OVA in the washed supernatants.

Loading of CpG into SFNs-CpG was verified by analyzing the nanoparticles' micro-analytical composition by a high-resolution scanning electron microscopy (TESCAN, Mira 3 XMU) equipped with an In-Beam SE detector operating at 8 kV and by energy dispersive spectrometry operating at 20 kV. Before the analysis, the samples were coated with carbon using a Cressington 208C.

The dimensional distribution of SFNs was analyzed using NanoSight NS300 equipment (Malvern Panalytical, Great Malvern, Worcestershire, UK); the mean size, polydispersity index (PDI) and zeta potential were analyzed by Zetasizer Nano Zs (Malvern Panalytical) (see online supplemental material). Chemical-physical characterization was performed by recording Mid-infrared (IR) (650–4000 cm^{-1}) spectra on powder samples using a Bruker Equinox 55 spectrometer equipped with a pyroelectric detector (deuterated-triglycine-sulfate (DTGS) type) with a resolution of 4 cm^{-1}. Following the procedures reported in the online supplemental material, temperature and enthalpy values were measured by differential scanning calorimetry (DSC) by a NEXTA DSC (Hitachi, Europark Fichtenhain A12, Krefeld, Germany) equipped with a DSC821e module and an intracooler device for subambient temperature analysis (Julabo FT 900); a Mettler STARe thermogravimetric analysis (TGA) system (PerkinElmer Pyris 1, Wellesley, Minneapolis, Minnesota, USA) with simultaneous DSC (TGA/DSC1) measured mass losses on heating.

Finally, the residual humidity, osmolarity and pH of the reconstituted product were measured (see online supplemental material).

Analysis of SFNs internalization by cancer cells

Analyses of SFNs internalization were performed on cancer cell lines and on tumor cells incubated either ex vivo or in vivo with SFNs. Analyses were conducted using either curcumin-loaded SFNs (SFNs-CUR) or SFNs-OVA. In the latter case, an fluorescein isothiocyanate (FITC) rabbit anti-OVA antibody (Abcam, Cambridge, UK) was used as a revealing agent. SFNs internalization was detected by either flow cytometry, using an FACSCanto II flow cytometry (BD) equipped with three lasers (488 nm, 640 nm, 405 nm) using FACSDiva software V.6 (BD), or confocal microscopy, using an Olympus FV500 confocal microscope (Olympus Corporation). Detailed

information on these procedures is provided in the online supplemental material.

Mice

Mice, 7–10 weeks old, female C57BL/6J were purchased from Envigo RMS (San Pietro al Natisone, Udine, Italy) and housed under specific pathogen-free conditions in the animal facility at the Istituto di Ricovero e Cura a Carattere Scientifico (IRCCS) Ospedale Policlinico San Martino, Genoa, Italy. All the procedures were carried out by animal facilities qualified staff according to the guidelines provided in Italian Ministero della Salute D.Lgs 26/2014. The protocol concerning the experiments followed the recommendation and received approval from the Institutional Animal Care and Use Committee (Organizzazione Per il Benessere Animale of IRCCS Ospedale Policlinico San Martino of Genoa) and the National Istituto Superiore di Sanità (protocol # 1000/2020-PR).

Analysis of SFNs internalization by DCs

The analysis of SFNs internalization by DCs was performed by flow cytometry on splenic DCs and DCs present in the TME. Detailed information on these procedures is provided in the online supplemental material.

Adipose adult stromal cells generation

Adipose adult stromal cells were generated as described in detail in the online supplemental material.

MTT assay

Methyl thiazolyl diphenyl-tetrazolium bromide (MTT) assay to assess cell viability was performed as described in the online supplemental material.

Administration of SFNs to tumor-challenged mice

Seven-week-old C57BL/6J female mice were immunized subcutaneously with a suspension of OVA (60 µg) (Merck, Darmstadt, Germania) and CpG 1826 (TIB MolBiol, Genoa, Italy) (30 µg), dissolved in 100 µL saline phosphate buffer without calcium and magnesium (PBS). Two subsequent boosters were administered 15 and 30 days after the first immunization. Ten days after the last booster, B16/F10 mouse melanoma cells or MB49 bladder cancer cells (10^5 cells/mouse) were injected subcutaneously into the mice. Neoplastic nodules were seen at the injection site 7–10 days after tumor cell administration. Mice, randomly distributed among the different treatment and untreated control groups (six mice per group), were administered with SNFs, SFNs-OVA and SFNs-CpG suspended in PBS at 1 mg/mL and sonicated at 59 MHz for 15–30 min at room temperature before subcutaneous injection into the peritumoral area (200 µg per mouse). Each mouse received three nanoparticle injections 1 week apart. Mice were observed daily by researchers who administered the treatments, and blind operators registered tumor sizes. Tumor masses were measured with a caliper at 2–3 days intervals by measuring long and short axes. Volume was calculated according to the formula: tumor volume = ½ (length × width^2) in cm^3. Mice were sacrificed when tumors reached >1 cm^3 or ulceration/bleeding developed.

The experiments aimed at demonstrating the eventual therapeutic effects of SFNs were performed only on the orthotopic B16/F10 melanoma model, more representative of the corresponding human disease than the heterotopic MB49 bladder cancer model, and sized based on our previous experience with the model, following the 3R principle (replacement, reduction and refinement). Tumor measures and laboratory analyses were conducted blind from the treatment group.

Intracellular staining for interferon-γ and interleukin-10 detection

Splenocytes and intratumoral T lymphocytes were purified from OVA hyper-immune C57BL/6J mice challenged with MB49 bladder cancer cells treated or not with SFNs: specimens were minced and passed through a cell strainer to obtain a homogenous cell suspension. Then, lymphocytes were purified by centrifugation on a Ficoll gradient Lympholyte-H Cell Separation Media (Cedarlane, Burlington, Canada). After red blood cell lysis (red blood cell lysing buffer, Merck), splenocytes or tumor-infiltrating lymphocytes were seeded in 96 wells of round-bottomed plates (Corning, Somerville, Massachusetts, USA) in triplicate at 10^6 cells/well in a volume of 100 µL of culture medium (Gibco Life Technologies, Milan, Italy) in the presence or not of OVA (100 µg/mL) overnight. At the end of incubation, the cells were stained with Efluor V450 rat anti-mouse CD3 (Thermo Fisher catalog no 48-0032-82) and PE-Cyanine7 rat anti-mouse CD8 (BD catalog no 552877) antibodies, fixed and permeabilized by BD Cytofix Cytoperm (BD), and incubated with allophycocyanine rat anti-mouse interleukin (IL)-10 (Thermo Fisher catalog no 17-7101-82) and FITC rat anti-mouse interferon (IFN)-γ (Thermo Fisher catalog no 11-7311-82) antibodies. Cells were then analyzed by LSRFortessa X20 flow cytometer (BD).

Cytotoxic assay

B16/F10 melanoma or MB49 bladder cancer cells were incubated overnight with SFNs-OVA or unloaded SFNs as a control in x-vivo medium (Lonza, Basilea, Switzerland) at 37°C in 5% CO_2. Then, the cells were labeled with 5 (6)-carboxyfluorescein diacetate N-succinimidyl ester (CFDA-SE) fluorescent dye (Thermo Fisher Scientific) to track the target cells. Then CFDA-SE labeled cells were seeded in 96 round-bottomed well plates (Corning) at 10^5 cells/well in 200 µL of culture medium. Next, these target cells were incubated overnight with 10^6/well effector T cells sorted (using Dynabeads FlowComp Mouse Pan-T, Thermo Fisher Scientific) from spleen or tumor of OVA hyper-immune mice challenged with either B16/F10 or MB49 cells and treated with SFNs-OVA. Finally, the target cell lysis was measured by adding the viability dye 7-aminoactinomycin D (7-AAD) (BD) at the end of the incubation and expressed as a

percentage of the CFDA-SE+7-AAD+cells. Samples were analyzed using an LSRFortessa X20 flow cytometer (BD).

Proteomic analysis

Sample preparation for liquid chromatography with tandem mass spectrometry analysis

Paraffin-embedded tissue sections from three mice per group of treatment were deparaffinized, proteins were extracted and digested, and the protein mixtures were analyzed by liquid chromatography with tandem mass spectrometry (LC-MS/MS) analysis, as previously reported.[14] The online supplemental material details sample preparation, chromatographic, and MS procedures.

MS/MS data processing

All raw files produced by LC-MS/MS were processed by the SEQUEST HT algorithm in Proteome Discoverer V.2.5 software (Thermo Fisher Scientific, California, USA). Experimental MS/MS spectra were compared with the theoretical mass spectra obtained by in silico digestion of a *Mus musculus* protein database containing 55,315 sequences (www.uniprot.org, accessed on March 1, 2022). The following searching criteria were set: trypsin enzyme, the maximum number of missed cleavages per peptide was set to two, mass tolerances of ±50 ppm for precursor ions and ±0.8 Da for fragment ions. Percolator node was used with a target-decoy strategy to give a final false discovery rate ≤0.01 based on q values, considering a maximum deltaCN of 0.05. Only peptides with peptide lengths of 5–30 amino acids, confidence at 'Medium' level and rank 1 were considered. Protein grouping and strict parsimony principles were applied.

Protein profiles preprocessing, statistical evaluations and quantitative analysis

Peptide spectrum matches (PSMs) of the identified proteins were normalized using a total signal normalization method and compared using a label-free quantification approach as previously reported.[13] Briefly, data matrix dimensionality (MB49 bladder carcinoma, 24 samples×3011 distinct proteins; B16/F10 melanoma, 24 samples×2735 distinct proteins) was reduced by linear discriminant analysis (LDA) and proteins with p value≤0.05 were retained. Pairwise comparisons (CTR vs SFNs-OVA, CTR vs SFNs-CpG) were performed; fold change of proteins selected by LDA was estimated by DAve index[15] comparing the average PSMs (avPSMs). Specifically, positive DAve values indicate proteins upregulated in CTR, whereas negative DAve values indicate proteins upregulated in SFNs-OVA or SFNs-CpG. Finally, differentially expressed proteins (DEPs) selected by LDA were processed by Spearman's rank correlation and hierarchical clustering by applying Ward's method and the Euclidean distance metric. All processing was performed by JMP V.15.2 SAS software.

MB49 bladder carcinoma and B16/F10 melanoma PPI network models

Mus musculus PPI network models were reconstructed starting from all proteins identified in MB49 bladder carcinoma and B16/F10 melanoma using the STRING Cytoscape's application[16]; physical and/or functional interactions were filtered by considering only those 'experiments' or/and 'databases' annotated, with a STRING score ≥0.15 and ≥0.35, respectively. Using the same approach, other two PPI network models were reconstructed starting from DEPs selected for MB49 bladder carcinoma and B16/F10 melanoma, respectively; DEPs were grouped in functional modules by the support of the GO enrichment tool inserted in STRING Cytoscape's Application.[16]

Reconstructed networks were globally analyzed at the topological level by Analyzer application integrated into Cytoscape V.3.8.2.[17] In addition, Centiscape Cytoscape's application[18] calculated betweenness and centroid centralities, and nodes with above-average values were considered PPI hubs.[19] Finally, the statistical significance of all topological results was tested by considering randomized network models[20]; they were reconstructed and analyzed by an in-house R script based on VertexSort (to build random models), igraph (to compute centralities), and ggplot2 (to plot results) libraries; results were visualized in the form of violin plots.

Statistical analysis

Raw data were processed through STATGRAPHICS XVII (StatPoint Technologies, Warrenton, Virginia, USA). A general linear analysis of variance model was generated to evaluate the data. In detail, tumor size data in mice were analyzed considering the treatment and the time as fixed factors and the tumor size as the response variable. The function was then followed by a least significant difference test to estimate the differences between means. Statistical significance was set at $p<0.05$.

RESULTS

Preparation and characterization of SFNs

Injectable formulations containing SFNs, SFNs-OVA and SFNs-CpG were prepared and characterized before in vitro and in vivo testing (figure 1).

Figure 1A shows the morphological analysis of the formulations containing SFNs, SFNs-OVA and SFNs-CpG at three different magnifications (rows a, b and c). As seen at all magnifications, especially row c, the nanoparticles are immersed in a homogeneous matrix of mannitol. At all magnifications, especially rows a and b, the nanoparticles appear round, without apparent aggregates, and with smooth surfaces. Figure 1B shows that the yield percentage was consistently above 70%. The OVA loading percentage was 32.7% for SFNs-OVA. Overall, high encapsulation efficiency for OVA was obtained. For SFNs-CpG, the CpG loading was verified by analyzing their micro-analytical composition. The relative abundance of

A

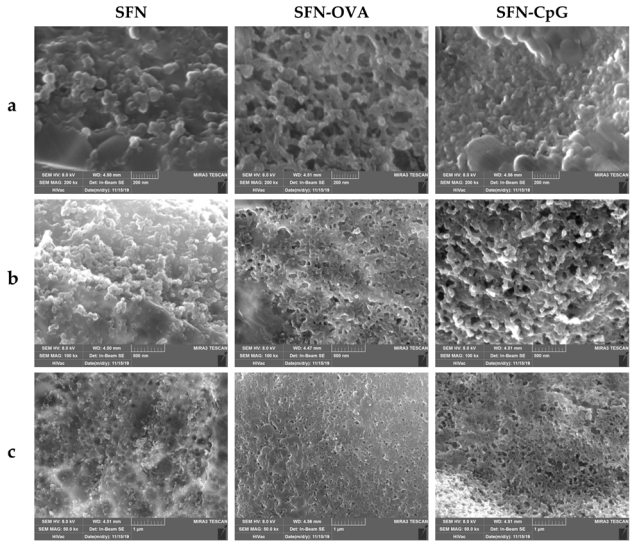

B

Formulation	Yield (%)	Actual drug loading (%)		Assumed drug loading (%)		Encapsulation efficiency (%)	
		OVA	CpG	OVA	CpG	OVA	CpG
SFN	93.6	-	-	-	-	-	-
SFN-OVA	91.7	32.7 ± 0.45	-	33	-	97.0 ± 0.4	-
SFN-CpG	75.2	-	7.36 ± 0.720	-	7	-	-

C

Formulation	Mean diameter ± standard deviation (nm)	Mode ± standard deviation (nm)	d_{10}	d_{50}	d_{90}	Zeta potential (mV)
SFNs	151.7 ± 3.0	103.5 ± 3.6	91.0 ± 1.9	136.6 ± 4.7	219.0 ± 6.4	-17.97
SFN-OVA	141.1 ± 4.6	93.7 ± 3.1	78.9 ± 5.8	111.5 ± 4.1	228.7 ± 19.1	-13.13
SFN-CpG	144.4 ± 4.2	102.7 ± 5.6	84.2 ± 0.9	107.5 ± 4.2	221.9 ± 12.4	-12.97

D

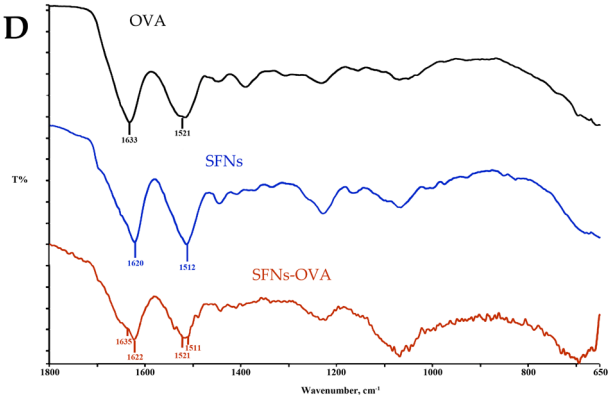

Figure 1 Characterization of SFNs. (A) Morphological investigation by SEM of SFNs, SFNs-OVA and SFNs-CpG at 200 k× (a), 100 k× (b) and 50 k× (c). (B) Yield, encapsulation efficiency and drug loading for the formulations prepared. Data are reported as mean±SD, n=3. (C) Mean diameter, mode, d_{10}, d_{50} and d_{90} for all the samples. Values are reported in nm as mean value±SD, n=5. Z potential is reported in mV. (D) Physico-chemical characterization by IR: enlarged IR spectra between 1800 and 650 cm^{-1} for OVA, SFNs and SFNs-OVA. IR, infrared; OVA, ovalbumin; SFNs, silk fibroin nanoparticles; SEM, scanning electron microscopy.

phosphorus atoms in the mixture was traced back to the percentage amount of CpG, which was 7.36%±0.720 w/w.

All nanoparticle formulations showed a mean diameter of about 150 nm (figure 1C) and a negative surface charge. No significant increase in particle size or change in Z potential was observed after the loading of SFNs with OVA or CpG. The PDI values were lower than 0.3 for all the formulations, confirming that the samples are monodisperse. Overall, the nanoparticle size, morphology and shape are optimal for cancer cells' uptake.[21]

Figure 1D shows the IR spectra between 1800 and 650 cm^{-1}. The protein amide I and II bands are present between 1600–1700 and 1500–1600 cm^{-1}, respectively, the most sensitive region of the IR spectrum for protein secondary structure analysis. In particular, the band at 1633 cm^{-1} in the OVA sample confirmed the presence of

β-sheet structure. Even in the SFNs spectrum, the high content of β-sheet domains is revealed by the characteristic bands in the spectral region of amide I at 1620 cm^{-1} (C=O stretching) and amide II at 1512 cm^{-1} (N–H bending). For SNFs-OVA, the typical bands of amide I and II of the two protein components are distinguishable. This technique did not reveal the presence of CpG in SFNs-CpG as below the sensitivity (data not shown).

The DSC thermal analysis supported the spectroscopic data: all the samples showed a typical profile of an amorphous compound with an endothermic effect around 270°C, associated with a loss of mass in the thermogravimetric curve, linked to sample decomposition (data not shown).

The residual humidity of freeze-dried formulations never exceeded 3%, and the osmolarity value was always between 320 and 350 mOsm/Kg. Moreover, the measured pH value was always in the range of 7.2–7.6.

Internalization of SFNs by cancer cells and DCs

Experiments were conducted to demonstrate that nanoparticles can be effectively up-taken by tumor cells and that this phenomenon is not restricted to a specific cell line or histological type. This first set of experiments was performed using SFNs-CUR, taking advantage of the autofluorescence emitted by curcumin, that makes the test fast and very sensitive. Interestingly, all tested cancer cells showed the capacity to internalize SFNs-CUR although with variable efficiencies, ranging from 40% (LLC1 cells at 1 hour) to 99% (5637 cells at 1 hour) of the total cell population (figure 2, panels A and B). Repeating the experiments using SFNs-OVA, that would have been subsequently administered to mice in the in vivo experiments, we observed again that all tested cell lines internalized the nanoparticles (online supplemental figure S1). Notably, internalization of soluble OVA (i.e., not carried by SFNs) was negligible unless the antigen was mixed with unloaded nanoparticles (a phenomenon likely due to a partial spontaneous OVA absorption on SFNs followed by their internalization by cancer cells). Next, the experiments were repeated on B16/F10 melanoma cells and MB49 bladder cancer cells purified from excised tumors exposed either ex vivo or in vivo to SFNs-OVA. Figure 2C,D show cell internalization of OVA in all experimental conditions.

We also observed that both splenic DCs and DCs present within TME could uptake fibroin nanoparticles (figure 2E and F).

These findings collectively suggest that fibroin nanoparticles are an effective tool to vehicle antigen and adjuvant into both tumor cells and DCs, providing the immunological basis for redirecting effective immune responses within the TME.

In the view of administering SFNs in vivo a relevant issue concerns their eventual direct cytotoxicity. Analysis of cell viability in the above reported tests revealed that SFNs internalization induced a moderate level of cytotoxicity on cancer cells (no more than 20% mortality) but not on healthy DCs, suggesting that nanoparticles may slightly impact on viability of cancer cells but not of healthy cells (online supplemental figure S2A). These data were confirmed by an MTT assay that showed a moderate loss of viability only by cancer cells after 4 hours of exposition to SFNs (again no more than 20% mortality), while viability of one line of adipose tissue-derived stem cells from a healthy donor was not affected (online supplemental figure S2B).

Assessment of immunological and biological effects mediated by SFNs-OVA and SFNs-CpG on TME

Based on the above, we tested the effects of SNFs, SFNs-OVA and SFNs-CpG in vivo. In particular, we addressed two issues: (a) whether SNFs-OVA could redirect into TME and against tumor cells a pre-existing immune response to a non-tumor antigen such as OVA; (b) whether local administrations of either SFNs-OVA or SFNs-CpG were able to induce proteomic changes within TME.

Concerning the first issue, splenic and tumor-infiltrating T lymphocytes were purified from B16/F10 and MB49 cell challenged OVA-hyperimmune mice peritumorally treated with SFNs or SFNs-OVA. Figure 3A and B show that only tumor cells pre-incubated with SFNs-OVA, but not those pre-incubated with unloaded SFNs, were efficiently killed by splenic (14% and 18% of cell lysis for B16/F10 and MB49 cells, respectively) and tumor-infiltrating T cells (19% and 16% of cell lysis for B16F10 and MB49 cells, respectively).

Since in the MB49 tumor we found a richer T-cell tumor infiltrate than in the B16/F10 melanoma, we could also perform experiments testing OVA-specific IFN-γ production by tumor-infiltrating T lymphocytes. Figure 3C shows that IFN-γ-secreting CD4+ and CD8+ OVA-specific T splenocytes were observed in OVA pre-immunized animals, as expected. The frequency of these cells increased in animals treated with SFNs-OVA (figure 3D). When intratumoral T cells were analyzed, IFN-γ-secreting CD4+ and CD8+ OVA-specific T lymphocytes were observed in animals treated with SFNs-OVA but not in untreated ones (figure 3E and F). In the same experiments, the frequency of IL-10-secreting OVA-specific T splenocytes was negligible (figure 3C–3F), suggesting that SFN-OVA immunization privileges the expansion of potential effectors over regulatory T cells.

Concerning the landscape of proteomic variations induced by SFNs-OVA and SFNs-CpG treatments, 2735 and 2463 proteins were identified in B16/F10 melanoma and MB49 bladder cancer, respectively; only 1067 proteins were shared by both models, likely as a result of the different biology of the respective tissues (online supplemental figure S3, datafiles S1 and S2). By comparing the characterized protein profiles, 245 and 332 proteins were found differentially expressed in B16/F10 melanoma and MB49 bladder cancer models, respectively (online supplemental figure S3, datafiles S3 and S4). Of note,

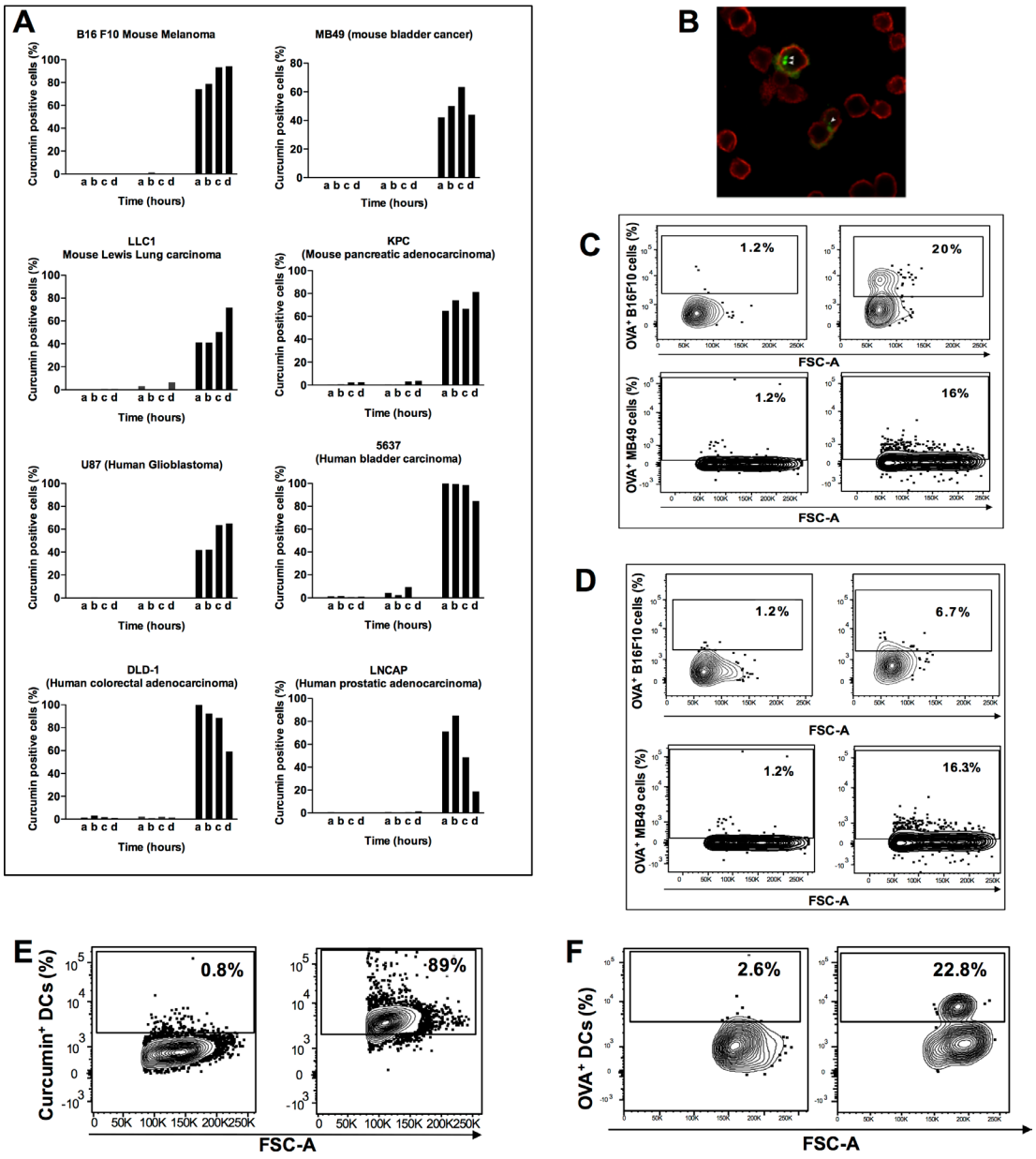

Figure 2 SFNs internalization by cancer cells and DCs. (A) Different mouse or human cancer cell lines were incubated for (a) 1 hour, (b) 2 hours, (c) 4 hours, and (d) 24 hours, alone (left bars) or in the presence of unloaded SFNs (middle bars) or curcumin loaded SFNs (right bars), and evaluated by flow cytometry using a green light-emitting laser; (B) Tumor cells derived from tumors excised from MB49 challenged mice were incubated with curcumin loaded SFNs for 4 hours and evaluated by confocal microscopy (plasma membrane of cells: red signal; curcumin SFNs: green signal). (C) B16/F10 melanoma cells (upper row) and MB49 bladder cancer cells (lower row) purified from an excised tumor were incubated (right panels) or not (left panels) for 4 hours with SFNs-OVA, then fixed and permeabilized before incubation with an anti-OVA FITC labeled mAb and the following cytometric analysis. (D) B16/F10 melanoma cells (upper row) and MB49 bladder cancer cells (lower row) purified from an excised tumor treated peritumorally (right panels) or not (left panels) in vivo with SFNs-OVA were fixed and permeabilized before incubation with an anti-OVA FITC labeled mAb and the following cytometric analysis. (E) Splenic DCs from C57BL/6J mice were incubated (right panel) or not (left panel) for 24 hours with curcumin-loaded SFNs and evaluated by flow cytometry; (F) DCs purified from B16/F10 melanoma tumor excised from SFNs-OVA treated (right panel) or not treated (left panel) mice were fixed and permeabilized before incubation with an anti-OVA FITC labeled mAb and the following cytometric analysis. DCs, dendritic cells; FITC, fluorescein isothiocyanate; FSC-A, forward scatter; mAb, monoclonal antibody; OVA, ovalbumin; SFNs, silk fibroin nanoparticles.

a set of them resulted regulated with the same trend in both models (table 1).

In this context, following SFNs-OVA and SFNs-CpG treatments, we observed downregulation of proteins involved in metastatic progression of cancer cells, such as Hmga1,[22] or erythrocytes (Ank1, Hba-a1, Hbb-b2, Hbb-bs) and blood vessel (Plg) development. On the other hand, proteins involved in endocytosis/major

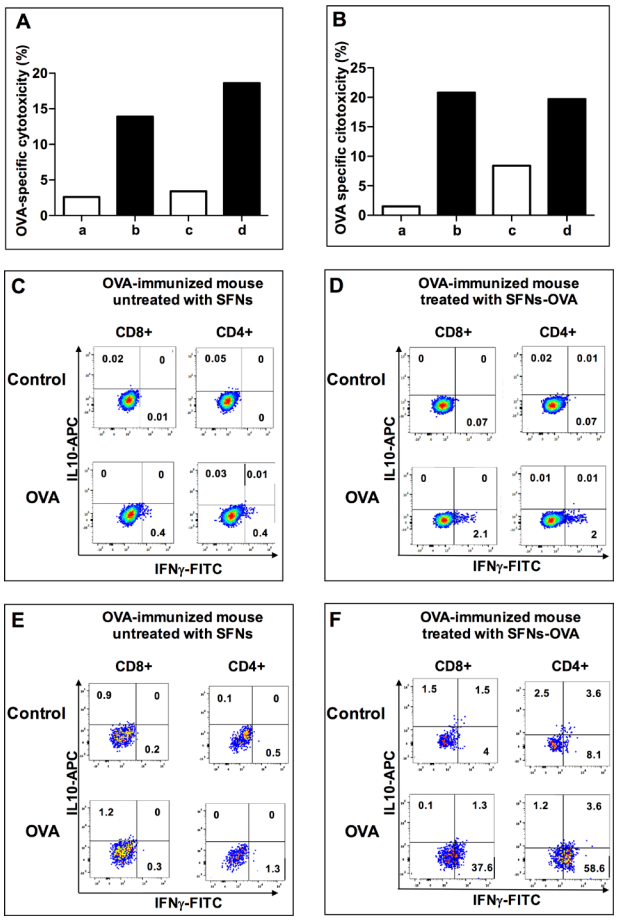

Figure 3 Intratumor expansion of IFN-γ-secreting and cytotoxic OVA-specific T lymphocytes by treatment with SFNs-OVA of tumor-challenged mice pre-immunized against OVA. (A) Cytotoxic activity against B16/F10 melanoma cells pre-exposed to unloaded SFNs (white) or SFNs-OVA (black) by either splenocytes (a–b) or tumor-infiltrating T lymphocytes (c–d) from a representative OVA pre-immunized C57BL/6J mouse challenged with B16-F10 cells and intratumorally treated with SFNs-OVA. (B) Cytotoxic activity against MB49 bladder carcinoma cells pre-exposed to unloaded SFNs (white) or SFNs-OVA (black) by either splenocytes (a–b) or tumor-infiltrating T lymphocytes (c–d) from a representative OVA pre-immunized C57BL/6J mouse challenged with MB49 cells and intratumorally treated with SFNs-OVA. (C) Expansion of OVA-specific T splenocytes in a representative OVA pre-immunized C57BL/6J mouse challenged with MB49 bladder carcinoma cells. Upper row: frequencies of IFN-γ-secreting and IL-10-secreting T splenocytes in a non-antigen stimulated in vitro culture; lower row: frequencies of IFN-γ and IL-10-secreting splenocytes in an OVA stimulated in vitro culture; (D) Expansion of OVA-specific T splenocytes in a representative OVA pre-immunized C57BL/6J mice challenged with MB49 bladder carcinoma cells and intratumorally treated with SFNs-OVA. Upper row: frequencies of IFN-γ-secreting and IL-10-secreting T splenocytes in a non-antigen stimulated in vitro culture; lower row: frequencies of IFN-γ-secreting and IL-10-secreting T splenocytes in an OVA stimulated in vitro culture; (E) Expansion of tumor-infiltrating OVA-specific T lymphocytes in a representative OVA pre-immunized C57BL/6J mouse challenged with MB49bladder carcinoma cells. Upper row: frequencies of IFN-γ-secreting and IL-10-secreting T lymphocytes in a non-antigen stimulated in vitro culture; lower row: frequencies of IFN-γ-secreting and IL-10-secreting T lymphocytes in an OVA stimulated in vitro culture; (F) Expansion of tumor-infiltrating OVA-specific T lymphocytes in a representative OVA pre-immunized C57BL/6J mouse challenged with MB49 bladder carcinoma cells and peritumorally treated with SFNs-OVA. Upper row: frequencies of IFN-γ-secreting and IL-10-secreting T lymphocytes in a non-antigen stimulated in vitro culture; lower row: frequencies of IFN-γ-secreting and IL-10-secreting T lymphocytes in an OVA stimulated in vitro culture. All the experiments were replicated three times. APC, allophycocyanine; FITC, fluorescein isothiocyanate; IFN, interferon; IL, interleukin; OVA, ovalbumin; SFNs, silk fibroin nanoparticles.

histocompatibility complex class II antigen presentation (Capza2, Rab7a, Cltc) and collagen-containing extracellular matrix (Dcn, Lum, Col1a1) were upregulated.

Similarly to their effects on protein expression, SNFs-OVA and SFN-CpG treatments modulated specific functional modules by inducing an analogous expression trend in both models: proteins involved in the immune system function and the vesicle-mediated transport increased their expression, while those related to angiogenesis and T-complex were downregulated (figure 4, online supplemental figures S4–S5).

Indeed, the different biology between the two cancer models could explain some differences and specificities observed following SFNs-OVA and SFNs-CpG treatments, such as downregulation of keratins, potential prognostic markers in melanoma,[23] and SERPINs,[24] that appeared

Table 1 Differentially expressed proteins with the same expression trend in both models

Gene name	B16/F10melanoma		MB49 bladder cancer	
	CTR vs SFNs-OVA*	CTR vs SFNs-CpG	CTR vs SFNs-OVA	CTR vs SFNs-CpG
Ank1	2.0	2.0	1.6	2.0
Ero1a	1.1	2.0	0.2	0.4
Hba-a1	1.1	1.2	1.0	0.7
Hbb-b2	0.9	0.8	0.8	1.3
Hbbs	1.5	1.5	0.7	1.2
Hmga1	2.0	2.0	2.0	2.0
Myadm	2.0	2.0	2.0	1.6
Plec	1.4	0.9	0.4	1.2
Plg	1.5	0.8	1.0	0.9
Snrpf	2.0	1.4	2.0	2.0
Stom	2.0	2.0	2.0	2.0
Aldh2	−0.4	−0.8	−1.0	−1.5
Capza2	−1.4	−1.6	−0.4	−0.8
Cltc	−0.8	−0.6	−0.5	−0.5
Col1a1	−1.1	−1.0	−0.9	−1.3
Dcn	−1.4	−1.4	−2.0	−2.0
Lum	−2.0	−2.0	−2.0	−2.0
Msn	−0.4	−0.7	−1.0	−1.3
Rab7a	−1.0	−1.4	−1.0	−0.3
Rps16	−0.9	−0.7	−0.5	−0.2

*For each pairwise comparison (CTR vs SFNs-OVA; CTR vs SFNs-CpG) DAve index is shown; positive DAve values indicate proteins upregulated in CTR (downregulated in SFNs treatments), while negative DAve values indicate proteins upregulated following SFNs treatments (downregulated in CTR).
CTR, control; OVA, ovalbumin; SFN, silk fibroin nanoparticle.

more consistent in the B16/F10 melanoma model than in the MB49 one (online supplemental figure S6).

Comparing the effects differentially mediated by SFNs-OVA and SFNs-CpG treatments, SFNs-OVA were found to be more effective in reducing angiogenesis, while SFNs-CpG in reducing keratins expression and in upregulating proteins involved in immune system activity (online supplemental figures S4–S6).

Hub proteins as key players of the proteome modulation mediated by SFNs-OVA and SFNs-CpG treatments

Interesting indications that support the efficacy of SFNs-OVA and SFNs-CpG treatments emerged from the topological analysis of PPI network models (online supplemental figure S7).

In this context, concerning the B16/F10 melanoma model, both Akt1 and Pik3r2, the best-ranked hubs in untreated tumors, were not identified in any B16/F10 samples treated with SFNs-OVA and SFNs-CpG (Data file S5), likely sign of tumor suppressive effect based on the well-known protumoral effects of both pathways reported in melanoma and other cancers.[25 26] Conversely, Itgb2, whose expression was reported to correlate with the infiltration of all types of immune cells,[27 28] potentially predisposing to improved effectiveness of immunotherapy and improved overall survival, was the best-ranked hub in all B16/F10 samples treated with SFNs-OVA and SFNs-CpG (Data online supplemental file 5). Fau was another interesting hub found in all B16/F10 samples treated with SFNs-OVA and SFNs-CpG since it has been proposed as a candidate tumor suppressor protein acting by regulation of apoptosis in human cells.[29]

Concerning the MB49 bladder cancer model, we found high mobility group protein HMGI-C (Hmga2) as the best-ranked hub protein (Data file S6); this protein, which was not identified in any MB49 samples treated with SFNs-OVA and SFNs-CpG, has been widely associated with cancer progression,[30] also in the bladder,[31] and is specifically targeted to inhibits bladder cancer metastasis.[32 33] On the opposite, cAMP-dependent protein kinase (PKA) catalytic subunit beta (Prkacb), a catalytic subunit of cAMP-dependent PKA that regulates numerous fundamental biological processes such as metabolism, development, memory, and immune response, resulted the best hub of all MB49 samples treated with SFNs-OVA and SFNs-CpG and of B16/F10 melanoma samples treated with SFNs-OVA (Data files S5 and S6). This is of relevance since Prkacb gene encodes several splice variants, including Cβ2, which is enriched in T cells, B cells and natural killer cells,[34] and its increased expression is associated with a favorable prognosis in different cancers.[35] The best-ranked hubs following treatment with SFNs-OVA in MB49 samples were cytotoxic granule-associated RNA binding protein TIA1 (Tia1) and nuclear factor of kappa light polypeptide gene enhancer in B cells 1 (Nfkb1). Noteworthy, Tia1 has been described as an important tumor suppressor molecule,[29] and other authors speculated that CD8/Tia1+infiltrating TME confer superior survival to patients with localized osteosarcoma.[36] Also of note, the knockout of Nfkb1, an important regulator of NF-κB activity in vivo, has been associated in mouse models with increased inflammation and susceptibility to certain forms of DNA damage, leading to cancer and a rapid aging phenotype.[37]

Therapeutic efficacy of the different SNFs formulations

OVA hyperimmune, B16/F10 melanoma-challenged C57BL/6J mice were untreated or treated peritumorally with either unloaded SFNs, SFNs-OVA, SFNs-CpG or the combination of SFNs-OVA plus SFNs-CpG. Both treatments with SFNs-OVA and SFNs-CpG significantly slowed tumor growth compared with the last two control groups of mice (figure 5). When B16/F10 melanoma-challenged mice were treated with a combination of SNFs-OVA and SFNs-CpG, tumor growth was significantly reduced compared with control mice and mice treated with either SFNs-OVA alone or SFNs-CpG alone (figure 5), showing a remarkable additive effect likely due to the association of their mechanisms of action. Proteomic analyses were performed on tumor specimens from mice treated with the combination of SFNs-OVA and SFNs-CpG to assess this possibility (figure 6).

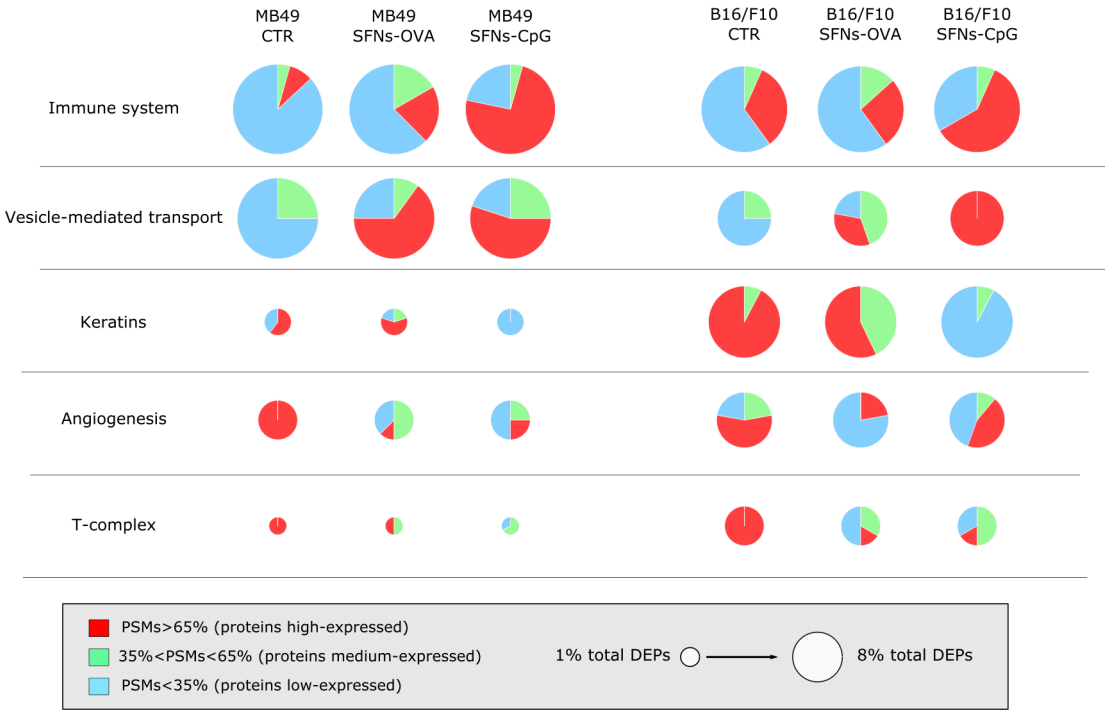

Figure 4 Proteomic and systems biology outcomes of SFNs administration at the tumor site. The analyses evidence the functional modules affected by SNFs-OVA and SFN-CpG treatments in both MB49 bladder cancer and B16/F10 melanoma models. Red, green and blue color codes indicate the percentage of proteins with high-, medium- and low expression, respectively, based on a PSMs-based label-free quantification. The pie chart size is proportional to the number of DEPs per module. CTR, control; DEP, differentially expressed protein; OVA, ovalbumin; SFNs, silk fibroin nanoparticles.

Correlation among DEP profiles was observed, indicating a consistent proteome remodeling and a synergic effect of SFNs-OVA and SFNs-CpG treatment (figure 6). This mainly appeared evident for keratins, complement and coagulation cascades, angiogenesis, SERPINs and erythrocyte-related proteins, which were mainly downregulated following the action of both SFNs-OVA and SFNs-CpG. Of note, keratins' downregulation appeared

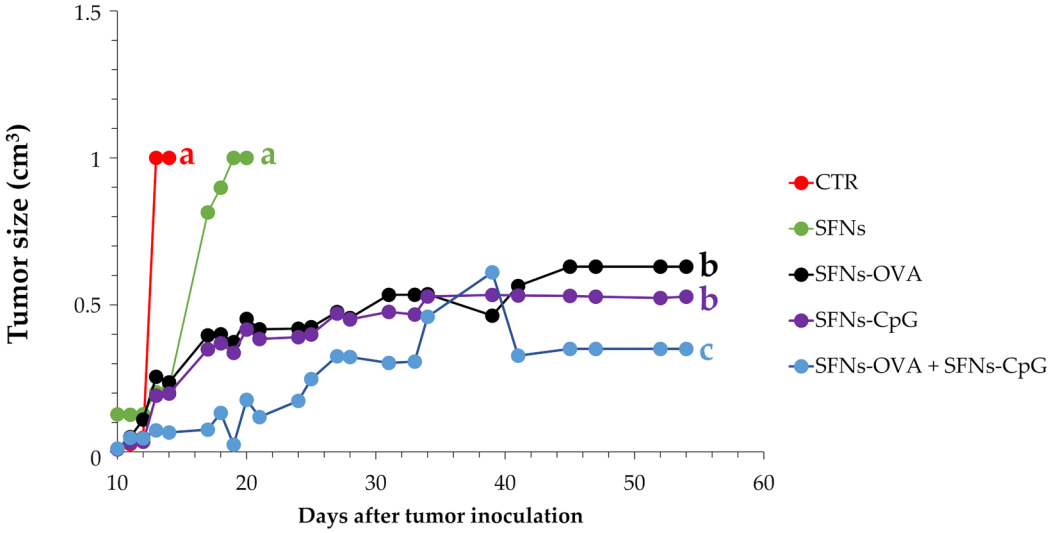

Figure 5 Effects of SFNs-OVA, SFNs-CpG, and their combination on B16/F10 melanoma growth. Tumor size is shown as a function of time (days after tumor inoculation) and treatment with or without SFNs. Mice (six per group) were sacrificed when the tumor reached 1 cm^3. Data are reported as mean values, and error bars were not displayed on the plots for clarity, but uncertainties were within ~15%. Different letters indicate a significant difference between the means of the corresponding groups: in particular, a p value<0.00001 was found in the comparisons a versus b and a versus c, while a p value<0.001 was observed in the comparison b versus c. The same letters indicate no significant differences (p>0.05) (multifactor analysis of variance, and Fisher's least significant difference, least significant difference, to discriminate among the means). CTR, control; OVA, ovalbumin; SFNs, silk fibroin nanoparticles.

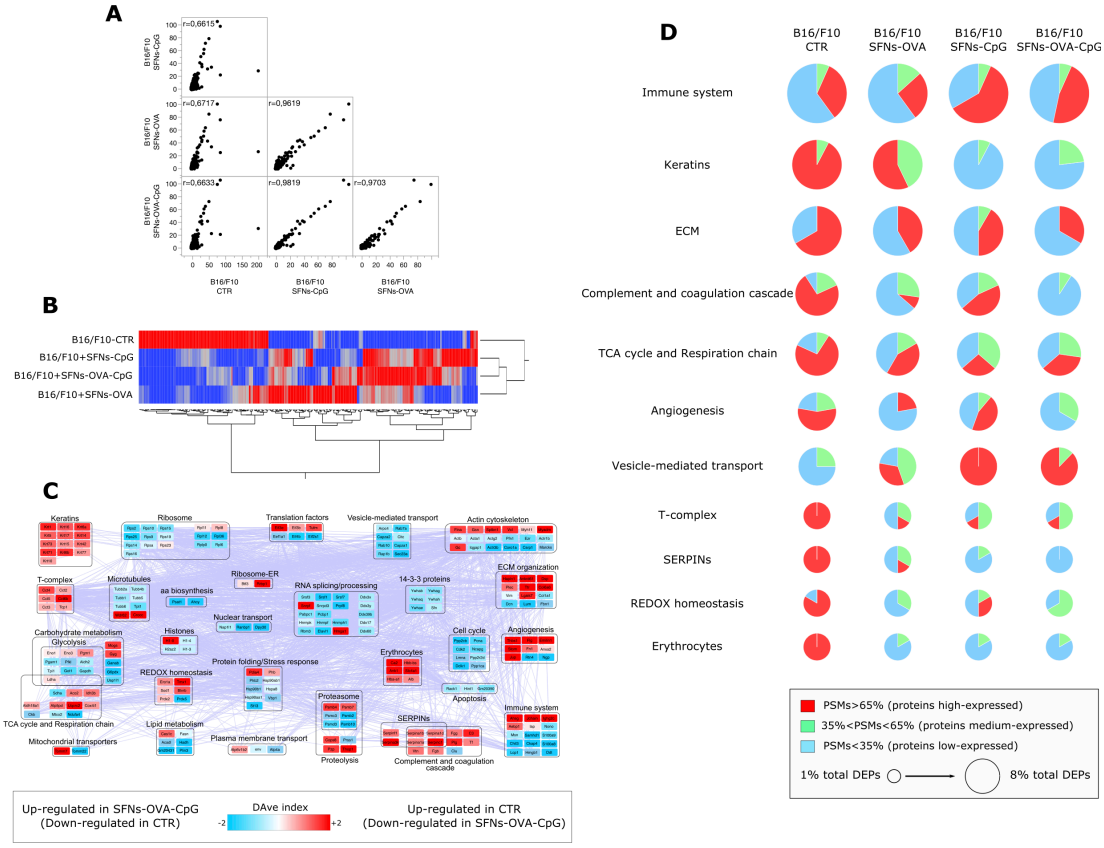

Figure 6 Proteome and functional modules characterized by nLC-hrMS/MS analysis of tissues from the B16/F10 melanoma model. (A) Spearman's correlation and hierarchical clustering (B) among profiles of DEPs. (C) PPI network model reconstructed by Cytoscape's STRING application starting from proteins differentially expressed by comparing B16/F10 melanoma model untreated (CTR) and treated with SFNs-OVA plus SFNs-CpG. Proteins were grouped in functional modules. The red color code (positive DAve values) indicates proteins upregulated in CTR (vs SFNs-OVA plus SFNs-CpG samples), while the blue color code (negative DAve values) indicates proteins upregulated in SFNs-OVA plus SFNs-CpG samples (vs CTR). (D) Functional modules most affected by SNFs treatments in B16/F10 melanoma model. Red, green and blue color codes indicate the percentage of proteins with high expression, medium expression and low expression, respectively, based on a PSMs-based label-free quantification. The pie chart size is proportional to the number of DEPs per module. CTR, control; DEP, differentially expressed protein; ECM, extracellular matrix; OVA, ovalbumin; PSMs, peptide spectrum matches; SFNs, silk fibroin nanoparticles; TCA, tricarboxylic acid cycle.

mainly mediated by the presence of CpG, while OVA mainly affected the downregulation of the complement and coagulation cascades, suggesting not only an additive mechanism of action but complementary as well.

DISCUSSION

In this study, we explored an innovative active immunotherapy approach aimed at redirecting a previously consolidated immune response toward the tumor against a re-call antigen. In our system, a non-tumor-associated antigen was delivered within tumor cells using SFNs. SF has been selected as the material to nanoencapsulate antigen and adjuvant because it is biocompatible, it provides mechanical durability, and its enzyme-mediated degradation supports the sustained intracellular release after nanoparticle uptake by cancer cells.[21] Clearly, based on the use of SFNs, our system provides a safety profile that escapes the concerns related to administering live pathogens to potentially immune-compromised patients, which has been recently reported.[38] Also, following administration in mice, the lack of inflammatory signs at peripheral tissues seems to rule out the risks related to the onset of inflammatory/autoimmune manifestations; this is probably linked to the fact that, in our model, SFNs are administered at the tumor site, and both tumor and DCs exert a preferential uptake. In this regard, the selective uptake of SFNs by tumors may be further refined through the functionalization of the nanoparticle surface with ligands able to provide active targeting, and many examples in the literature exploited the large amounts of available amino and carboxyl groups in fibroin peptides to link oligonucleotides or peptides.[39–44] This may also avoid the onset of an autoimmune response when the nanoparticles are uptaken by healthy instead of tumor cells.

Our data also showed that our approach effectively redirected immunity against a re-call antigen toward

the tumor, involving in this process both innate and adoptive harms of the immune response (in particular, DCs, which were shown to efficiently uptake SFNs, and T cells, respectively). Concerning DCs, their involvement is important since these cells orchestrate innate and adaptive immune responses, so their function is crucial for effective anticancer immunity.[45] Concerning T cells, both CD4+ and CD8+ IFN-γ-secreting/cytotoxic T cells were detected among tumor-infiltrating lymphocytes of SFNs-OVA treated mice, specifically demonstrating the efficiency of our 'Trojan horse' strategy in redirecting the anti-OVA immune response against tumor cells.

The proteomic analyses of tumors treated with SFNs, and their evaluation at a holistic level by network models, allowed us to appreciate the involvement of not strictly immune-mediated mechanisms among the effects of the treatments.

Indeed, our data envisage the possibility of translating into clinics this 'Trojan-horse', immune response-centered strategy, that is, adopting, as immunogens, antigens of the compulsory vaccines recommended by the international health institutes for the prevention of infectious diseases. The advantage of this 'Trojan-horse' approach would be that each single patient with cancer, independently from the tumor's histological nature, could have already at play the appropriate immunological background to be treated. Hence, this approach would recapitulate the essence of personalized medicine with the need for universality. The 'Trojan-horse' approach could also synergize well with immune checkpoint inhibitors, favoring the unleashing of T cells effector activities. Finally, based on the continuous improvement of technologies for local site delivery of immunotherapies,[46] our innovative strategy could find a role in the treatment with eradication purpose of non-metastatic tumors, such as glioblastoma, as well as in palliative therapy of all surgically unresectable tumor masses. However, to ensure clinical success, many challenges in the translation from bench to bedside still must be addressed for SFNs, ranging from the technological and Good Manufacturing Practice large-scale manufacturing challenges, including quality control and batch release requirements, to the biological ones, including biocompatibility, biodegradability and safety, as we recently discussed in detail.[47]

Author affiliations
[1]Department of Pharmaceutical Sciences, University of Piemonte Orientale, Novara, Piemonte, Italy
[2]Department of Internal Medicine and Centre of Excellence for Biomedical Research, University of Genoa, Genova, Liguria, Italy
[3]Department of Drug Sciences, University of Pavia, Pavia, Lombardia, Italy
[4]PharmaExceed S.r.l, Pavia, Lombardia, Italy
[5]Institute for Biomedical Technologies, ITB CNR, Segrate, Lombardia, Italy
[6]Anatomic Pathology Unit, IRCCS Ospedale Policlinico San Martino, Genova, Liguria, Italy
[7]Department of Surgical and Integrated Diagnostic Sciences, University of Genoa, Genova, Liguria, Italy
[8]Biotherapy Unit, IRCCS Ospedale Policlinico San Martino, Genova, Liguria, Italy

Acknowledgements The authors thank Dr Sara Tengattini from University of Pavia, Department of Drug Sciences for OVA quantitative analysis, and Dr Ilaria Giuseppina Tredici from the Arvedi Laboratory, CISRiC (Centro Interdipartimentale di Studi e Ricerche per la Conservazione del Patrimonio Culturale), Pavia, Italy for the scanning electron microscopy and energy dispersive spectrometry analyses. Also, The authors also thank Professor Lorenzo Moretta and Professor Paola de Candia for their precious suggestions and comments on the manuscript.

Contributors Guarantor: GF. Conceptualization: GF, MLT, DDS. Methodology: EB, FF, TA, SP, PM, RR, GP, LM, DF, GF. Investigation: EB, FF, TA, SP, PM, RR, GP, LM, MG, GIA, MM, DF. Visualization: GF, MLT, DDS, DF, FF, LM. Funding acquisition: GF, MLT, DDS, PM. Project administration: GF, MLT. Supervision: GF, MLT, DDS. Writing—original draft: GF, MLT, DDS. Writing—review and editing: GF, MLT, DDS, FF, DF, EB.

Funding This research was funded by grants from: Ministero della Salute, Progetto 5M-2019-2366468 – 5 per mille, 'Generazione di organoidi tumorali da neoplasia solide ed ematologiche'; PON ELIXIR CNR-BiOMICS (PIR01_00017), Elixir Implementation Study Proteomics (2019–2021 and 2021–2023) and Italian Ministry of Health (RF2019-12370396); Interreg V-A Italy-Switzerland 2014–2020—ATEx—Advanced Therapies Experiences (Project ID 637541).

Competing interests Data presented in this manuscript pertain to the Italian Patent Application N. 102019000008658 'Immunizzazione antitumorale mediata da nanoparticelle e basata su un'immunità preesistente' filed on June 11, 2019, granted on April 21, 2021, and the international patent application PCT/IB2020/055456 'Nanoparticles for use in the redirection against the tumour of a non-tumour-specific immune response, based on a pre-existing immunity', Publication number WO/2020/250153, filed on June 10, 2020.The authors who are co-inventors in these patents are EB, FF, DF, SP, MLT and GF.

Patient consent for publication Not applicable.

Ethics approval Not applicable.

Provenance and peer review Not commissioned; externally peer reviewed.

Data availability statement All data relevant to the study are included in the article or uploaded as supplementary information. All data are available in the main text or the Supplemental materials.

ORCID iDs
Elia Bari http://orcid.org/0000-0003-0241-0620
Giuseppina Iliana Astone http://orcid.org/0000-0003-4206-3491
Maria Luisa Torre http://orcid.org/0000-0001-8062-6836
Gilberto Filaci http://orcid.org/0000-0001-6445-8414

REFERENCES

1 Rosenberg SA, Yang JC, Restifo NP. Cancer immunotherapy: moving beyond current vaccines. *Nat Med* 2004;10:909–15.
2 Small EJ, Schellhammer PF, Higano CS, *et al*. Placebo-Controlled phase III trial of immunologic therapy with sipuleucel-T (APC8015) in patients with metastatic, asymptomatic hormone refractory prostate cancer. *J Clin Oncol* 2006;24:3089–94.
3 Saxena M, van der Burg SH, Melief CJM, *et al*. Therapeutic cancer vaccines. *Nat Rev Cancer* 2021;21:360–78.
4 Lee C-H, Yelensky R, Jooss K, *et al*. Update on tumor neoantigens and their utility: why it is good to be different. *Trends Immunol* 2018;39:536–48.
5 Rammensee H-G, Singh-Jasuja H. Hla ligandome tumor antigen discovery for personalized vaccine approach. *Expert Rev Vaccines* 2013;12:1211–7.

6 Januszkiewicz-Lewandowska D, Gowin E, Bocian J, *et al*. Vaccine-Derived immunity in children with Cancer-Analysis of anti-tetanus and Anti-Diphtheria antibodies changes after completion of antineoplastic therapy. *Pediatr Blood Cancer* 2015;62:2108–13.
7 Sau S, Alsaab HO, Bhise K, *et al*. Multifunctional nanoparticles for cancer immunotherapy: a groundbreaking approach for reprogramming malfunctioned tumor environment. *J Control Release* 2018;274:24–34.
8 Gao S, Yang D, Fang Y, *et al*. Engineering nanoparticles for targeted remodeling of the tumor microenvironment to improve cancer immunotherapy. *Theranostics* 2019;9:126–51.
9 Nasirmoghadas P, Mousakhani A, Behzad F, *et al*. Nanoparticles in cancer immunotherapies: an innovative strategy. *Biotechnol Prog* 2021;37:e3070.
10 Perteghella S, Crivelli B, Catenacci L, *et al*. Stem cell-extracellular vesicles as drug delivery systems: new frontiers for silk/curcumin nanoparticles. *Int J Pharm* 2017;520:86–97.
11 Crivelli B, Perteghella S, Bari E. Silk nanoparticles: from inert supports to bioactive natural carriers for drug delivery. *Soft Matter* 2017.
12 Crivelli B, Bari E, Perteghella S, *et al*. Silk fibroin nanoparticles for celecoxib and curcumin delivery: ROS-scavenging and anti-inflammatory activities in an in vitro model of osteoarthritis. *Eur J Pharm Biopharm* 2019;137:37–45.
13 Palma C, La Rocca C, Gigantino V, *et al*. Caloric restriction promotes immunometabolic reprogramming leading to protection from tuberculosis. *Cell Metab* 2021;33:300–18.
14 Bari E, Di Silvestre D, Mastracci L. GMP-compliant sponge-like dressing containing MSC lyo-secretome: proteomic network of healing in a murine wound model. *Eur J Pharm Biopharma* 2020.
15 Di Silvestre D, Brambilla F, Mauri PL. Multidimensional protein identification technology for direct-tissue proteomics of heart. *Methods Mol Biol* 2013;1005:25–38.
16 Doncheva NT, Morris JH, Gorodkin J, *et al*. Cytoscape StringApp: network analysis and visualization of proteomics data. *J Proteome Res* 2019;18:623–32.
17 Su G, Morris JH, Demchak B, *et al*. Biological network exploration with Cytoscape 3. *Curr Protoc Bioinformatics* 2014;47:11–24.
18 Scardoni G, Tosadori G, Faizan M, *et al*. Biological network analysis with CentiScaPe: centralities and experimental dataset integration. *F1000Res* 2014;3:139.
19 Burrello J, Tetti M, Forestiero V, *et al*. Characterization of circulating extracellular vesicle surface antigens in patients with primary aldosteronism. *Hypertension* 2021;78:726–37.
20 Tosadori G, Bestvina I, Spoto F, *et al*. Creating, generating and comparing random network models with NetworkRandomizer. *F1000Res* 2016;5:2524.
21 Donahue ND, Acar H, Wilhelm S. Concepts of nanoparticle cellular uptake, intracellular trafficking, and kinetics in nanomedicine. *Adv Drug Deliv Rev* 2019;143:68–96.
22 Wang Y, Hu L, Zheng Y, *et al*. Hmga1 in cancer: cancer classification by location. *J Cell Mol Med* 2019;23:2293–302.
23 Han W, Hu C, Fan Z-J, *et al*. Transcript levels of keratin 1/5/6/14/15/16/17 as potential prognostic indicators in melanoma patients. *Sci Rep* 2021;11:1023.
24 Lorenz N, Loef EJ, Verdon DJ, *et al*. Human T cell activation induces synaptic translocation and alters expression of the serine protease inhibitor neuroserpin and its target protease. *J Leukoc Biol* 2015;97:699–710.
25 Kircher DA, Trombetti KA, Silvis MR, *et al*. AKT1^{E17K} Activates Focal Adhesion Kinase and Promotes Melanoma Brain Metastasis. *Mol Cancer Res* 2019;17:1787–800.
26 Liu J, Zhong F, Cao L, *et al*. 7-Dehydrocholesterol suppresses melanoma cell proliferation and invasion via Akt1/NF-κB signaling. *Oncol Lett* 2020;20:1.
27 Nurzat Y, Su W, Min P, *et al*. Identification of therapeutic targets and prognostic biomarkers among integrin subunits in the skin cutaneous melanoma microenvironment. *Front Oncol* 2021;11:751875.
28 Kwak M, Erdag G, Leick KM, Leick LaRoche KM, *et al*. Associations of immune cell homing gene signatures and infiltrates of lymphocyte subsets in human melanomas: discordance with CD163+ myeloid cell infiltrates. *J Transl Med* 2021;19:371–23.
29 Liu Y, Liu R, Yang F, *et al*. miR-19A promotes colorectal cancer proliferation and migration by targeting TIA1. *Mol Cancer* 2017;16:53.
30 Mansoori B, Mohammadi A, Ditzel HJ, *et al*. Hmga2 as a critical regulator in cancer development. *Genes* 2021;12:269.
31 Yang GL, Zhang LH, Bo JJ, *et al*. Overexpression of HMGA2 in bladder cancer and its association with clinicopathologic features and prognosis HMGA2 as a prognostic marker of bladder cancer. *Eur J Surg Oncol* 2011;37:265–71.
32 Chen Z, Li Q, Wang S, *et al*. miR-485-5p inhibits bladder cancer metastasis by targeting HMGA2. *Int J Mol Med* 2015;36:1136–42.
33 Shi Z, Li X, Wu D, *et al*. Silencing of HMGA2 suppresses cellular proliferation, migration, invasion, and epithelial-mesenchymal transition in bladder cancer. *Tumour Biol* 2016;37:7515–23.
34 Moen LV, Sener Z, Volchenkov R, *et al*. Ablation of the Cβ2 subunit of PKA in immune cells leads to increased susceptibility to systemic inflammation in mice. *Eur J Immunol* 2017;47:1880–9.
35 Tang J, Luo Y, Wu G. A glycolysis-related gene expression signature in predicting recurrence of breast cancer. *Aging* 2020;12:24983–94.
36 Palmerini E, Agostinelli C, Picci P, *et al*. Tumoral immune-infiltrate (IF), PD-L1 expression and role of CD8/TIA-1 lymphocytes in localized osteosarcoma patients treated within protocol ISG-OS1. *Oncotarget* 2017;8:111836–46.
37 Cartwright T, Perkins ND, L Wilson C. Nfkb1: a suppressor of inflammation, ageing and cancer. *Febs J* 2016;283:1812–22.
38 Selvanesan BC, Chandra D, Quispe-Tintaya W, *et al*. *Listeria* delivers tetanus toxoid protein to pancreatic tumors and induces cancer cell death in mice. *Sci Transl Med* 2022;14:eabc1600.
39 Mao B, Liu C, Zheng W, *et al*. Cyclic cRGDfk peptide and chlorin E6 functionalized silk fibroin nanoparticles for targeted drug delivery and photodynamic therapy. *Biomaterials* 2018;161:306–20.
40 Mottaghitalab F, Kiani M, Farokhi M, *et al*. Targeted delivery system based on Gemcitabine-Loaded silk fibroin nanoparticles for lung cancer therapy. *ACS Appl Mater Interfaces* 2017;9:31600–11.
41 Bian X, Wu P, Sha H, *et al*. Anti-EGFR-iRGD recombinant protein conjugated silk fibroin nanoparticles for enhanced tumor targeting and antitumor efficiency. *Onco Targets Ther* 2016;9:3153–62.
42 Gou S, Huang Y, Wan Y, *et al*. Multi-bioresponsive silk fibroin-based nanoparticles with on-demand cytoplasmic drug release capacity for CD44-targeted alleviation of ulcerative colitis. *Biomaterials* 2019;212:39–54.
43 Rodriguez-Nogales A, Algieri F, De Matteis L, *et al*. Intestinal anti-inflammatory effects of RGD-functionalized silk fibroin nanoparticles in trinitrobenzenesulfonic acid-induced experimental colitis in rats. *Int J Nanomedicine* 2016;11:5945–58.
44 Bari E, Serra M, Paolillo M, *et al*. Silk fibroin nanoparticle functionalization with Arg-Gly-Asp cyclopentapeptide promotes active targeting for tumor site-specific delivery. *Cancers* 2021;13:1185.
45 Plesca I, Müller L, Böttcher JP, *et al*. Tumor-Associated human dendritic cell subsets: phenotype, functional orientation, and clinical relevance. *Eur J Immunol* 2022;52:1750–8.
46 Wang J, Zhang Y, Pi J, *et al*. Localized delivery of immunotherapeutics: a rising trend in the field. *J Control Release* 2021;340:149–67.
47 Bari E. From bench to bedside: the long way towards GMP scale-up, preclinical and clinical trials for Silk-based drug delivery systems.. In: *Silk-Based drug delivery systems*, 2021: 179–204.

Data file S1. Proteins identified by analyzing B16/F10 melanoma model untreated (CTR, n=3 biol. rep x 2 tech. rep), treated with SNFs-OVA (SNFs-OVA, n=3 biol. rep x 2 tech. rep), treated with SNFs-CpG (SNFs-CpG, n=3 biol. rep x 2 tech. rep), treated with SNFs-OVA-CpG (SNFs-OVA-CpG, n=3 biol. rep x 2 tech. rep). Peptide spectru

Annotations					PSMs (B16/F10 MELANOMA MODEL)																									Av. PSMs			
ID UNIPROT	Gene Name	Protein name	MW [kDa]	calc. pI	CTR1	CTR2	CTR3	CTR4	CTR5	CTR6	SNFs-OVA1	SNFs-OVA2	SNFs-OVA3	SNFs-OVA4	SNFs-OVA5	SNFs-OVA6	SFNs-CpG1	SFNs-CpG2	SFNs-CpG3	SFNs-CpG4	SFNs-CpG5	SFNs-CpG6	SFNs-OVA-CpG1	SFNs-OVA-CpG2	SFNs-OVA-CpG3	SFNs-OVA-CpG4	SFNs-OVA-CpG5	SFNs-OVA-CpG6	IF	CTR	SFNs-OVA	SFNs-CpG	SFNs-OVA-CpG
P68134	Acta1	Actin, alpha skeletal muscle	42	5,39	55,6	53,8	35,4	37,3	33,6	39,7	76,5	60,3	63,1	63,4	60,8	60,4	68,9	63,3	71,6	83,8	74,9	68,7	63,2	65,3	57,7	64,2	72,5	70,2	100,0	42,5	64,1	71,9	65,5
V9GXQ2	Actb	Predicted gene 17087	41,7	7,37	77,6	70,8	83,8	82,3	76,7	79,3	94,1	92,3	105,1	112,5	101,4	100,7	113,1	101,4	91,0	98,1	116,2	115,2	102,0	99,2	82,7	89,6	113,0	111,3	100,0	78,4	101,0	105,9	99,6
Q8BFZ3	Actbl2	Beta-actin-like protein 2	42	5,49	35,3	35,0	53,7	56,6	49,2	54,1	43,1	43,5	67,3	67,5	62,8	64,2	67,1	54,0	43,0	44,0	75,8	68,7	56,9	54,8	40,4	45,2	68,4	70,2	100,0	47,3	58,1	58,8	56,0
P63268	Actg2	Actin, gamma-enteric smooth muscle	41,9	5,48	47,6	45,7	34,1	34,7	31,2	37,3	69,5	52,4	58,9	58,3	57,0	56,6	53,3	49,3	63,4	75,7	69,0	63,7	61,4	61,8	51,0	59,7	68,4	66,2	100,0	38,4	58,8	62,4	61,4
A1BN54	Actn1	Alpha actinin 1a	102,7	5,48	6,2	5,4	7,9	9,0	7,2	8,4	6,2	5,3	5,3	7,2	7,7	7,7	5,5	6,5	6,1	6,1	7,9	9,1	5,4	8,7	3,8	5,4	8,3	7,0	100,0	7,3	6,5	6,9	6,5
A0A1L1SV25	Actn4	Alpha-actinin-4	107	5,36	6,2	8,1	9,2	10,3	8,4	9,6	7,0	6,2	5,3	8,2	7,7	7,7	5,5	6,5	6,1	6,1	7,9	9,1	5,4	8,7	3,8	5,4	9,3	7,0	100,0	8,6	7,0	6,9	6,6
P07724	Alb	Albumin	68,6	6,07	69,7	69,9	57,6	55,3	53,9	57,7	17,6	21,3	42,0	44,0	38,6	42,2	46,9	43,7	28,6	32,7	26,6	29,3	25,3	23,5	22,1	27,1	19,7	20,0	100,0	60,7	34,3	34,6	23,0
P47738	Aldh2	Aldehyde dehydrogenase, mitochondrial	56,5	7,62	3,5	4,5	3,9	5,1	3,6	4,8	1,8	4,4	7,4	8,2	8,7	5,8	10,1	12,1	10,2	8,2	7,9	11,1	5,4	8,7	10,6	13,6	4,1	5,0	100,0	4,2	6,0	9,9	7,9
A6ZI44	Aldoa	Fructose-bisphosphate aldolase	45,1	7,91	20,3	17,0	23,6	27,0	25,2	24,0	19,4	21,3	26,3	22,5	24,1	19,2	35,8	36,3	22,5	23,5	14,8	17,2	24,4	23,5	24,0	25,3	19,7	20,0	100,0	22,9	22,1	25,0	22,8
P07356	Anxa2	Annexin A2	38,7	7,69	6,2	8,1	2,6	2,6	3,6	2,4	6,2	4,4	5,3	8,2	7,7	5,8	4,6	6,5	8,2	8,2	5,9	10,1	3,6	2,6	2,9	5,4	2,1	3,0	100,0	4,2	6,3	7,2	3,3
P48036	Anxa5	Annexin A5	35,7	4,96	11,5	14,3	17,0	16,7	14,4	13,2	12,3	12,4	11,6	17,4	13,5	16,3	19,3	16,7	11,2	18,4	13,8	13,1	20,8	20,9	14,4	15,4	16,6	16,0	100,0	14,5	13,9	15,4	17,3
Q99PT1	Arhgdia	Rho GDP-dissociation inhibitor 1	23,4	5,2	1,8	1,8	3,9	2,6	2,4	3,6	1,8	1,8	3,2	4,1	1,9	2,9	4,6	3,7	2,0	4,1	5,9	4,0	2,7	2,6	3,8	1,8	6,2	7,0	100,0	2,7	2,6	4,1	4,0
Q03265	Atp5f1a	ATP synthase subunit alpha, mitochondrial	59,7	9,19	24,7	26,9	40,6	38,6	37,2	37,3	21,1	22,2	34,7	37,8	33,8	29,7	29,4	28,8	24,5	21,5	34,5	42,5	29,8	31,3	30,8	19,0	30,1	34,1	100,0	34,2	29,9	30,2	29,2
P56480	Atp5f1b	ATP synthase subunit beta, mitochondrial	56,3	5,34	42,3	37,7	44,5	41,1	39,6	31,2	40,5	39,9	56,7	58,3	52,1	58,5	67,1	61,4	41,9	31,7	69,0	50,5	56,0	51,4	50,0	41,6	49,7	56,1	100,0	39,4	51,0	53,6	50,8
P35564	Canx	Calnexin	67,2	4,64	3,5	3,6	2,6	5,1	6,0	3,6	3,5	6,2	5,3	5,1	5,8	3,8	14,7	16,7	3,1	4,1	4,9	7,1	9,9	12,2	3,8	3,6	5,2	4,0	100,0	4,1	5,0	8,4	6,5
P80314	Cct2	T-complex protein 1 subunit beta	57,4	6,4	8,8	9,0	15,7	14,1	16,8	15,6	6,2	7,1	8,4	9,2	7,7	9,6	3,7	5,6	4,1	6,1	9,9	11,1	5,4	4,4	5,8	5,4	9,3	11,0	100,0	13,3	8,0	6,7	6,9
P80318	Cct3	T-complex protein 1 subunit gamma	60,6	6,7	4,4	3,6	6,5	5,1	6,0	4,8	6,2	5,3	4,2	3,1	3,9	3,8	1,8	1,9	1,0	4,1	3,0	3,0	1,8	1,7	2,9	3,6	4,1	3,0	100,0	5,1	4,4	2,5	2,9
Q52KG9	Cct6a	Chaperonin containing Tcp1, subunit 6a (Zeta)	58	6,9	5,3	5,4	5,2	5,1	4,8	6,0	8,8	2,7	2,1	2,0	8,7	9,6	7,4	8,4	2,0	5,1	4,9	6,1	7,2	6,1	5,8	2,7	3,1	5,0	100,0	5,3	5,6	5,6	5,0
Q04447	Ckb	Creatine kinase B-type	42,7	5,67	19,4	25,1	21,0	14,1	20,4	20,4	27,3	27,5	24,2	22,5	24,1	23,0	16,5	13,0	18,4	17,4	17,7	21,2	17,2	17,4	19,2	22,6	17,6	16,0	100,0	20,1	24,8	17,4	18,3
Q68FD5	Cltc	Clathrin heavy chain 1	191,4	5,69	14,1	11,7	9,2	6,4	9,6	4,8	20,2	23,1	21,0	19,4	21,2	21,1	17,5	15,8	18,4	16,4	15,8	18,2	18,1	20,0	16,4	15,4	18,7	15,0	100,0	9,3	21,0	17,0	17,2
Q01149	Col1a2	Collagen alpha-2(I) chain	129,5	9,19	7,9	8,1	10,5	9,0	2,4	1,2	7,0	9,8	7,4	8,2	6,8	7,7	3,7	3,7	18,4	17,4	4,9	4,0	9,0	9,6	14,4	15,4	3,1	2,0	100,0	6,5	7,8	8,7	8,9
E9PWQ3	Col6a3	Collagen, type VI, alpha 3	353,7	6,93	5,3	4,5	9,2	7,7	15,6	12,0	14,1	12,4	5,3	3,1	7,7	7,7	12,9	14,9	26,6	28,6	18,7	16,2	9,9	7,0	5,8	7,2	42,5	41,1	100,0	9,0	8,4	19,6	18,9
Q501J6	Ddx17	Probable ATP-dependent RNA helicase DDX17	72,4	8,59	2,6	3,6	2,6	5,1	2,4	2,4	1,8	2,7	3,2	2,0	3,9	3,8	1,8	1,9	3,1	4,1	2,0	3,0	4,5	6,1	4,8	3,6	4,1	4,0	100,0	3,1	2,9	2,6	4,5
Q62167	Ddx3x	ATP-dependent RNA helicase DDX3X	73,1	7,18	5,3	6,3	3,9	3,9	3,6	4,8	8,8	9,8	7,4	3,1	8,7	8,6	3,7	2,8	4,1	6,1	4,9	6,1	9,9	12,2	6,7	9,0	8,3	8,0	100,0	4,6	7,7	4,6	9,0
Q61656	Ddx5	Probable ATP-dependent RNA helicase DDX5	69,2	8,92	6,2	8,1	2,6	5,1	2,4	2,4	7,0	7,1	6,3	5,1	4,8	7,7	2,8	3,7	7,2	8,2	3,9	5,1	8,1	9,6	8,7	7,2	4,1	4,0	100,0	4,5	6,3	5,1	7,0
P31001	Des	Desmin	53,5	5,27	7,1	3,6	2,6	5,1	4,8	3,6	7,0	8,0	6,3	5,1	3,9	4,8	3,7	4,7	10,2	10,2	5,9	4,0	8,1	6,1	8,7	9,0	6,2	8,0	100,0	4,5	5,8	6,5	7,7
O08553	Dpysl2	Dihydropyrimidinase-related protein 2	62,2	6,38	2,6	4,5	3,9	6,4	7,2	3,6	1,8	2,7	4,2	3,1	3,9	1,9	1,8	3,7	4,1	4,1	2,0	2,0	0,9	1,7	3,8	3,6	5,2	5,0	100,0	4,7	2,9	3,0	3,4
Q9JHU4	Dync1h1	Cytoplasmic dynein 1 heavy chain 1	531,7	6,42	4,4	4,5	6,5	3,9	2,4	2,4	5,3	5,3	3,2	2,0	1,9	5,8	3,7	4,7	3,1	6,1	5,9	3,0	8,1	10,4	3,8	2,7	5,2	7,0	100,0	4,0	3,9	4,4	6,2
P10126	Eef1a1	Elongation factor 1-alpha 1	50,1	9,01	37,1	37,7	13,1	15,4	14,4	13,2	40,5	46,1	31,5	30,7	30,9	25,9	20,2	20,5	25,6	26,6	28,6	27,3	19,0	21,8	29,8	23,5	19,7	22,1	100,0	21,8	34,3	24,8	22,6
Q80T06	Eef1d	Elongation factor 1-delta	31,3	5,06	1,8	1,8	5,2	5,1	6,0	7,2	2,6	2,7	5,3	6,1	4,8	5,8	5,5	3,7	3,1	2,0	4,9	4,0	4,5	2,6	1,9	2,7	5,2	6,0	100,0	4,5	4,5	3,9	3,8
Q9D8N0	Eef1g	Elongation factor 1-gamma	50	6,74	4,4	4,5	2,6	5,1	3,6	3,6	3,5	3,5	6,3	6,1	5,8	6,7	3,7	1,9	8,2	5,1	2,0	4,0	1,8	3,5	6,7	9,0	4,1	4,0	100,0	4,0	5,3	4,1	4,9
P58252	Eef2	Elongation factor 2	95,3	6,83	15,9	13,4	19,6	18,0	22,8	18,0	17,6	16,0	20,0	18,4	20,3	23,0	13,8	12,1	13,3	20,4	16,7	17,2	20,8	18,3	21,2	18,1	16,6	18,0	100,0	18,0	19,2	15,6	18,8
P60843	Eif4a1	Eukaryotic initiation factor 4A-I	46,1	5,48	9,7	9,9	11,8	11,6	9,6	10,8	8,8	12,4	11,6	11,2	10,6	10,5	5,5	8,4	6,1	9,2	12,8	9,1	6,3	6,1	8,7	7,2	13,5	16,0	100,0	10,6	10,9	8,5	9,6
P10630	Eif4a2	Eukaryotic initiation factor 4A-II	46,4	5,48	7,1	7,2	5,2	3,9	4,8	4,8	7,0	9,8	8,4	9,2	6,8	6,7	4,6	6,5	4,1	7,2	9,9	8,1	6,3	5,2	6,7	5,4	6,2	8,0	100,0	5,5	8,0	6,7	6,3
P17182	Eno1	Alpha-enolase	47,1	6,8	30,9	31,4	66,8	59,1	55,1	50,5	40,5	40,8	50,4	47,0	41,5	39,3	36,8	37,2	28,6	26,6	29,6	32,3	56,0	47,9	32,7	39,8	39,4	37,1	100,0	49,0	43,3	31,9	42,1
P10404	env	MLV-related proviral Env polyprotein	69,6	7,96	2,6	1,8	2,6	2,6	1,2	1,2	2,6	3,5	5,3	4,1	1,9	3,8	2,8	3,7	4,1	4,1	3,0	3,0	3,6	3,5	1,9	3,6	2,1	2,0	100,0	2,0	3,5	3,4	2,8
P19096	Fasn	Fatty acid synthase	272,3	6,58	15,0	11,7	19,6	20,6	20,4	16,8	22,0	22,2	27,3	26,6	29,0	30,7	27,6	23,3	12,3	16,4	23,6	16,2	25,3	22,6	23,1	22,6	17,6	19,0	100,0	17,3	26,3	19,9	21,7
Q8VCM7	Fgg	Fibrinogen gamma chain	49,4	5,86	19,4	21,5	13,1	10,3	13,2	12,0	1,8	1,8	6,3	6,1	6,8	8,6	3,7	3,7	9,2	14,3	33,5	34,4	2,7	3,5	6,7	7,2	5,2	3,0	100,0	14,9	5,2	16,5	4,7
A0A087WS56	Fn1	Fibronectin	249,4	5,82	15,9	16,1	24,9	21,9	19,2	20,4	1,8	0,9	7,4	6,1	7,7	8,6	3,7	3,7	17,4	17,4	53,2	56,6	2,7	2,6	4,8	5,4	10,4	10,0	100,0	19,7	5,4	25,3	6,0
V9GX06	Gapdh	Predicted gene 11214 (Fragment)	19,9	7,42	8,8	13,4	2,6	3,9	7,2	6,0	17,6	15,1	15,8	17,4	12,6	18,2	19,3	23,3	19,4	20,4	10,8	10,1	24,4	24,4	26,0	22,6	9,3	10,0	100,0	7,0	16,1	17,2	19,4
A0A1D5RLD8	Gm10358	Glyceraldehyde-3-phosphate dehydrogenase	35,8	8,25	48,5	62,8	45,8	52,7	52,7	56,5	73,9	77,2	90,4	94,1	85,0	91,1	91,0	94,9	75,7	65,4	71,9	75,8	80,3	81,0	74,1	71,5	68,4	62,1	100,0	53,2	85,3	79,1	72,9
P05202	Got2	Aspartate aminotransferase, mitochondrial	47,4	9	5,3	0,9	6,5	5,1	4,8	7,2	4,4	4,4	6,3	6,1	3,9	4,8	6,4	3,7	4,1	2,0	2,0	2,0	8,1	6,1	2,9	2,7	3,1	4,0	100,0	5,0	5,0	3,4	4,5
P06745	Gpi	Glucose-6-phosphate isomerase	62,7	8,13	7,1	5,4	18,3	15,4	18,0	20,4	10,6	10,6	18,9	15,3	13,5	15,3	15,6	15,8	13,3	12,3	9,9	9,1	10,8	13,1	13,5	12,7	11,4	13,0	100,0	14,1	14,1	12,7	12,4
P19157	Gstp1	Glutathione S-transferase P 1	23,6	7,87	1,8	2,7	6,5	6,4	6,0	6,0	4,4	2,7	3,2	6,1	3,9	1,9	3,7	3,7	3,1	4,1	6,9	5,1	3,6	3,5	4,8	6,3	5,2	8,0	100,0	4,9	3,7	4,4	5,2
Q8CGP4	H2ac1	Histone H2A	14	11,21	22,1	19,7	44,5	34,7	40,8	39,7	22,9	24,8	31,5	32,7	29,0	27,8	35,8	33,5	20,5	23,5	34,5	34,4	34,3	30,5	23,1	19,0	33,2	37,1	100,0	33,6	28,1	30,4	29,5
Q64523	H2ac20	Histone H2A type 2-C	14	10,9	28,2	31,4	43,2	36,0	40,8	36,1	37,0	34,6	34,7	35,8	32,8	31,6	47,8	41,9	33,7	33,7	38,4	36,4	37,9	36,6	36,5	33,5	44,6	42,1	100,0	35,9	34,4	38,7	38,5
Q64522	H2ac21	Histone H2A type 2-B	14	10,89	14,1	17,0	19,6	24,4	24,0	21,6	22,9	18,6	20,0	21,5	19,3	16,3	30,3	23,3	21,5	23,5	21,7	25,3	20,8	20,9	22,1	24,4	30,1	24,1	100,0	20,1	19,8	24,3	23,7
Q8BFU2	H2aw	Histone H2A type 3	14,1	11,05	29,1	26,9	44,5	34,7	40,8	39,7	31,7	30,2	31,5	32,7	29,0	27,8	39,5	40,0	30,7	28,6	35,5	35,4	34,3	32,2	35,6	29,9	36,3	39,1	100,0	35,9	30,5	34,9	34,6
Q3THW5	H2az2	Histone H2A.V	13,5	10,58	14,1	12,6	7,9	7,7	7,2	7,2	12,3	14,2	13,7	13,3	12,6	13,4	15,6	14,0	14,3	15,3	13,8	14,2	20,8	15,7	17,3	16,3	10,4	11,0	100,0	9,4	13,2	14,5	15,2
P70696	H2bc1	Histone H2B type 1-A	14,2	10,29	12,4	9,9	9,2	9,0	7,2	13,2	12,3	12,4	8,4	8,2	7,7	6,7	10,1	5,6	15,3	17,4	7,9	5,1	4,5	5,2	13,5	12,7	9,3	5,0	100,0	10,1	9,3	10,2	8,4
Q64475	H2bc3	Histone H2B type 1-B	13,9	10,32	30,9	26,9	34,1	33,4	27,6	32,4	34,3	32,8	34,7	31,7	33,8	27,8	35,8	31,6	38,9	34,8	33,5	30,3	26,2	25,2	30,8	34,4	36,3	29,1	100,0	30,9	32,5	34,2	30,3
P84244	H3-3a	Histone H3.3	15,3	11,27	21,2	18,8	11,8	7,7	10,8	8,4	22,9	24,8	10,5	15,3	11,6	12,5	11,9	14,0	26,6	23,5	7,9	8,1	9,9	11,3	21,2	24,4	6,2	6,0	100,0	13,1	16,3	15,3	13,2
P62806	H4c1	Histone H4	11,4	11,36	64,4	62,8	35,4	36,0	37,2	36,1	60,7	60,3	59,9	50,1	54,1	54,7	75,4	78,2	63,4	54,2	48,3	40,4	46,0	44,4	57,7	55,2	37,3	40,1	100,0	45,3	56,6	60,0	46,8
Q91VB8	Hba-a1	Alpha globin 1	15,1	8,22	33,5	28,7	117,9	127,3	109,1	108,2	4,4	4,4	30,5	36,8	38,6	37,4	26,7	28,8	13,3	12,3	28,6	25,3	21,7	23,5	15,4	15,4	23,8	30,1	100,0	87,4	25,4	22,5	21,6
P02089	Hbb-b2	Hemoglobin subunit beta-2	15,9	8,05	7,9	11,7	22,3	19,3	21,6	28,8	3,5	3,5	9,5	9,2	8,7	7,7	10,1	9,3	6,1	7,2	6,9	6,1	17,2	12,2	5,8	8,1	6,2	6,0	100,0	18,6	7,0	7,6	9,2
A8DUK4	Hbb-bs	Beta-globin	15,7	7,69	58,2	66,3	290,8	291,8	237,4	264,4	13,2	10,6	36,8	37,8	33,8	28,8	39,5	37,2	22,5	24,5	28,6	21,2	46,9	38,3	21,2	19,9	26,9	32,1	100,0	201,5	26,8	28,9	30,9
Q64525	Hist2h2bb	Histone H2B type 2-B	13,9	10,32	30,9	26,9	34,1	33,4	27,6	32,4	34,3	33,7	34,7	32,7	35,7	29,7	36,8	32,6	37,8	32,7	35,5	32,3	28,0	26,1	31,7	35,3	37,3	30,1	100,0	30,9	33,5	34,6	31,4
P61979	Hnrnpk	Heterogeneous nuclear ribonucleoprotein K	50,9	5,54	8,8	9,0	3,9	6,4	6,0	4,8	8,8	11,5	8,4	12,3	10,6	10,5	7,4	7,4	10,2	7,2	8,9	7,1	12,6	7,8	7,7	10,9	8,3	7,0	100,0	6,5	10,4	8,0	9,1
P07901	Hsp90aa1	Heat shock protein HSP 90-alpha	84,7	5,01	20,3	20,6	19,6	15,4	15,6	16,8	32,6	28,4	35,7	32,7	31,9	34,5	25,7	31,6	20,5	23,5	20,7	20,2	37,9	38,3	27,9	25,3	20,7	20,0	100,0	18,1	32,6	23,7	28,4
P11499	Hsp90ab1	Heat shock protein HSP 90-beta	83,2	5,03	33,5	41,2	31,4	27,0	31,2	28,8	45,7	43,5	50,4	45,0	43,5	41,2	41,4	42,8	32,7	35,8	30,5	28,3	46,9	42,7	35,6	34,4	34,2	34,1	100,0	32,2	44,9	35,3	38,0
P08113	Hsp90b1	Endoplasmin	92,4	4,82	15,9	15,2	14,4	16,7	10,8	16,8	23,8	23,1	16,8	16,4	21,2	19,2	14,7	15,8	9,2	14,3	14,8	10,1	15,3	13,9	16,4	17,2	18,7	12,0	100,0	15,0	20,1	13,2	15,6
Q61696	Hspa1a	Heat shock 70 kDa protein 1A	70	5,72	4,4	3,6	6,5	5,1	4,8	4,8	3,5	3,5	6,3	6,1	5,8	4,8	5,5	5,6	4,1	6,1	5,9	6,1	8,1	7,0	5,8	7,2	5,2	5,0	100,0	4,9	5,0	5,5	6,4
P17156	Hspa2	Heat shock-related 70 kDa protein 2	69,6	5,67	15,9	13,4	18,3	18,0	16,8	13,2	15,0	14,2	21,0	19,4	20,3	18,2	20,2	20,5	13,3	18,4	20,7	23,3	20,8	17,4	19,2	18,1	17,6	19,0	100,0	15,9	18,0	19,4	18,7
P20029	Hspa5	Endoplasmic reticulum chaperone BiP	72,4	5,16	21,2	15,2	30,1	28,3	31,2	27,6	22,9	25,7	29,4	31,7	26,1	25,9	29,4	36,3	28,6	24,5	25,6	27,3	29,8	25,2	26,0	28,9	28,0	27,1	100,0	25,6	26,9	28,6	27,5
P63017	Hspa8	Heat shock cognate 71 kDa protein	70,8	5,52	29,1	26,0	34,1	36,0	33,6	30,0	30,8	37,3	49,4	49,1	37,7	49,9	31,3	34,4	32,7	35,8	47,3	52,6	44,2	38,3	48,1	47,0	39,4	39,1	100,0	31,5	42,3	39,0	42,7
P63038	Hspd1	60 kDa heat shock protein, mitochondrial	60,9	6,18	30,9	36,8	60,2	52,7	73,1	68,5	29,9	30,2	36,8	35,8	63,7	58,5	49,6	42,8	21,5	23,5	50,2	50,5	47,8	47,0	28,9	37,1	47,7	55,1	100,0	53,7	42,5	39,7	43,9
P03975	Iap	IgE-binding protein	62,7	9,31	7,9	8,1	17,0	19,3	19,2	15,6	15,8	12,4	20,0	20,4	16,4	19,2	5,5	11,2	5,1	4,1	14,8	14,2	15,3	14,8	12,5	9,0	10,4	11,0	100,0	14,5	17,4	9,1	12,2
P70168	Kpnb1	Importin subunit beta-1	97,1	4,78	1,8	1,8	5,2	3,9	3,6	4,8	4,4	4,4	4,2	3,1	1,9	4,8	1,8	1,9	2,0	2,0	4,9	2,0	4,5	4,4	2,9	2,7	3,1	2,0	100,0	3,5	3,8	2,5	3,3
A0A1B0GSX0	Ldha	L-lactate dehydrogenase	39,7	8,35	19,4	21,5	18,3	14,1	18,0	12,0	25,5	24,0	24,2	20,4	28,0	27,8	15,6	15,8	13,3	16,4	12,8	14,2	12,6	13,9	19,2	15,4	9,3	9,0	100,0	17,2	25,0	14,7	13,3
P48678	Lmna	Prelamin-A/C	74,2	6,98	11,5	12,6	7,9	11,6	8,4	7,2	11,4	11,5	11,6	8,2	11,6	6,7	3,7	1,9	10,2	9,2	5,9	5,1	8,1	7,0	11,5	10,0	8,3	8,0	100,0	9,8	10,2	6,0	8,8
P08249	Mdh2	Malate dehydrogenase, mitochondrial	35,6	8,68	4,4	4,5	14,4	15,4	20,4	14,4	5,3	6,2	16,8	14,3	11,6	13,4	11,9	14,0	8,2	10,2	7,9	9,1	13,5	12,2	5,8	4,5	10,4	10,0	100,0	12,3	11,3	10,2	9,4
P00405	Mtco2	Cytochrome c oxidase subunit 2	26	4,73	4,4	3,6	6,5	5,1	3,6	4,8	7,0	7,1	6,3	8,2	3,9	5,8	8,3	9,3	5,1	5,1	7,9	8,1	10,8	10,4	7,7	4,5	8,3	10,0	100,0	4,7	6,4	7,3	8,6
Q8VDD5	Myh9	Myosin-9	226,2	5,66	12,4	7,2	22,3	23,1	28,8	20,4	7,9	10,6	4,2	5,1	9,7	6,7	16,5	10,2	19,4	12,3	30,5	23,3	7,2	7,8	7,7	5,4	30,1	25,1	100,0	19,0	7,4	18,7	13,9
A0A1W2P7Q9	Myl6	Myosin light polypeptide 6	17,7	4,65	5,3	4,5	5,2	6,4	9,6	8,4	3,5	0,9	6,3	5,1	4,8	5,8	2,8	5,6	4,1	4,1	6,9	6,1	7,2	6,1	3,8	3,6	3,1	6,0	100,0	6,6	4,4	4,9	5,0
P09405	Ncl	Nucleolin	76,7	4,75	11,5	16,1	3,9	6,4	6,0	7,2	13,2	12,4	17,9	12,3	13,5	9,6	11,0	10,2	9,2	8,2	13,8	16,2	9,0	8,7	14,4	18,1	9,3	8,0	100,0	8,5	13,1	11,4	11,3
Q61937	Npm1	Nucleophosmin	32,5	4,77	7,9	4,5	7,9	7,7	4,8	6,0	5,3	6,2	10,5	9,2	9,7	9,6	10,1	7,4	2,0	4,1	10,8	9,1	9,0	5,2	7,7	6,3	11,4	9,0	100,0	6,5	8,4	7,3	8,1
P09103	P4hb	Protein disulfide-isomerase	57	4,88	15,0	18,8	19,6	14,1	18,0	13,2	22,0	18,6	14,7	11,2	14,5	14,4	16,5	19,5	10,2	14,3	6,9	3,0	9,9	11,3	11,5	12,7	12,4	12,0	100,0	16,5	15,9	11,8	11,7
P27773	Pdia3	Protein disulfide-isomerase A3	56,6	6,21	6,2	8,1	13,1	10,3	7,2	10,8	8,8	11,5	10,5	10,2	11,6	12,5	16,5	14,9	6,1	8,2	12,8	13,1	13,5	12,2	11,5	10,0	9,3	12,0	100,0	9,3	10,9	11,9	11,4
Q3TML0	Pdia6	Protein disulfide-isomerase A6	48,7	5,19	1,8	0,9	9,2	9,0	14,4	15,6	4,4	4,4	9,5	11,2	9,7	10,5	9,2	4,7	1,0	4,1	8,9	10,1	8,1	7,8	4,8	7,2	9,3	13,0	100,0	8,5	8,3	6,3	8,4
Q9DBJ1	Pgam1	Phosphoglycerate mutase 1	28,8	7,18	12,4	11,7	5,2	3,9	1,2	2,4	17,6	12,4	9,5	10,2	11,6	12,5	24,8	24,2	15,3	16,4	4,9	4,0	19,9	16,5	19,2	12,7	13,5	13,0	100,0	6,1	12,3	14,9	15,8
P09411	Pgk1	Phosphoglycerate kinase 1	44,5	7,9	18,5	18,8	17,0	18,0	20,4	16,8	19,4	19,5	26,3	29,6	24,1	24,9	29,4	35,4	12,3	16,4	20,7	25,3	21,7	27,9	20,2	19,9	19,7	21,0	100,0	18,3	24,0	23,2	21,7
P67778	Phb	Prohibitin	29,8	5,76	4,4	6,3	11,8	14,1	9,6	10,8	5,3	4,4	5,3	9,2	4,8	4,8	2,8	4,7	3,1	5,1	7,9	8,1	2,7	3,5	7,7	7,2	3,1	4,0	100,0	9,5	5,6	5,3	4,7
O35129	Phb2	Prohibitin-2	33,3	9,83	13,2	15,2	11,8	10,3	12,0	12,0	16,7	18,6	14,7	14,3	11,6	16,3	12,9	14,9	12,3	7,2	6,9	7,1	14,4	13,9	15,4	14,5	7,3	8,0	100,0	12,4	15,4	10,2	12,3
Q61753	Phgdh	D-3-phosphoglycerate dehydrogenase	56,5	6,54	1,8	1,8	5,2	5,1	4,8	4,8	3,5	8,0	6,3	3,1	3,9	5,8	5,5	6,5	3,1	2,0	3,0	2,0	0,9	1,7	5,8	2,7	5,2	4,0	100,0	3,9	5,1	3,7	3,4
G3X925	Pklr	Pyruvate kinase	62,2	7,09	4,4	1,8	3,9	2,6	3,6	3,6	3,5	0,9	4,2	4,1	4,8	3,8	3,7	3,7	5,1	4,1	3,9	4,0	3,6	3,5	5,8	2,7	4,1	4,0	100,0	3,3	3,6	4,1	4,0
P52480	Pkm	Pyruvate kinase PKM	57,8	7,47	71,5	76,2	57,6	56,6	68,3	64,9	87,1	96,7	76,7	75,7	76,3	69,0	72,6	71,6	77,7	84,9	57,1	51,6	62,3	69,6	94,3	100,4	53,9	50,1	100,0	65,8	80,3	69,3	71,8
Q62009	Postn	Periostin	93,1	7,53	1,8	0,9	1,3	1,3	2,4	2,4	0,9	2,7	2,1	3,1	2,9	3,8	2,8	2,8	4,1	2,0	7,9	6,1	2,7	2,6	1,9	1,8	8,3	8,0	100,0	1,7	2,6	4,3	4,2
P17742	Ppia	Peptidyl-prolyl cis-trans isomerase A	18	7,9	22,9	18,8	18,3	19,3	20,4	19,2	25,5	24,0	29,4	24,5	23,2	23,0	32,2	28,8	24,5	20,4	14,8	18,2	25,3	22,6	27,9	27,1	20,7	19,0	100,0	19,8	24,9	23,2	23,8
P35700	Prdx1	Peroxiredoxin-1	22,2	8,12	12,4	11,7	11,8	12,9	8,4	9,6	8,8	13,3	17,9	21,5	17,4	19,2	23,9	22,3	14,3	15,3	10,8	12,1	19,9	20,9	17,3	19,0	10,4	10,0	100,0	11,1	16,3	16,5	16,2
Q61171	Prdx2	Peroxiredoxin-2	21,8	5,41	3,5	3,6	5,2	6,4	4,8	4,8	1,8	2,7	4,2	2,0	2,9	3,8	6,4	7,4	3,1	4,1	2,0	4,0	1,8	2,6	3,8	3,6	3,1	3,0	100,0	4,7	2,9	4,5	3,0
P68040	Rack1	Receptor of activated protein C kinase 1	35,1	7,69	5,3	7,2	2,6	3,9	1,2	1,2	6,2	6,2	4,2	5,1	6,8	7,7	5,5	3,7	8,2	7,2	4,9	7,1	6,3	7,8	7,7	7,2	9,3	8,0	100,0	3,6	6,0	6,1	7,7
O89086	Rbm3	RNA-binding protein 3	16,6	7,5	1,8	1,8	1,3	2,6	1,2	1,2	2,6	3,5	5,3	3,1	2,9	5,8	5,5	6,5	5,1	4,1	3,9	6,1	6,3	7,0	3,8	7,2	4,1	4,0	100,0	1,6	3,9	5,2	5,4
Q9CXW4	Rpl11	60S ribosomal protein L11	20,2	9,6	1,8	1,8	2,6	2,6	2,4	2,4	3,5	2,7	3,2	2,0	2,9	3,8	2,8	1,9	1,0	2,0	2,0	2,0	1,8	1,7	1,0	1,8	2,1	3,0	100,0	2,3	3,0	1,9	1,9
P47963	Rpl13	60S ribosomal protein L13	24,3	11,55	3,5	4,5	7,9	7,7	7,2	8,4	4,4	7,1	11,6	8,2	7,7	6,7	10,1	12,1	8,2	4,1	7,9	9,1	9,0	7,8	7,7	8,1	10,4	9,0	100,0	6,5	7,6	8,6	8,7
A0A1B0GQU8	Rpl18	60S ribosomal protein L18	18,1	11,91	7,1	6,3	6,5	7,7	3,6	4,8	6,2	5,3	6,3	8,2	4,8	5,8	4,6	5,6	6,1	7,2	4,9	6,1	7,2	3,5	7,7	6,3	4,1	6,0	100,0	6,0	6,1	5,7	5,8
Q8BP67	Rpl24	60S ribosomal protein L24	17,8	11,25	1,8	3,6	1,3	2,6	2,4	2,4	5,3	2,7	2,1	2,0	1,9	1,9	4,6	5,6	3,1	4,1	2,0	2,0	2,7	2,6	5,8	2,7	2,1	2,0	100,0	2,3	2,7	3,6	3,0
P14148	Rpl7	60S ribosomal protein L7	31,4	10,89	7,9	5,4	2,6	3,9	2,4	2,4	6,2	6,2	2,1	4,1	2,9	2,9	4,6	4,7	4,1	4,1	3,0	7,1	6,3	6,1	5,8	6,3	4,1	6,0	100,0	4,1	4,1	4,6	5,8
P62918	Rpl8	60S ribosomal protein L8	28	11,03	1,8	1,8	3,9	3,9	4,8	4,8	1,8	1,8	1,1	2,0	1,0	1,9	0,9	0,9	2,0	3,1	2,0	2,0	1,8	1,7	2,9	2,7	2,1	2,0	100,0	3,5	1,6	1,8	2,2
P47955	Rplp1	60S acidic ribosomal protein P1	11,5	4,32	1,8	1,8	5,2	5,1	4,8	4,8	3,5	3,5	6,3	5,1	3,9	3,8	3,7	3,7	4,1	3,1	3,9	4,0	3,6	4,4	2,9	2,7	5,2	5,0	100,0	3,9	4,4	3,8	4,0
Q91YQ5	Rpn1	Dolichyl-diphosphooligosaccharide--protein glycosy	68,5	6,46	3,5	3,6	3,9	2,6	4,8	4,8	5,3	2,7	2,1	4,1	4,8	3,8	3,7	4,7	5,1	4,1	3,9	4,0	0,9	1,7	3,8	3,6	4,1	4,0	100,0	3,9	3,8	4,3	3,0
Q9DBG6	Rpn2	Dolichyl-diphosphooligosaccharide--protein glycosy	69	5,81	0,9	2,7	3,9	5,1	6,0	3,6	3,5	3,5	9,5	6,1	5,8	7,7	6,4	5,6	3,1	2,0	8,9	8,1	4,5	3,5	4,8	2,7	6,2	7,0	100,0	3,7	6,0	5,7	4,8
P14131	Rps16	40S ribosomal protein S16	16,4	10,21	4,4	5,4	2,6	2,6	3,6	2,4	7,9	6,2	9,5	10,2	8,7	9,6	6,4	8,4	8,2	7,2	6,9	7,1	8,1	7,0	5,8	7,2	7,3	5,0	100,0	3,5	8,7	7,4	6,7
G3UYV7	Rps28	40S ribosomal protein S28 (Fragment)	6,3	9,96	3,5	3,6	2,6	5,1	4,8	3,6	4,4	5,3	6,3	6,1	5,8	5,8	3,7	3,7	4,1	3,1	5,9	6,1	7,2	7,0	5,8	5,4	3,1	4,0	100,0	3,9	5,6	4,4	5,4
P62908	Rps3	40S ribosomal protein S3	26,7	9,66	11,5	13,4	5,2	3,9	4,8	7,2	12,3	13,3	7,4	8,2	6,8	9,6	7,4	9,3	11,2	12,3	4,9	8,1	5,4	7,8	13,5	13,6	5,2	6,0	100,0	7,7	9,6	8,9	8,6
P62702	Rps4x	40S ribosomal protein S4, X isoform	29,6	10,15	7,1	4,5	1,3	1,3	2,4	1,2	3,5	5,3	3,2	4,1	4,8	4,8	0,9	0,9	3,1	4,1	3,0	5,1	1,8	0,9	2,9	3,6	5,2	3,0	100,0	3,0	4,3	2,8	2,9
P62082	Rps7	40S ribosomal protein S7	22,1	10,1	7,1	6,3	3,9	7,7	6,0	8,4	7,9	9,8	4,2	6,1	4,8	7,7	7,4	8,4	6,1	8,2	5,9	6,1	5,4	5,2	5,8	8,1	8,3	9,0	100,0	6,6	6,8	7,0	7,0
P14206	Rpsa	40S ribosomal protein SA	32,8	4,87	7,1	8,1	5,2	3,9	6,0	4,8	15,0	15,1	10,5	12,3	9,7	13,4	8,3	8,4	7,2	11,2	11,8	11,1	9,0	9,6	4,8	9,0	6,2	8,0	100,0	5,8	12,6	9,7	7,8
P07758	Serpina1a	Alpha-1-antitrypsin 1-1	46	5,72	7,9	8,1	6,5	7,7	6,0	6,0	1,8	0,9	7,4	6,1	5,8	9,6	3,7	3,7	3,1	3,1	3,9	4,0	4,5	3,5	1,9	1,8	1,0	2,0	100,0	7,0	5,3	3,6	2,5
P22599	Serpina1b	Alpha-1-antitrypsin 1-2	45,9	5,54	8,8	9,9	3,9	5,1	4,8	4,8	1,8	0,9	5,3	5,1	3,9	6,7	1,8	2,8	2,0	1,0	3,0	2,0	2,7	1,7	1,9	1,8	1,0	2,0	100,0	6,2	3,9	2,1	1,9
Q00897	Serpina1d	Alpha-1-antitrypsin 1-4	46	5,44	7,9	9,9	5,2	3,9	3,6	3,6	1,8	0,9	5,3	3,1	2,9	4,8	1,8	2,8	2,0	1,0	2,0	2,0	2,7	1,7	1,9	1,8	1,0	2,0	100,0	5,7	3,1	1,9	1,9
P19324	Serpinh1	Serpin H1	46,5	8,82	15,9	20,6	13,1	11,6	21,6	20,4	22,0	22,2	14,7	13,3	28,0	22,1	21,1	24,2	20,5	15,3	11,8	18,2	19,0	18,3	11,5	16,3	34,2	27,1	100,0	17,2	20,4	18,5	21,1
O70456	Sfn	14-3-3 protein sigma	27,7	4,78	6,2	3,6	1,3	2,6	1,2	2,4	5,3	1,8	5,3	10,2	5,8	6,7	0,9	1,9	4,1	4,1	1,0	4,0	7,2	6,1	3,8	3,6	5,2	4,0	100,0	2,9	5,8	2,7	5,0
Q8VIJ6	Sfpq	Splicing factor, proline- and glutamine-rich	75,4	9,44	4,4	6,3	1,3	2,6	4,8	3,6	4,4	4,4	4,2	3,1	6,8	4,8	4,6	7,4	4,1	4,1	4,9	7,1	2,7	6,1	5,8	3,6	6,2	9,0	100,0	3,8	4,6	5,4	5,6
P62315	Snrpd1	Small nuclear ribonucleoprotein Sm D1	13,3	11,56	3,5	2,7	2,6	3,9	9,6	7,2	3,5	1,8	5,3	3,1	6,8	5,8	3,7	3,7	4,1	3,1	7,9	7,1	3,6	4,4	4,8	2,7	8,3	7,0	100,0	4,9	4,4	4,6	5,1
P11983	Tcp1	T-complex protein 1 subunit alpha	60,4	6,16	2,6	1,8	6,5	6,4	6,0	4,8	3,5	1,8	1,1	1,0	1,0	3,8	5,5	2,8	1,0	2,0	1,0	3,0	1,8	1,7	1,9	1,8	4,1	3,0	100,0	4,7	2,0	2,6	2,4
Q921I1	Tf	Serotransferrin	76,7	7,18	9,7	10,8	18,3	19,3	20,4	18,0	1,8	2,7	11,6	13,3	10,6	18,2	14,7	10,2	9,2	5,1	12,8	16,2	6,3	4,4	7,7	6,3	4,1	5,0	100,0	16,1	9,7	11,4	5,6
P17751	Tpi1	Triosephosphate isomerase	26,7	7,3	15,9	9,9	13,1	10,3	15,6	10,8	16,7	16,9	20,0	24,5	16,4	23,0	23,0	25,1	17,4	19,4	14,8	12,1	19,0	14,8	22,1	23,5	13,5	14,0	100,0	12,6	19,6	18,6	17,8
Q8BSH3	Tpm1	Tropomyosin alpha-1 chain	32,7	4,77	7,1	6,3	6,5	3,9	7,2	9,6	8,8	9,8	1,1	2,0	5,8	1,9	8,3	7,4	15,3	12,3	6,9	4,0	3,6	5,2	9,6	15,4	10,4	11,0	100,0	6,8	4,9	9,0	9,2
P58774	Tpm2	Tropomyosin beta chain	32,8	4,7	2,6	1,8	6,5	3,9	7,2	9,6	6,2	8,0	1,1	2,0	5,8	1,9	6,4	5,6	12,3	9,2	5,9	3,0	3,6	3,5	4,8	10,0	10,4	11,0	100,0	5,3	4,2	7,1	7,2
E9Q5J9	Tpm3	Tropomyosin alpha-3 chain	33,3	4,79	6,2	7,2	7,9	5,1	9,6	13,2	11,4	8,9	1,1	2,0	6,8	1,9	6,4	5,6	15,3	12,3	6,9	4,0	4,5	5,2	9,6	12,7	11,4	12,0	100,0	8,2	5,3	8,4	9,2
D3Z2H9	Tpm3-rs7	Tropomyosin 3, related sequence 7	29	4,81	6,2	7,2	6,5	5,1	9,6	13,2	11,4	8,9	1,1	2,0	5,8	1,9	6,4	5,6	14,3	12,3	6,9	4,0	3,6	3,5	9,6	12,7	10,4	11,0	100,0	8,0	5,2	7,9	8,5
Q9CQN1	Trap1	Heat shock protein 75 kDa, mitochondrial	80,2	6,68	3,5	3,6	5,2	5,1	4,8	4,8	3,5	3,5	5,3	4,1	3,9	3,8	3,7	3,7	6,1	5,1	3,9	4,0	6,3	6,1	5,8	5,4	4,1	4,0	100,0	4,5	4,0	4,4	5,3
P68369	Tuba1a	Tubulin alpha-1A chain	50,1	5,06	29,1	24,2	14,4	12,9	10,8	14,4	33,4	29,3	24,2	17,4	19,3	25,9	32,2	27,9	16,4	20,4	21,7	31,3	33,4	24,4	24,0	19,9	26,9	29,1	100,0	17,6	24,9	25,0	26,3
A0A0A0MQA5	Tuba4a	Tubulin alpha chain (Fragment)	52,9	5,19	16,8	17,9	7,9	7,7	8,4	12,0	22,9	20,4	16,8	13,3	15,4	19,2	24,8	19,5	10,2	9,2	13,8	24,3	25,3	20,0	11,5	8,1	14,5	17,0	100,0	11,8	18,0	17,0	16,1
A2AQ07	Tubb1	Tubulin beta-1 chain	50,4	5,07	7,9	5,4	3,9	5,1	4,8	7,2	13,2	9,8	13,7	11,2	10,6	9,6	14,7	14,9	10,2	10,2	11,8	11,1	21,7	21,8	11,5	8,1	6,2	9,0	100,0	5,7	11,3	12,2	13,1
Q7TMM9	Tubb2a	Tubulin beta-2A chain	49,9	4,89	31,8	28,7	24,9	25,7	18,0	25,2	37,8	35,5	39,9	36,8	38,6	35,5	56,1	56,8	31,7	30,7	35,5	38,4	56,9	56,6	26,9	24,4	39,4	43,1	100,0	25,7	37,4	41,5	41,2
Q9ERD7	Tubb3	Tubulin beta-3 chain	50,4	4,93	21,2	17,9	21,0	21,9	19,2	25,2	22,9	24,0	32,6	30,7	29,0	27,8	37,7	41,9	23,5	22,5	31,5	28,3	44,2	43,5	25,0	23,5	24,9	27,1	100,0	21,1	27,8	30,9	31,4
P68372	Tubb4b	Tubulin beta-4B chain	49,8	4,89	37,1	32,3	27,5	25,7	21,6	28,8	44,9	47,0	53,6	50,1	50,2	47,0	66,2	69,8	38,9	34,8	47,3	49,5	64,1	65,3	38,5	35,3	45,6	49,1	100,0	28,8	48,8	51,1	49,6
P99024	Tubb5	Tubulin beta-5 chain	49,6	4,89	45,0	38,6	36,7	37,3	28,8	36,1	44,9	47,0	57,8	53,2	52,1	50,8	74,5	74,4	40,9	44,0	51,2	50,5	68,6	70,5	41,4	38,9	53,9	55,1	100,0	37,1	51,0	55,9	54,7
Q922F4	Tubb6	Tubulin beta-6 chain	50,1	4,89	15,0	11,7	9,2	10,3	9,6	13,2	18,5	16,9	22,1	21,5	20,3	19,2	27,6	33,5	17,4	16,4	23,6	21,2	29,8	31,3	20,2	14,5	14,5	18,0	100,0	11,5	19,7	23,3	21,4
E9Q5F6	Ubc	Polyubiquitin-C (Fragment)	22,6	7,4	18,5	16,1	7,9	6,4	6,0	6,0	19,4	16,0	8,4	9,2	14,5	12,5	11,9	12,1	16,4	13,0	7,9	9,1	12,6	10,4	15,4	14,5	5,2	6,0	100,0	11,8	13,3	11,8	10,7
Q01853	Vcp	Transitional endoplasmic reticulum ATPase	89,3	5,26	7,9	10,8	19,6	25,7	19,2	22,8	15,0	14,2	18,9	16,4	12,6	13,4	12,9	15,8	14,3	12,3	9,9	15,2	16,2	13,9	17,3	13,6	11,4	13,0	100,0	17,7	15,1	13,4	14,2

Data file S2. Proteins identified by analyzing MB49 Bladder cancer model untreated (CTR, n=3 biol. rep x 2 tech. rep), treated with SNFs-OVA (SNFs-OVA, n=3 biol. rep x 2 tech. rep) and treated with SNFs-CpG (SNFs-CpG, n=3 biol. rep x 2 tech. rep). Peptide spectrum matches (PSMs) per sample an

Annotations					PSMs (MB49 BLADDER CANCER MODEL)																			Av. PSMs		
ID UNIPROT	Gene Name	Protein name	MW [kDa]	calc. pI	CTR1	CTR2	CTR3	CTR4	CTR5	CTR6	SNFs-OVA1	SNFs-OVA2	SNFs-OVA3	SNFs-OVA4	SNFs-OVA5	SNFs-OVA6	SFNs-CpG1	SFNs-CpG2	SFNs-CpG3	SFNs-CpG4	SFNs-CpG5	SFNs-CpG6	IF	CTR	SFNs-OVA	SFNs-CpG
P68134	Acta1	Actin, alpha skeletal muscle	42	5,39	90,9	88,1	71,0	76,2	77,0	73,6	72,0	76,9	67,5	61,3	71,4	81,5	112,4	106,6	114,7	107,3	157,7	127,2	100	79,5	71,8	121,0
P60710	Actb	Actin, cytoplasmic 1	41,7	5,48	153,5	161,3	112,3	118,3	121,7	113,8	130,1	113,9	108,6	114,7	92,8	100,0	187,3	178,4	152,2	142,4	222,0	194,3	100	130,1	110,0	179,4
Q8BFZ3	Actbl2	Beta-actin-like protein 2	42	5,49	102,0	96,2	66,5	73,5	67,0	62,5	81,1	69,1	59,7	61,3	53,0	55,7	108,0	105,5	101,1	98,0	132,4	101,5	100	77,9	63,3	107,8
P63268	Actg2	Actin, gamma-enteric smooth muscle	41,9	5,48	74,7	74,1	69,2	74,4	73,7	68,1	62,0	65,2	58,7	55,4	67,3	75,3	111,3	107,7	105,3	101,1	141,3	114,3	100	72,4	64,0	113,5
A1BN54	Actn1	Alpha actinin 1a	102,7	5,48	16,2	18,0	19,8	17,0	16,7	16,7	15,0	16,5	12,7	12,6	15,3	14,4	9,9	9,8	20,8	18,6	15,1	10,0	100	17,4	14,4	14,0
A0A1L1SV25	Actn4	Alpha-actinin-4	107	5,36	15,1	16,0	14,4	15,2	14,5	13,4	14,0	14,6	11,7	11,7	15,3	17,5	9,9	9,8	15,6	15,5	15,1	10,0	100	14,8	14,1	12,7
E9Q616	Ahnak	AHNAK nucleoprotein (desmoyokin)	603,9	6,3	5,0	7,0	15,3	11,7	8,9	7,8	6,0	4,9	3,9	2,9	3,1	5,2	6,6	5,4	5,2	4,1	3,8	2,9	100	9,3	4,3	4,7
P07724	Alb	Albumin	68,6	6,07	39,4	35,1	27,8	26,0	33,5	32,4	27,0	27,3	32,3	26,3	38,7	39,2	45,2	41,3	24,0	23,7	46,7	50,0	100	32,4	31,8	38,5
A6ZI44	Aldoa	Fructose-bisphosphate aldolase	45,1	7,91	17,2	17,0	17,1	16,1	20,1	20,1	9,0	10,7	13,7	13,6	8,2	14,4	4,4	5,4	13,6	14,4	6,3	7,1	100	17,9	11,6	8,5
P10107	Anxa1	Annexin A1	38,7	7,37	19,2	23,0	26,9	25,1	24,6	27,9	25,0	22,4	27,4	25,3	15,3	17,5	8,8	7,6	30,2	28,9	13,9	11,4	100	24,5	22,1	16,8
P07356	Anxa2	Annexin A2	38,7	7,69	38,4	37,1	44,9	39,4	35,7	34,6	28,0	38,0	42,1	40,8	28,5	30,9	13,2	15,2	31,3	26,8	15,1	8,6	100	38,4	34,7	18,4
O35639	Anxa3	Annexin A3	36,4	5,76	8,1	9,0	14,4	14,3	14,5	14,5	9,0	7,8	10,8	11,7	3,1	4,1	3,3	3,3	11,5	11,4	5,0	2,9	100	12,5	7,7	6,2
P97429	Anxa4	Annexin A4	35,9	5,57	7,1	9,0	12,6	12,6	12,3	12,3	7,0	7,8	9,8	9,7	3,1	2,1	4,4	4,4	7,3	7,2	5,0	2,9	100	11,0	6,6	5,2
P48036	Anxa5	Annexin A5	35,7	4,96	15,1	15,0	21,6	25,1	29,0	29,0	21,0	19,5	25,4	23,3	18,3	17,5	25,3	23,9	21,9	19,6	31,5	31,4	100	22,5	20,9	25,6
P14824	Anxa6	Annexin A6	75,8	5,5	1,0	5,0	3,6	5,4	3,3	5,6	4,0	3,9	5,9	4,9	7,1	7,2	9,9	10,9	7,3	7,2	13,9	15,7	100	4,0	5,5	10,8
Q00623	Apoa1	Apolipoprotein A-I	30,6	5,73	2,0	2,0	3,6	4,5	6,7	5,6	2,0	1,9	2,9	2,9	3,1	2,1	2,2	2,2	2,1	2,1	2,5	2,9	100	4,1	2,5	2,3
P61205	Arf3	ADP-ribosylation factor 3	20,6	7,43	7,1	6,0	3,6	1,8	2,2	2,2	10,0	11,7	5,9	6,8	4,1	3,1	8,8	9,8	2,1	3,1	2,5	2,9	100	3,8	6,9	4,9
Q99PT1	Arhgdia	Rho GDP-dissociation inhibitor 1	23,4	5,2	6,1	4,0	3,6	4,5	3,3	4,5	4,0	1,9	2,9	3,9	4,1	5,2	5,5	5,4	3,1	4,1	1,3	2,9	100	4,3	3,7	3,7

Data file S3. Differentially expressed proteins (DEPs) identified by LDA (Prob<0.05) by comparing PSMs from B16/F10 melanoma model untreated (CTR, n=6), treated with SNFs-OVA (SNFs-OVA, n=6), tre (SNFs-OVA-CpG, n=6). Average and normalized (%) PSMs are shown. Pairwise comparisons (CTR vs SFNs-OVA; CTR vs SFNs-CpG; CTR vs SFNs-OVA-CpG) by DAve index are reported; positive DAve values SFNs treatments), while negative DAve values (in blue) indicate proteins up-regulated following SFNs treatments (down-regulated in CTR).

Annotations					LDA		Av. PSMs (B16/F10 MELANOMA MODEL)				Dave index		
ID UNIPROT	Gene name	Description	MW [kDa]	calc. pI	F Ratio	Prob>F	CTR	SFNs-OVA	SFNs-CpG	SFNs-OVA-CpG	CTR vs SFNs-OVA	CTR vs SFNs-CpG	CTR vs SFNs-OVA-CpG
A0A0R4J083	Acadl	Long-chain specific acyl-CoA dehydrogenase, mitochondrial	47,9	8,15	4	2,5E-02	0,0	0,0	0,7	0,0		-2,00	
Q99KI0	Aco2	Aconitate hydratase, mitochondrial	85,4	7,93	5	8,0E-03	4,7	0,7	1,3	1,6	1,50	1,16	1,00
P68134	Acta1	Actin, alpha skeletal muscle	42	5,39	19	5,0E-06	42,6	64,1	71,9	65,5	-0,40	-0,51	-0,42
V9GXQ2	Actb	Predicted gene 17087	41,7	7,37	11	1,9E-04	78,4	101,0	105,8	99,6	-0,25	-0,30	-0,24
P63268	Actg2	Actin, gamma-enteric smooth muscle	41,9	5,48	15	2,8E-05	38,4	58,8	62,4	61,4	-0,42	-0,48	-0,46
Q8R5C5	Actr1b	Beta-centractin	42,3	6,4	3	3,7E-02	0,6	1,9	1,0	1,3	-1,04	-0,47	-0,71
Q641P0	Actr3b	Actin-related protein 3B	47,5	6,02	8	1,1E-03	0,0	1,6	2,1	1,2	-2,00	-2,00	-2,00
Q640N1	Aebp1	Adipocyte enhancer-binding protein 1	128,3	5,08	4	2,9E-02	2,1	0,0	0,0	0,5	2,00	2,00	1,19
P50247	Ahcy	Adenosylhomocysteinase	47,7	6,54	3	4,1E-02	0,0	0,7	0,6	1,2	-2,00	-2,00	-2,00
A0A338P7H5	Ahsg	Alpha-2-HS-glycoprotein	32,2	6,95	6	6,3E-03	1,4	1,3	0,3	0,0		1,25	2,00
P07724	Alb	Albumin	68,6	6,07	23	1,2E-06	60,7	34,3	34,6	23,0	0,56	0,55	0,90
Q9Z110	Aldh18a1	Delta-1-pyrroline-5-carboxylate synthase	87,2	7,55	6	6,2E-03	2,1	0,6	0,5	1,1	1,12	1,26	0,66
P47738	Aldh2	Aldehyde dehydrogenase, mitochondrial	56,5	7,62	6	4,3E-03	4,2	6,1	9,9	7,9	-0,35	-0,80	-0,60
G5E8J2	Ank1	Ankyrin-1	202,4	6,65	10	3,2E-04	1,7	0,0	0,0	0,0	2,00	2,00	2,00
Q9CQM6	Ankrd61	Ankyrin repeat domain-containing protein 61	46,6	8,85	5	9,6E-03	0,6	0,0	0,0	0,0	2,00	2,00	2,00
P07356	Anxa2	Annexin A2	38,7	7,69	6	3,8E-03	4,3	6,3	7,3	3,3	-0,38	-0,52	0,26
P59999	Arpc4	Actin-related protein 2/3 complex subunit 4	19,7	8,43	5	1,3E-02	1,8	1,2	4,2	3,5	0,42	-0,79	-0,62
E9QNX7	Atp4a	Sodium/potassium-transporting ATPase subunit alpha	114	5,81	3	4,1E-02	0,0	0,5	0,5	0,0	-2,00	-2,00	
Q9DCX2	Atp5pd	ATP synthase subunit d, mitochondrial	18,7	5,69	5	7,2E-03	4,0	1,4	1,8	1,3	0,94	0,76	1,02
P62814	Atp6v1b2	V-type proton ATPase subunit B, brain isoform	56,5	5,81	5	8,5E-03	3,4	0,2	1,6	1,6	1,81	0,71	0,74
Q923D2	Blvrb	Flavin reductase (NADPH)	22,2	7,01	16	1,5E-05	2,1	0,0	0,3	0,5	2,00	1,46	1,28
Q64152	Btf3	Transcription factor BTF3	22	9,52	5	1,3E-02	1,6	0,4	0,0	1,3	1,28	2,00	0,22
P01027	C3	Complement C3	186,4	6,73	13	5,8E-05	18,0	2,6	5,5	1,3	1,49	1,07	1,74
P00920	Ca2	Carbonic anhydrase 2	29	7,01	5	1,4E-02	1,5	0,0	0,0	0,0	2,00	2,00	2,00
P47753	Capza1	F-actin-capping protein subunit alpha-1	32,9	5,55	3	4,1E-02	0,2	1,2	1,5	1,4	-1,41	-1,52	-1,51
P47754	Capza2	F-actin-capping protein subunit alpha-2	32,9	5,85	4	3,2E-02	0,2	1,2	1,8	1,7	-1,41	-1,59	-1,59
P80314	Cct2	T-complex protein 1 subunit beta	57,4	6,4	8	1,4E-03	13,3	8,0	6,8	6,9	0,50	0,66	0,64
P80318	Cct3	T-complex protein 1 subunit gamma	60,6	6,7	8	9,7E-04	5,1	4,4	2,5	2,9		0,69	0,56
P80315	Cct4	T-complex protein 1 subunit delta	58	8,02	6	3,1E-03	7,8	1,2	1,1	1,3	1,47	1,49	1,43
P80316	Cct5	T-complex protein 1 subunit epsilon	59,6	6,02	17	8,2E-06	10,6	2,5	4,1	4,1	1,25	0,89	0,89
Q61390	Cct6b	T-complex protein 1 subunit zeta-2	58,1	7,36	9	6,0E-04	2,1	0,0	0,0	0,0	2,00	2,00	2,00
P97377	Cdk2	Cyclin-dependent kinase 2	39	8,54	3	4,9E-02	0,3	2,2	1,8	1,7	-1,52	-1,42	-1,40
P23953	Ces1c	Carboxylesterase 1C	61	5,06	11	1,5E-04	8,4	2,6	2,5	2,2	1,05	1,09	1,18
O35744	Chil3	Chitinase-like protein 3	44,4	5,69	6	4,2E-03	0,0	0,0	1,2	0,3		-2,00	-2,00
Q8BMK4	Ckap4	Cytoskeleton-associated protein 4	63,7	5,64	9	6,5E-04	0,0	0,0	1,1	0,3		-2,00	-2,00
Q04447	Ckb	Creatine kinase B-type	42,7	5,67	9	6,6E-04	20,1	24,8	17,4	18,3	-0,21		
Q68FD5	Cltc	Clathrin heavy chain 1	191,4	5,69	32	8,7E-08	9,3	21,0	17,0	17,3	-0,77	-0,59	-0,60
Q06890	Clu	Clusterin	51,6	5,67	5	9,0E-03	0,0	0,0	1,5	0,0		-2,00	
P11087	Col1a1	Collagen alpha-1(I) chain	137,9	5,85	3	4,6E-02	2,8	9,2	8,9	6,9	-1,06	-1,04	-0,83
E9Q6A6	Col6a6	Collagen alpha-6(VI) chain	246,3	6,9	6	4,7E-03	2,0	0,0	0,2	0,0	2,00	1,69	2,00
Q8VBV7	Cops8	COP9 signalosome complex subunit 8	23,2	5,2	5	6,5E-03	1,1	0,0	0,0	0,2	2,00	2,00	1,45
O89053	Coro1a	Coronin-1A	51	6,48	10	2,7E-04	0,0	0,2	3,3	1,5	-2,00	-2,00	-2,00
P19783	Cox4i1	Cytochrome c oxidase subunit 4 isoform 1, mitochondrial	19,5	9,23	4	1,7E-02	1,5	0,0	0,7	0,6	2,00	0,76	0,78
Q8CJ40	Crocc	Rootletin	226,8	5,55	8	8,1E-04	0,2	0,0	1,0	0,0	2,00	-1,31	2,00
P97315	Csrp1	Cysteine and glycine-rich protein 1	20,6	8,57	4	2,0E-02	0,0	0,5	0,5	1,5	-2,00	-2,00	-2,00
Q9JLM8	Dclk1	Serine/threonine-protein kinase DCLK1	84,1	8,87	4	1,6E-02	0,0	0,5	1,3	0,5	-2,00	-2,00	-2,00
P28654	Dcn	Decorin	39,8	8,68	7	2,5E-03	0,5	2,3	2,5	2,5	-1,35	-1,39	-1,39
G3UZN1	Ddt	D-dopachrome decarboxylase	8,2	7,34	4	1,8E-02	0,0	0,3	1,0	1,1	-2,00	-2,00	-2,00
Q501J6	Ddx17	Probable ATP-dependent RNA helicase DDX17	72,4	8,59	5	1,2E-02	3,1	2,9	2,7	4,5		0,16	-0,37
Q9Z1N5	Ddx39b	Spliceosome RNA helicase Ddx39b	49	5,67	8	9,1E-04	0,8	2,9	2,1	2,5	-1,13	-0,90	-1,04
Q62167	Ddx3x	ATP-dependent RNA helicase DDX3X	73,1	7,18	10	3,5E-04	4,6	7,7	4,6	9,0	-0,50		-0,64
Q62095	Ddx3y	ATP-dependent RNA helicase DDX3Y	73,4	7,53	4	3,1E-02	3,4	4,9	2,7	6,1	-0,35	0,25	-0,55
E9PZQ1	Ddx60	DExD/H box helicase 60	197,5	7,55	3	3,6E-02	1,3	1,3	0,3	2,8		1,17	-0,75
Q99LT0	Dpy30	Protein dpy-30 homolog	11,2	4,88	3	3,7E-02	0,0	1,1	0,2	0,5	-2,00	-2,00	-2,00
E9Q557	Dsp	Desmoplakin	332,7	6,8	9	5,3E-04	2,2	0,2	0,0	0,0	1,72	2,00	2,00
P10126	Eef1a1	Elongation factor 1-alpha 1	50,1	9,01	3	3,7E-02	21,8	34,3	24,8	22,7	-0,44		
Q6ZWX6	Eif2s1	Eukaryotic translation initiation factor 2 subunit 1	36,1	5,08	8	1,3E-03	0,0	0,3	1,3	1,9	-2,00	-2,00	-2,00
Q8JZQ9	Eif3b	Eukaryotic translation initiation factor 3 subunit B	91,3	5,02	5	8,8E-03	2,0	0,8	1,8	0,9	0,86		0,71
P60229	Eif3e	Eukaryotic translation initiation factor 3 subunit E	52,2	6,04	10	2,6E-04	1,4	0,2	0,0	0,0	1,61	2,00	2,00
Q8BGD9	Eif4b	Eukaryotic translation initiation factor 4B	68,8	5,67	4	1,5E-02	0,2	1,8	1,3	2,2	-1,69	-1,58	-1,74
P70372	Elavl1	ELAV-like protein 1	36,1	9,04	5	8,9E-03	0,2	1,6	1,9	2,0	-1,66	-1,71	-1,73
Q99K41	Emilin1	EMILIN-1	107,5	5,3	4	1,8E-02	1,0	0,0	0,0	0,0	2,00	2,00	2,00
P17182	Eno1	Alpha-enolase	47,1	6,8	4	2,9E-02	49,0	43,3	31,9	42,2		0,42	0,15
P21550	Eno3	Beta-enolase	47	7,18	4	3,1E-02	11,0	9,0	4,1	7,9	0,20	0,92	0,33
P10404	env	MLV-related proviral Env polyprotein	69,6	7,96	4	2,1E-02	2,0	3,5	3,5	2,8	-0,55	-0,53	-0,33
Q8R180	Ero1a	ERO1-like protein alpha	54,1	6,54	4	1,6E-02	1,6	0,5	0,0	0,6	1,13	2,00	0,94
P26040	Ezr	Ezrin	69,4	6,1	17	9,4E-06	1,6	3,7	6,2	5,8	-0,78	-1,18	-1,13
P19096	Fasn	Fatty acid synthase	272,3	6,58	5	8,7E-03	17,4	26,3	19,9	21,7	-0,41		-0,22
Q61554	Fbn1	Fibrillin-1	312,1	4,92	4	2,5E-02	0,0	0,0	0,7	0,0		-2,00	
Q8K0E8	Fgb	Fibrinogen beta chain	54,7	7,08	4	2,3E-02	9,1	1,1	22,1	3,3	1,57	-0,83	0,94
Q8VCM7	Fgg	Fibrinogen gamma chain	49,4	5,86	4	2,1E-02	14,9	5,2	16,5	4,7	0,96		1,04
A0A0A6YWE2	Flg	Filaggrin	27,3	10,92	7	2,1E-03	6,2	0,5	0,0	0,0	1,71	2,00	2,00
Q8BTM8	Flna	Filamin-A	281	6,04	10	3,0E-04	10,2	1,9	2,8	1,5	1,37	1,13	1,50
A0A087WS56	Fn1	Fibronectin	249,4	5,82	4	2,2E-02	19,7	5,4	25,3	6,0	1,14	-0,25	1,07
A3KG36	G6pdx	Glucose-6-phosphate 1-dehydrogenase (Fragment)	45,2	6,27	4	2,2E-02	0,0	0,0	0,9	1,4		-2,00	-2,00
Q8BHN3	Ganab	Neutral alpha-glucosidase AB	106,8	6,06	4	2,9E-02	0,0	1,1	2,6	2,6	-2,00	-2,00	-2,00
V9GX06	Gapdh	Predicted gene 11214 (Fragment)	19,9	7,42	7	2,6E-03	7,0	16,1	17,2	19,5	-0,79	-0,85	-0,94
P21614	Gc	Vitamin D-binding protein	53,6	5,5	5	1,1E-02	13,2	3,3	4,4	1,6	1,21	0,99	1,57
A0A1D5RLD8	Gm10358	Glyceraldehyde-3-phosphate dehydrogenase	35,8	8,25	16	1,4E-05	53,2	85,3	79,1	72,9	-0,46	-0,39	-0,31
E9PZF0	Gm20390	Nucleoside diphosphate kinase	30,2	8,72	4	2,0E-02	1,8	6,4	4,1	5,0	-1,13	-0,79	-0,94
E9PY39	Gm20431	Predicted gene 20431	42,1	6,76	6	6,0E-03	0,0	0,6	0,8	1,6	-2,00	-2,00	-2,00
P05201	Got1	Aspartate aminotransferase, cytoplasmic	46,2	7,14	3	3,5E-02	1,1	4,1	4,7	5,3	-1,17	-1,26	-1,33
P13020	Gsn	Gelsolin	85,9	6,18	6	3,1E-03	4,1	2,2	1,0	0,9	0,61	1,22	1,28
K3W4S6	Gyg	Glycogenin	41,9	6,02	4	1,8E-02	1,1	0,2	0,0	0,2	1,45	2,00	1,45
P10922	H1-0	Histone H1.0	20,8	10,9	4	3,1E-02	0,7	0,7	0,0	0,0		2,00	2,00
P43277	H1-3	Histone H1.3	22,1	11,03	8	1,0E-03	4,6	11,2	8,6	7,2	-0,83	-0,60	-0,44
P43274	H1-4	Histone H1.4	22	11,11	3	4,9E-02	4,8	9,9	7,2	7,0	-0,69	-0,40	-0,38
Q3THW5	H2az2	Histone H2A.V	13,5	10,58	6	3,9E-03	9,5	13,3	14,5	15,3	-0,33	-0,42	-0,47
Q61425	Hadh	Hydroxyacyl-coenzyme A dehydrogenase, mitochondrial	34,4	8,65	8	1,2E-03	0,0	0,8	1,8	1,4	-2,00	-2,00	-2,00
Q9QUP5	Hapln1	Hyaluronan and proteoglycan link protein 1	40,5	7,8	81	2,4E-11	2,3	0,3	0,0	0,0	1,53	2,00	2,00
Q91VB8	Hba-a1	Alpha globin 1	15,1	8,22	11	2,0E-04	87,5	25,4	22,5	21,7	1,10	1,18	1,21
P02089	Hbb-b2	Hemoglobin subunit beta-2	15,9	8,05	8	1,2E-03	18,6	7,0	7,6	9,3	0,90	0,84	0,67
A8DUK4	Hbb-bs	Beta-globin	15,7	7,69	14	3,0E-05	201,5	26,8	28,9	30,9	1,53	1,50	1,47
P70349	Hint1	Histidine triad nucleotide-binding protein 1	13,8	6,87	5	8,2E-03	0,4	2,2	1,1	0,7	-1,34	-0,88	-0,51
A0A384DV79	Hmga1	High mobility group protein HMG-I/HMG-Y	12	10,43	10	3,2E-04	1,7	0,0	0,0	0,0	2,00	2,00	2,00
P63158	Hmgb1	High mobility group protein B1	24,9	5,74	5	6,5E-03	0,0	1,5	0,3	0,0	-2,00	-2,00	
Q9Z2X1	Hnrnpf	Heterogeneous nuclear ribonucleoprotein F	45,7	5,49	3	3,8E-02	1,0	3,2	3,4	2,9	-1,09	-1,13	-1,00
Q8C2Q7	Hnrnph1	Heterogeneous nuclear ribonucleoprotein H	51,2	6,8	4	2,8E-02	0,6	3,0	2,6	2,7	-1,32	-1,25	-1,27
P61979	Hnrnpk	Heterogeneous nuclear ribonucleoprotein K	50,9	5,54	5	1,0E-02	6,5	10,4	8,0	9,1	-0,46	-0,21	-0,33
P07901	Hsp90aa1	Heat shock protein HSP 90-alpha	84,7	5,01	10	3,7E-04	18,1	32,6	23,7	28,4	-0,58	-0,27	-0,44
P11499	Hsp90ab1	Heat shock protein HSP 90-beta	83,2	5,03	7	1,9E-03	32,2	44,9	35,3	38,0	-0,33		-0,17
P08113	Hsp90b1	Endoplasmin	92,4	4,82	7	1,6E-03	15,0	20,1	13,2	15,6	-0,29		
P63017	Hspa8	Heat shock cognate 71 kDa protein	70,8	5,52	4	2,9E-02	31,5	42,4	39,0	42,7	-0,30	-0,21	-0,30
P03975	Iap	IgE-binding protein	62,7	9,31	4	1,6E-02	14,5	17,4	9,2	12,2	-0,18	0,45	0,18
Q91VA7	Idh3b	Isocitrate dehydrogenase [NAD] subunit, mitochondrial	42,2	8,6	5	1,3E-02	1,5	0,0	0,3	0,5	2,00	1,25	1,03
A0A0A6YXW6	Igha	Immunoglobulin heavy constant alpha (Fragment)	42	4,94	11	1,7E-04	3,5	1,0	0,0	0,0	1,13	2,00	2,00
A0A0A6YVP0	Ighg2b	Immunoglobulin heavy constant gamma 2B (Fragment)	44,3	6,52	8	7,9E-04	10,7	5,1	3,2	2,2	0,72	1,07	1,32
A0A0A6YY53	Ighg2c	Immunoglobulin heavy constant gamma 2C (Fragment)	36,5	8,02	9	6,3E-04	8,3	1,3	0,3	0,0	1,45	1,84	2,00
P01872	Ighm	Immunoglobulin heavy constant mu	49,9	7,01	35	3,8E-08	8,0	1,3	1,3	0,0	1,44	1,43	2,00
A0A075B5Y4	Ighv1-81	Immunoglobulin heavy variable 1-81 (Fragment)	13	8,79	7	1,5E-03	1,3	0,0	0,0	0,0	2,00	2,00	2,00
A0A0B4J1I9	Igkv4-55	Immunoglobulin kappa variable 4-55 (Fragment)	12,7	6,48	6	5,7E-03	3,3	1,0	0,8	0,0	1,07	1,24	2,00
Q9JKF1	Iqgap1	Ras GTPase-activating-like protein IQGAP1	188,6	6,48	3	3,7E-02	2,5	3,6	7,1	5,7	-0,36	-0,94	-0,76
P01592	Jchain	Immunoglobulin J chain	18	4,89	9	7,4E-04	1,5	0,0	0,0	0,0	2,00	2,00	2,00
Q02257	Jup	Junction plakoglobin	81,7	6,14	4	3,3E-02	0,6	1,0	0,0	0,0	-0,50	2,00	2,00
P04104	Krt1	Keratin, type II cytoskeletal 1	65,6	8,15	9	6,3E-04	6,0	7,0	1,0	0,4	-0,15	1,43	1,73
A2A513	Krt10	Keratin, type I cytoskeletal 10	57	5,07	8	9,2E-04	7,1	9,5	2,0	3,4	-0,28	1,12	0,71
Q61781	Krt14	Keratin, type I cytoskeletal 14	52,8	5,17	23	1,2E-06	31,6	13,8	3,9	5,3	0,78	1,56	1,43
Q61414	Krt15	Keratin, type I cytoskeletal 15	49,1	4,86	7	2,6E-03	11,0	9,1	2,0	4,6	0,20	1,38	0,83
Q9Z2K1	Krt16	Keratin, type I cytoskeletal 16	51,6	5,2	12	1,0E-04	14,9	5,8	0,5	3,1	0,88	1,87	1,31
Q9QWL7	Krt17	Keratin, type I cytoskeletal 17	48,1	5,06	15	2,1E-05	16,8	9,7	2,7	3,8	0,54	1,45	1,26
Q6IFX2	Krt42	Keratin, type I cytoskeletal 42	50,1	5,16	9	4,6E-04	8,9	5,8	1,5	2,7	0,42	1,42	1,07
Q922U2	Krt5	Keratin, type II cytoskeletal 5	61,7	7,75	4	1,9E-02	19,6	18,4	5,3	4,7		1,14	1,23
P50446	Krt6a	Keratin, type II cytoskeletal 6A	59,3	7,94	7	2,4E-03	23,9	12,2	1,8	2,5	0,65	1,72	1,62
Q3UV11	Krt6b	Keratin, type II cytoskeletal 6B	59,5	8,15	7	2,6E-03	24,2	12,2	1,8	2,5	0,66	1,72	1,62
Q9R0H5	Krt71	Keratin, type II cytoskeletal 71	57,3	6,99	7	2,4E-03	2,9	3,0	1,2	0,3		0,85	1,62
Q6NXH9	Krt73	Keratin, type II cytoskeletal 73	58,9	8,09	5	6,7E-03	1,2	2,8	0,2	0,3	-0,81	1,51	1,19
Q6IFZ6	Krt77	Keratin, type II cytoskeletal 1b	61,3	8,02	4	2,8E-02	15,3	13,1	5,0	6,9	0,16	1,01	0,76
Q61233	Lcp1	Plastin-2	70,1	5,33	5	9,0E-03	0,4	0,0	3,3	4,4	2,00	-1,56	-1,66
A0A1B0GSX0	Ldha	L-lactate dehydrogenase	39,7	8,35	18	7,9E-06	17,2	25,0	14,7	13,2	-0,37	0,16	0,26
Q9CRB1	Lgals7	Galectin	15,2	6,89	8	9,3E-04	7,0	5,1	2,0	0,5	0,32	1,11	1,74
P48678	Lmna	Prelamin-A/C	74,2	6,98	4	2,6E-02	9,9	10,2	6,0	8,8		0,49	
P51885	Lum	Lumican	38,2	6,43	8	1,4E-03	0,0	0,5	1,4	1,2	-2,00	-2,00	-2,00
P26645	Marcks	Myristoylated alanine-rich C-kinase substrate	29,6	4,34	4	1,6E-02	0,0	0,3	0,6	0,0	-2,00	-2,00	
Q80UM7	Mogs	Mannosyl-oligosaccharide glucosidase	91,8	9	4	2,6E-02	1,3	0,6	0,0	0,2	0,68	2,00	1,53
P26041	Msn	Moesin	67,7	6,6	5	7,3E-03	6,0	8,9	11,9	13,0	-0,39	-0,67	-0,75
P00405	Mtco2	Cytochrome c oxidase subunit 2	26	4,73	6	6,4E-03	4,7	6,4	7,3	8,6	-0,31	-0,44	-0,59
A0A0N4SW94	Myadm	Myeloid-associated differentiation marker (Fragment)	8,6	8,38	10	3,2E-04	1,7	0,0	0,0	0,0	2,00	2,00	2,00
A0A2R8VHF9	Myh11	Myosin-11	223,2	5,5	4	2,5E-02	2,4	0,3	2,5	1,6	1,55		0,39
Q8BSH9	Nap1l1	Nucleosome assembly protein 1-like 1	44,6	4,56	5	8,5E-03	1,3	2,8	0,8	2,4	-0,74	0,44	-0,60
E9PWG6	Ncapg	Non-SMC condensin I complex, subunit G	112,8	5,55	3	4,5E-02	0,2	0,2	0,0	0,6		2,00	-1,22
Q62425	Ndufa4	Cytochrome c oxidase subunit NDUFA4	9,3	9,52	10	2,4E-04	0,0	1,2	1,1	1,9	-2,00	-2,00	-2,00
O08692	Ngp	Neutrophilic granule protein	19,3	5,31	4	2,2E-02	0,0	0,0	4,0	1,8		-2,00	-2,00
Q99K48	Nono	Non-POU domain-containing octamer-binding protein	54,5	8,95	4	3,0E-02	3,0	5,8	8,8	9,0	-0,64	-0,99	-1,01
P29341	Pabpc1	Polyadenylate-binding protein 1	70,6	9,5	4	2,7E-02	1,5	3,6	3,7	4,2	-0,81	-0,85	-0,95
P60335	Pcbp1	Poly(rC)-binding protein 1	37,5	7,09	6	3,8E-03	0,4	2,7	0,8	2,0	-1,44	-0,61	-1,29
P17918	Pcna	Proliferating cell nuclear antigen	28,8	4,77	3	3,8E-02	0,2	0,2	1,1	0,9		-1,53	-1,43
A0A0R4J0Z1	Pdia4	Protein disulfide-isomerase A4	72,3	5,22	5	8,4E-03	2,1	0,0	0,7	0,2	2,00	1,04	1,73
P12382	Pfkl	ATP-dependent 6-phosphofructokinase, liver type	85,3	7,17	6	6,2E-03	1,0	3,2	3,0	1,1	-1,02	-0,96	
P62962	Pfn1	Profilin-1	14,9	8,28	10	3,9E-04	2,9	7,4	6,7	8,3	-0,89	-0,81	-0,97
Q9DBJ1	Pgam1	Phosphoglycerate mutase 1	28,8	7,18	4	2,8E-02	6,1	12,3	14,9	15,8	-0,67	-0,84	-0,88
Q9D0F9	Pgm1	Phosphoglucomutase-1	61,4	6,57	7	2,2E-03	3,0	0,5	0,5	1,2	1,44	1,45	0,88
P67778	Phb	Prohibitin	29,8	5,76	4	1,6E-02	9,5	5,6	5,3	4,7	0,51	0,57	0,68
O35129	Phb2	Prohibitin-2	33,3	9,83	3	4,7E-02	12,4	15,4	10,2	12,3	-0,21	0,19	
Q9QXS1	Plec	Plectin	533,9	5,96	7	1,8E-03	3,3	0,6	1,2	1,0	1,37	0,94	1,11
P20918	Plg	Plasminogen	90,7	6,6	5	1,1E-02	3,9	0,5	1,7	0,3	1,53	0,80	1,70
Q9DBG5	Plin3	Perilipin-3	47,2	5,62	4	2,6E-02	0,0	0,0	0,5	1,5		-2,00	-2,00
P62137	Ppp1ca	Serine/threonine-protein phosphatase PP1-alpha catalytic subunit	37,5	6,33	3	4,2E-02	0,0	0,8	0,0	0,0	-2,00		
P62715	Ppp2cb	Serine/threonine-protein phosphatase 2A catalytic subunit beta isoform	35,6	5,43	7	2,4E-03	0,0	0,0	1,5	1,6		-2,00	-2,00
F6RV17	Ppp2r2d	Serine/threonine-protein phosphatase 2A 55 kDa regulatory subunit B	33,4	6,65	6	3,5E-03	0,2	1,3	1,5	0,3	-1,59	-1,63	-0,71
Q61171	Prdx2	Peroxiredoxin-2	21,8	5,41	3	4,0E-02	4,7	2,9	4,5	3,0	0,48		0,45
P99029	Prdx5	Peroxiredoxin-5, mitochondrial	21,9	8,85	7	2,1E-03	0,0	0,0	2,2	1,2		-2,00	-2,00
Q99PV0	Prpf8	Pre-mRNA-processing-splicing factor 8	273,4	8,84	9	6,5E-04	0,0	0,5	2,1	0,9	-2,00	-2,00	-2,00
Q9Z1R9	Prss1	Protease, serine 1 (trypsin 1)	26,1	4,94	4	3,0E-02	1,4	3,8	2,2	1,5	-0,91	-0,41	
Q3U6K9	Psat1	Phosphoserine aminotransferase	40,2	7,65	4	1,9E-02	0,0	1,1	0,0	0,6	-2,00		-2,00
O35955	Psmb10	Proteasome subunit beta type-10	29	6,87	8	9,9E-04	0,0	0,0	0,0	0,8			-2,00
Q9R1P3	Psmb2	Proteasome subunit beta type-2	22,9	7,02	6	5,5E-03	0,0	0,8	0,0	0,2	-2,00		-2,00
P99026	Psmb4	Proteasome subunit beta type-4	29,1	5,64	4	2,8E-02	1,2	0,2	0,0	0,2	1,57	2,00	1,57
P70195	Psmb7	Proteasome subunit beta type-7	29,9	7,99	6	4,7E-03	2,8	0,3	0,0	0,6	1,60	2,00	1,27
O88685	Psmc3	26S proteasome regulatory subunit 6A	49,5	5,19	3	4,4E-02	0,0	0,9	0,5	0,0	-2,00	-2,00	
P14685	Psmd3	26S proteasome non-ATPase regulatory subunit 3	60,7	8,44	5	8,4E-03	0,4	1,5	1,5	1,9	-1,22	-1,22	-1,38
Q61838	Pzp	Pregnancy zone protein	165,7	6,68	20	3,2E-06	11,1	4,2	4,2	1,4	0,91	0,91	1,54
P61027	Rab10	Ras-related protein Rab-10	22,5	8,38	7	1,7E-03	0,2	0,8	2,0	1,2	-1,15	-1,60	-1,40
P51150	Rab7a	Ras-related protein Rab-7a	23,5	6,7	5	1,3E-02	0,9	2,6	4,7	5,6	-0,98	-1,36	-1,46
P68040	Rack1	Receptor of activated protein C kinase 1	35,1	7,69	6	3,3E-03	3,6	6,0	6,1	7,7	-0,51	-0,52	-0,74
P34022	Ranbp1	Ran-specific GTPase-activating protein	23,6	5,22	6	5,6E-03	0,0	1,5	0,5	1,3	-2,00	-2,00	-2,00
Q99JI6	Rap1b	Ras-related protein Rap-1b	20,8	5,78	9	5,9E-04	0,5	1,3	2,3	1,8	-0,97	-1,35	-1,18
O89086	Rbm3	RNA-binding protein 3	16,6	7,5	12	8,4E-05	1,7	3,9	5,2	5,4	-0,80	-1,04	-1,06
Q9CXW4	Rpl11	60S ribosomal protein L11	20,2	9,6	5	1,0E-02	2,3	3,0	2,0	1,9	-0,28	0,15	0,18
P35979	Rpl12	60S ribosomal protein L12	17,8	9,42	4	1,9E-02	0,2	2,5	1,3	1,6	-1,70	-1,47	-1,56
Q6ZWZ4	Rpl36	60S ribosomal protein L36	12,2	11,59	4	2,0E-02	0,0	1,0	0,2	0,2	-2,00	-2,00	-2,00
P47911	Rpl6	60S ribosomal protein L6	33,5	10,7	9	6,9E-04	2,5	9,9	9,5	6,9	-1,19	-1,16	-0,93
P62918	Rpl8	60S ribosomal protein L8	28	11,03	6	5,2E-03	3,5	1,6	1,8	2,2	0,75	0,63	0,46
P14869	Rplp0	60S acidic ribosomal protein P0	34,2	6,25	3	4,2E-02	1,2	3,7	3,1	3,8	-1,02	-0,90	-1,06
P63325	Rps10	40S ribosomal protein S10	18,9	10,15	9	6,1E-04	1,2	4,3	2,4	3,3	-1,13	-0,69	-0,94
P62264	Rps14	40S ribosomal protein S14	16,3	10,05	6	3,3E-03	1,2	4,1	2,7	3,1	-1,11	-0,77	-0,89
P62843	Rps15	40S ribosomal protein S15	17	10,39	3	4,3E-02	1,8	1,8	3,6	5,6		-0,64	-1,01
P14131	Rps16	40S ribosomal protein S16	16,4	10,21	21	1,9E-06	3,5	8,7	7,4	6,7	-0,85	-0,71	-0,63
Q9CZX8	Rps19	40S ribosomal protein S19	19,4	10,45	4	3,2E-02	1,9	4,6	2,9	2,9	-0,84	-0,44	-0,42
P25444	Rps2	40S ribosomal protein S2	31,2	10,24	6	4,5E-03	0,8	5,2	4,4	4,0	-1,50	-1,42	-1,37
P62267	Rps23	40S ribosomal protein S23	15,8	10,49	4	3,1E-02	0,7	2,1	0,5	0,6	-0,95	0,38	0,15
A0A1L1SQA8	Rps25	40S ribosomal protein S25	10,3	9,99	5	6,6E-03	0,3	3,9	2,6	3,8	-1,71	-1,58	-1,70
Q6ZWN5	Rps9	40S ribosomal protein S9	22,6	10,65	4	2,0E-02	1,5	4,4	3,8	4,9	-0,96	-0,84	-1,05
P14206	Rpsa	40S ribosomal protein SA	32,8	4,87	14	4,3E-05	5,9	12,7	9,7	7,8	-0,74	-0,49	-0,28
A2AVJ7	Rrbp1	Ribosome-binding protein 1	158,3	9,19	9	6,0E-04	2,1	0,0	0,0	0,0	2,00	2,00	2,00
Q99P72	Rtn4	Reticulon-4	126,5	4,54	3	4,4E-02	0,0	0,0	0,8	0,3		-2,00	-2,00
P27005	S100a8	Protein S100-A8	10,3	5,68	6	4,6E-03	0,0	0,0	1,3	0,6		-2,00	-2,00
P31725	S100a9	Protein S100-A9	13	7,17	6	4,0E-03	1,3	2,7	7,5	5,8	-0,67	-1,40	-1,25
Q60710	Samhd1	Deoxynucleoside triphosphate triphosphohydrolase SAMHD1	75,8	7,93	4	3,0E-02	0,0	0,0	1,6	1,2		-2,00	-2,00
Q8K2B3	Sdha	Succinate dehydrogenase [ubiquinone] flavoprotein subunit, mitochondrial	72,5	7,37	7	2,2E-03	0,6	1,9	2,0	2,2	-1,05	-1,06	-1,14
E9Q1S3	Sec23a	Protein transport protein SEC23	82,9	7,46	4	2,2E-02	0,0	0,0	1,0	0,8		-2,00	-2,00
P07758	Serpina1a	Alpha-1-antitrypsin 1-1	46	5,72	7	2,2E-03	7,0	5,3	3,6	2,5	0,29	0,65	0,97
P22599	Serpina1b	Alpha-1-antitrypsin 1-2	45,9	5,54	8	9,2E-04	6,2	4,0	2,1	1,9	0,45	0,99	1,08
Q00897	Serpina1d	Alpha-1-antitrypsin 1-4	46	5,44	7	1,7E-03	5,7	3,1	1,9	1,9	0,58	0,98	1,02
P07759	Serpina3k	Serine protease inhibitor A3K	46,9	5,16	5	9,6E-03	17,8	2,3	1,7	0,0	1,54	1,66	2,00
P32261	Serpinc1	Antithrombin-III	52	6,46	16	1,5E-05	1,6	0,0	0,0	0,0	2,00	2,00	2,00
E9PWS2	Serpinf1	Pigment epithelium-derived factor	15,8	5,77	5	7,0E-03	2,9	0,2	0,0	0,9	1,78	2,00	1,09
O70456	Sfn	14-3-3 protein sigma	27,7	4,78	4	2,5E-02	2,9	5,9	2,7	5,0	-0,68		-0,53
P04919	Slc4a1	Band 3 anion transport protein	103,1	5,45	9	4,4E-04	2,3	0,0	0,0	0,0	2,00	2,00	2,00
P62320	Snrpd3	Small nuclear ribonucleoprotein Sm D3	13,9	10,32	7	2,3E-03	1,2	2,9	3,4	3,3	-0,80	-0,94	-0,91
P62307	Snrpf	Small nuclear ribonucleoprotein F	9,7	4,67	3	4,2E-02	0,8	0,0	0,2	0,0	2,00	1,38	2,00
P08228	Sod1	Superoxide dismutase [Cu-Zn]	15,9	6,51	3	4,9E-02	5,1	2,8	2,5	3,2	0,59	0,69	0,46
Q62261	Sptbn1	Spectrin beta chain, non-erythrocytic 1	274,1	5,58	11	1,7E-04	2,3	0,6	0,7	0,2	1,16	1,09	1,73
H7BX95	Srsf1	Serine/arginine-rich splicing factor 1	28,3	10,08	8	1,2E-03	0,0	0,3	2,2	2,2	-2,00	-2,00	-2,00
P84104	Srsf3	Serine/arginine-rich splicing factor 3	19,3	11,65	9	5,3E-04	1,8	3,1	3,6	4,7	-0,54	-0,67	-0,88
Q8BL97	Srsf7	Serine/arginine-rich splicing factor 7	30,8	11,9	9	6,0E-04	0,4	2,5	2,2	3,5	-1,51	-1,44	-1,63
E9Q1V0	St13	Hsc70-interacting protein (Fragment)	14,2	4,51	6	5,4E-03	0,0	0,8	0,0	0,2	-2,00		-2,00
P54116	Stom	Stomatin	31,4	6,93	10	3,2E-04	0,8	0,0	0,0	0,0	2,00	2,00	2,00
P11983	Tcp1	T-complex protein 1 subunit alpha	60,4	6,16	4	2,7E-02	4,7	2,0	2,6	2,4	0,79	0,59	0,65
Q921I1	Tf	Serotransferrin	76,7	7,18	6	5,8E-03	16,1	9,7	11,4	5,6	0,50	0,34	0,96
P35441	Thbs1	Thrombospondin-1	129,6	4,96	4	2,4E-02	1,9	0,0	0,7	0,0	2,00	0,95	2,00
A0A0R4IZY0	Thop1	Thimet oligopeptidase	78	5,99	4	2,0E-02	0,8	0,0	0,0	0,0	2,00	2,00	2,00
F6V084	Tmx1	Thioredoxin-related transmembrane protein 1 (Fragment)	14,4	5,06	10	3,2E-04	0,8	0,0	0,0	0,0	2,00	2,00	2,00
Q9CPQ3	Tomm22	Mitochondrial import receptor subunit TOM22 homolog	15,5	4,34	4	2,6E-02	0,0	0,0	1,0	0,9		-2,00	-2,00
Q9D173	Tomm7	Mitochondrial import receptor subunit TOM7 homolog	6,2	10,17	7	2,1E-03	1,1	0,0	0,0	0,0	2,00	2,00	2,00
P17751	Tpi1	Triosephosphate isomerase	26,7	7,3	4	2,8E-02	12,6	19,6	18,6	17,8	-0,43	-0,39	-0,34
P63028	Tpt1	Translationally-controlled tumor protein	19,5	4,86	4	1,8E-02	0,6	3,1	2,7	2,2	-1,34	-1,28	-1,15
P07309	Ttr	Transthyretin	15,8	6,16	7	2,5E-03	1,6	1,2	0,2	0,0	0,29	1,65	2,00
A2AQ07	Tubb1	Tubulin beta-1 chain	50,4	5,07	5	1,4E-02	5,7	11,4	12,2	13,1	-0,66	-0,72	-0,78
Q7TMM9	Tubb2a	Tubulin beta-2A chain	49,9	4,89	4	3,0E-02	25,7	37,4	41,5	41,2	-0,37	-0,47	-0,46
P68372	Tubb4b	Tubulin beta-4B chain	49,8	4,89	7	2,7E-03	28,8	48,8	51,1	49,7	-0,51	-0,56	-0,53
P99024	Tubb5	Tubulin beta-5 chain	49,6	4,89	4	2,1E-02	37,1	51,0	55,9	54,7	-0,32	-0,41	-0,38
Q922F4	Tubb6	Tubulin beta-6 chain	50,1	4,89	6	4,1E-03	11,5	19,8	23,3	21,4	-0,53	-0,68	-0,60
Q8BFR5	Tufm	Elongation factor Tu, mitochondrial	49,5	7,56	9	4,4E-04	2,1	0,2	0,8	0,3	1,74	0,90	1,46
Q3TW96	Uap1l1	UDP-N-acetylhexosamine pyrophosphorylase-like protein 1	56,6	5,43	12	1,2E-04	1,4	7,7	5,3	5,9	-1,39	-1,18	-1,24
Q9DB77	Uqcrc2	Cytochrome b-c1 complex subunit 2, mitochondrial	48,2	9,25	5	7,5E-03	1,5	0,3	0,2	0,0	1,26	1,59	2,00
P61759	Vbp1	Prefoldin subunit 3	22,4	6,28	5	9,7E-03	0,0	0,5	0,0	0,0	-2,00		
Q64727	Vcl	Vinculin	116,6	6	7	2,2E-03	9,3	0,0	1,6	0,8	2,00	1,40	1,67
P20152	Vim	Vimentin	53,7	5,12	5	1,2E-02	87,2	76,4	98,3	106,3			-0,20
P29788	Vtn	Vitronectin	54,8	5,88	4	3,1E-02	2,3	0,2	4,0	0,7	1,73	-0,55	1,08
~~Q3U3T8~~	~~Wdr62~~	~~WD repeat-containing protein 62~~	~~167,2~~	~~5,48~~	~~5~~	~~1,1E-02~~	~~0,6~~	~~0,0~~	~~0,0~~	~~0,0~~	~~2,00~~	~~2,00~~	~~2,00~~
Q9CQV8	Ywhab	14-3-3 protein beta/alpha	28,1	4,83	5	1,0E-02	3,6	8,7	7,2	8,1	-0,82	-0,66	-0,76
P62259	Ywhae	14-3-3 protein epsilon	29,2	4,74	18	7,4E-06	5,0	15,2	13,0	19,4	-1,01	-0,68	[illegible]
P61982	Ywhag	14-3-3 protein gamma	28,3	4,89	7	2,6E-03	2,7	7,3	5,9	8,1	-0,91	-0,73	-0,99
P68510	Ywhah	14-3-3 protein eta	28,2	4,89	7	2,3E-03	3,2	7,2	4,8	6,9	-0,77	-0,40	-0,74
P68254	Ywhaq	14-3-3 protein theta	27,8	4,78	4	2,9E-02	2,7	6,0	5,5	6,5	-0,75	-0,67	-0,82

Data file S4. Differentially expressed proteins (DEPs) identified by LDA (Prob<0.05) by comparing PSMs from MB49 Bladder cancer model untreated (CTR, n=6), treated with SNFs-OVA (SNFs-OVA, n=6) and treated with SNFs-CpG (SNFs-CpG, n=6). Average PSMs are shown. Pairwise comparisons (CTR vs SFNs-OVA; CTR vs SFNs-CpG) by DAve index are reported; positive DAve values (in red) indicate proteins up-regulated in CTR (down-regulated in SFNs treatments), while negative DAve values (in blue) indicate proteins up-regulated following SFNs treatments (down-regulated in CTR).

Annotations					LDA		Av. PSMs (MB49 BLADDER CANCER M			Dave index	
ID UNIPROT	Gene name	Description	MW [kDa]	calc. pI	F Ratio	Prob>F	CTR	SFNs-OVA	SFNs-CpG	CTR vs SFNs-OVA	CTR vs SFNs-CpG
Q9D8W5	Psmd12	26S proteasome non-ATPase regulatory subunit 12	52,9	7,06	124	4,2E-13	0	2	0	-2,00	
A0A0N4SW94	Myadm	Myeloid-associated differentiation marker (Fragment)	8,6	8,38	65	1,7E-10	2	0	0,2	2,00	1,64
P17426	Ap2a1	AP-2 complex subunit alpha-1	107,6	7,03	62	2,8E-10	0	1,7	0	-2,00	
O35955	Psmb10	Proteasome subunit beta type-10	29	6,87	45	4,5E-09	3,5	1,5	6,9	0,80	-0,65
P46935	Nedd4	E3 ubiquitin-protein ligase NEDD4	102,6	5,26	44	5,0E-09	0	1,5	0	-2,00	
E9Q9E1	Eif4g1	Eukaryotic translation initiation factor 4 gamma 1	175,2	5,38	25	6,6E-07	0,2	2,8	0,2	-1,73	
P17751	Tpi1	Triosephosphate isomerase	26,7	7,3	22	1,5E-06	8,6	11,3	3	-0,27	0,97
P50516	Atp6v1a	V-type proton ATPase catalytic subunit A	68,3	5,58	20	2,6E-06	0,5	0,3	3,2	0,50	-1,46
G5E8J2	Ank1	Ankyrin-1	202,4	6,65	19	4,9E-06	2	0,2	0	1,64	2,00
P14869	Rplp0	60S acidic ribosomal protein P0	34,2	6,25	16	1,8E-05	2,4	5,7	2,3	-0,81	
P63268	Actg2	Actin, gamma-enteric smooth muscle	41,9	5,48	15	2,0E-05	72,4	64	113,5		-0,44
P20918	Plg	Plasminogen	90,7	6,6	14	3,4E-05	4,9	1,6	1,8	1,02	0,93
P01872	Ighm	Immunoglobulin heavy constant mu	49,9	7,01	14	3,7E-05	0,6	0,4	2,8	0,40	-1,29
A0A0A6YVP0	Ighg2b	Immunoglobulin heavy constant gamma 2B (Fragment)	44,3	6,52	14	3,7E-05	0,7	4,5	8,8	-1,46	-1,71
Q61074	Ppm1g	Protein phosphatase 1G	58,7	4,39	13	6,4E-05	0,5	2	0,2	-1,20	0,86
Q8K297	Colgalt1	Procollagen galactosyltransferase 1	71	7,28	13	6,5E-05	0	1,5	0	-2,00	
P68134	Acta1	Actin, alpha skeletal muscle	42	5,39	13	6,9E-05	79,5	71,8	121		-0,41
Q9R1P1	Psmb3	Proteasome subunit beta type-3	22,9	6,55	13	7,1E-05	0	1,5	0	-2,00	
G3UVV4	Hk1	Hexokinase	101,8	6,67	12	9,4E-05	4,7	0	0,7	2,00	1,48
B7ZNL2	Nap1l4	Nap1l4 protein	43,9	4,68	12	9,5E-05	0,5	2,3	0	-1,29	2,00
P50518	Atp6v1e1	V-type proton ATPase subunit E 1	26,1	9,23	12	1,0E-04	0,2	0	1,5	2,00	-1,53
Q62167	Ddx3x	ATP-dependent RNA helicase DDX3X	73,1	7,18	12	1,3E-04	6,8	8,8	5,1	-0,26	0,29
P26883	Fkbp1a	Peptidyl-prolyl cis-trans isomerase FKBP1A	11,9	8,16	11	1,4E-04	1,3	2	0	-0,42	2,00
P97352	S100a13	Protein S100-A13	11,2	6,13	11	1,9E-04	1,8	0,5	0	1,13	2,00
P16045	Lgals1	Galectin-1	14,9	5,49	11	2,0E-04	2,7	1,8	0,2	0,40	1,72
P62849	Rps24	40S ribosomal protein S24	15,4	10,78	11	2,1E-04	0,3	3,2	0	-1,66	2,00
Q64522	H2ac21	Histone H2A type 2-B	14	10,89	10	2,5E-04	24	35,9	22,4	-0,40	
P60710	Actb	Actin, cytoplasmic 1	41,7	5,48	10	2,7E-04	130,2	110	179,4	0,17	-0,32
P54116	Stom	Stomatin	31,4	6,93	10	3,2E-04	0,6	0	0	2,00	2,00
Q9D6Z1	Nop56	Nucleolar protein 56	64,4	9,44	10	3,7E-04	0,2	1,5	0,4	-1,53	-0,67
P99029	Prdx5	Thioredoxin-dependent peroxiredoxin	21,9	9,25	10	3,8E-04	4,4	5,5	14,2	-0,22	-1,05
A0A140T8N1	Igkv1-88	Immunoglobulin kappa chain variable 1-88 (Fragment)	13,2	8,02	10	3,9E-04	0	0	1,6		-2,00
P62900	Rpl31	60S ribosomal protein L31	14,5	10,54	10	4,1E-04	0,2	2	0,4	-1,64	-0,67
P70696	H2bc1	Histone H2B type 1-A	14,2	10,29	9	4,4E-04	17,6	5,7	19,8	1,02	
A0A7N9VR94	Ahnak2	AHNAK nucleoprotein 2	368,2	5,88	9	4,6E-04	5,7	3,8	0,4	0,40	1,74
P50637	Tspo	Translocator protein	18,8	9,52	9	4,6E-04	0,2	0,3	0	-0,40	2,00
P09411	Pgk1	Phosphoglycerate kinase 1	44,5	7,9	9	5,0E-04	22,3	16,3	9,9	0,31	0,77
Q9CZN7	Shmt2	Serine hydroxymethyltransferase, mitochondrial	55,7	8,47	9	5,2E-04	4,2	2,8	0,4	0,40	1,65
Q8BFZ3	Actbl2	Beta-actin-like protein 2	42	5,49	9	5,3E-04	78	63,3	107,8	0,21	-0,32
G3UZI2	Syncrip	Heterogeneous nuclear ribonucleoprotein Q	58,7	7,56	9	6,1E-04	4,9	7,1	1,6	-0,37	1,02
Q8R1F1	Niban2	Protein Niban 2	84,8	5,94	9	6,4E-04	1,1	2	0	-0,58	2,00
Q08943	Ssrp1	FACT complex subunit SSRP1	80,8	6,76	9	6,4E-04	0	1,5	0,2	-2,00	-2,00
P47911	Rpl6	60S ribosomal protein L6	33,5	10,7	9	6,5E-04	4,9	8,6	1,1	-0,55	1,27
P68040	Rack1	Receptor of activated protein C kinase 1	35,1	7,69	9	7,2E-04	5,8	7,4	1,5	-0,24	1,18
Q64475	H2bc3	Histone H2B type 1-B	13,9	10,32	8	8,8E-04	50,8	39,4	58,1	0,25	
Q91XL1	Lrg1	Leucine-rich HEV glycoprotein	37,4	6,61	8	8,9E-04	1,8	0	0,2	2,00	1,60
D3Z2M0	Ctu2	Cytoplasmic tRNA 2-thiolation protein 2 (Fragment)	27,3	8,19	8	9,6E-04	1,5	1	0,8	0,40	0,61
Q9CZU6	Cs	Citrate synthase, mitochondrial	51,7	8,57	8	9,9E-04	1,6	4	1,7	-0,86	
Q9EPB4	Pycard	Apoptosis-associated speck-like protein containing a CARD	21,4	5,43	8	1,1E-03	0	0,2	4,6	-2,00	-2,00
Q80X19	Col14a1	Collagen alpha-1(XIV) chain	192,9	5,1	8	1,1E-03	0	3,3	13,3	-2,00	-2,00
Q64525	Hist2h2bb	Histone H2B type 2-B	13,9	10,32	8	1,2E-03	53,3	39,4	58,3	0,30	
Q8VDM4	Psmd2	26S proteasome non-ATPase regulatory subunit 2	100,1	5,17	8	1,2E-03	1	2	0,2	-0,67	1,33
P14483	H2-Ab1	H-2 class II histocompatibility antigen, A beta chain	30,1	7,24	8	1,3E-03	0,5	1,5	5,1	-1,00	-1,64
Q542I8	Itgb2	Integrin beta	84,8	7,05	8	1,3E-03	1,5	2,5	5,1	-0,50	-1,09
A0A384DV79	Hmga1	High mobility group protein HMG-I/HMG-Y	10,5	10,43	8	1,4E-03	1,3	0	0	2,00	2,00
Q923D2	Blvrb	Flavin reductase (NADPH)	22,2	7,01	8	1,4E-03	1,7	0,9	2,3	0,62	-0,30
P17182	Eno1	Alpha-enolase	47,1	6,8	8	1,5E-03	43,5	29,2	26,4	0,39	0,49
A6ZI44	Aldoa	Fructose-bisphosphate aldolase	45,1	7,91	7	1,5E-03	17,9	11,6	8,5	0,43	0,71
E9QLG3	Mga	MAX gene-associated protein	332,9	7,58	7	1,6E-03	0	1,8	0,2	-2,00	-2,00
Q9JLZ6	Hic2	Hypermethylated in cancer 2 protein	66,7	6,35	7	1,6E-03	0	1	0	-2,00	
F6WR04	Ctss	Cathepsin S	38,6	7,15	7	1,7E-03	0	0	3,2		-2,00
A0A0R4J2B2	Kctd12	BTB/POZ domain-containing protein KCTD12	35,9	5,81	7	1,8E-03	0	0,2	5,7	-2,00	-2,00
A0A0A6YY53	Ighg2c	Immunoglobulin heavy constant gamma 2C (Fragment)	36,5	8,02	7	1,8E-03	0	0	4,5		-2,00
Q14AA6	1700009N14Rik	GTP-binding nuclear protein Ran	24,3	7,97	7	1,9E-03	0	1,3	0	-2,00	
Q99K94	Stat1	Signal transducer and activator of transcription	87,1	6,02	7	1,9E-03	0	0,8	7,7	-2,00	-2,00
A0A498WGD8	Txnl1	Thioredoxin-like protein 1	32,7	5,07	7	2,1E-03	0,9	1,4	0,2	-0,43	1,27
P14733	Lmnb1	Lamin-B1	66,7	5,16	7	2,2E-03	6,6	0,7	3,2	1,62	0,69
P62814	Atp6v1b2	V-type proton ATPase subunit B, brain isoform	56,5	5,81	7	2,2E-03	0	0	2,2		-2,00
Q9WTI7	Myo1c	Unconventional myosin-Ic	121,9	9,35	7	2,2E-03	0,3	0,2	1,6	0,40	-1,37
Q61937	Npm1	Nucleophosmin	32,5	4,77	7	2,2E-03	5,8	7,5	1,2	-0,26	1,31
A0A0N4SV32	Serbp1	Plasminogen activator inhibitor 1 RNA-binding protein	39,6	9,66	7	2,3E-03	0,6	2,3	0,6	-1,17	
A0A1B0GS13	Bax	Apoptosis regulator BAX (Fragment)	12,6	4,94	7	2,5E-03	2,3	1,5	0,5	0,42	1,29
Q8R0W0	Eppk1	Epiplakin	724,2	6,07	7	2,5E-03	1,8	3,5	0,7	-0,64	0,88
P25444	Rps2	40S ribosomal protein S2	31,2	10,24	7	2,6E-03	2,5	5,6	0,8	-0,77	1,03
I7HLV2	Rpl10	60S ribosomal protein L10 (Fragment)	23,1	10,01	7	2,7E-03	2,1	1,5	0,2	0,33	1,65
P99026	Psmb4	Proteasome subunit beta type-4	29,1	5,64	7	2,8E-03	0,2	0,3	1,5	-0,40	-1,53
Q9D1A2	Cndp2	Cytosolic non-specific dipeptidase	52,7	5,66	7	2,8E-03	0,8	2,8	14	-1,11	-1,78
Q8BSH9	Nap1l1	Nucleosome assembly protein 1-like 1	44,6	4,56	7	2,8E-03	1,5	3,8	0,4	-0,87	1,16
Q9DBJ1	Pgam1	Phosphoglycerate mutase 1	28,8	7,18	7	2,8E-03	8,9	8	3,9		0,78
Q8BG07	Pld4	5'-3' exonuclease PLD4	56,1	7,31	7	2,9E-03	0	0	2,5		-2,00
Q9Z1R9	Prss1	Protease, serine 1 (trypsin 1)	26,1	4,94	7	2,9E-03	0,3	1,8	0,6	-1,43	-0,67
P19324	Serpinh1	Serpin H1	46,5	8,82	6	3,3E-03	3,3	17,6	15,4	-1,37	-1,29
Q62433	Ndrg1	Protein NDRG1	43	6,1	6	3,4E-03	1,3	0	0,4	2,00	1,06
O09131	Gsto1	Glutathione S-transferase omega-1	27,5	7,36	6	3,6E-03	2,4	0,2	0	1,69	2,00
P97351	Rps3a	40S ribosomal protein S3a	29,9	9,73	6	3,7E-03	1	0	0	2,00	2,00
E9PWS2	Serpinf1	Pigment epithelium-derived factor	15,8	5,77	6	3,7E-03	0,3	0,2	2,6	0,40	-1,59
Q61233	Lcp1	Plastin-2	70,1	5,33	6	3,8E-03	2,9	3,3	22		-1,53
P58252	Eef2	Elongation factor 2	95,3	6,83	6	3,8E-03	15,2	18,7	9,9	-0,21	0,42
P62855	Rps26	40S ribosomal protein S26	13	11	6	3,8E-03	5,4	4,1	0,9	0,27	1,43
E9Q5L2	Itih4	Inter alpha-trypsin inhibitor, heavy chain 4	102,8	6,37	6	3,9E-03	1,5	0	0	2,00	2,00
P54071	Idh2	Isocitrate dehydrogenase [NADP], mitochondrial	50,9	8,69	6	3,9E-03	0	1,2	0	-2,00	
P14131	Rps16	40S ribosomal protein S16	16,4	10,21	6	4,0E-03	4,6	8	5,4	-0,54	-0,16
A0A0A0MQA5	Tuba4a	Tubulin alpha chain (Fragment)	52,9	5,19	6	4,3E-03	30,8	26,1	22,9	0,17	0,29
Q9ERD7	Tubb3	Tubulin beta-3 chain	50,4	4,93	6	4,3E-03	38	44,9	38,2	-0,17	
P28654	Dcn	Decorin	39,8	8,68	6	4,3E-03	0	4,3	3,1	-2,00	-2,00
P28063	Psmb8	Proteasome subunit beta type-8	30,2	6,68	6	4,3E-03	0	0	1,2		-2,00
P51150	Rab7a	Ras-related protein Rab-7a	23,5	6,7	6	4,5E-03	2,7	7,6	3,8	-0,95	-0,34
Q921M7	Cyrib	CYFIP-related Rac1 interactor B	36,8	6,06	6	4,6E-03	0	1,5	3,2	-2,00	-2,00
E9Q8F0	Rbm39	RNA-binding protein 39	47	10,52	6	4,6E-03	0,4	1,8	0,5	-1,27	-0,22
A0A0G2JEB3	Fdps	Farnesyl pyrophosphate synthase (Fragment)	25,9	7,21	6	4,7E-03	1,8	5,1	0,2	-0,96	1,60
P62806	H4c1	Histone H4	11,4	11,36	6	4,7E-03	66,6	46,6	62,9	0,35	
Q91X72	Hpx	Hemopexin	51,3	7,8	6	4,8E-03	2,6	0,7	7,9	1,15	-1,01
Q60710	Samhd1	Deoxynucleoside triphosphate triphosphohydrolase SAMHD1	75,8	7,93	6	4,9E-03	2	2,9	9,2	-0,37	-1,29
Q64433	Hspe1	10 kDa heat shock protein, mitochondrial	11	8,35	6	4,9E-03	3,2	2,8	0,2		1,76
P63276	Rps17	40S ribosomal protein S17	15,5	9,85	6	5,1E-03	1,2	2,3	0,5	-0,63	0,82
Q99M73	Krt84	Keratin, type II cuticular Hb4	64,9	7,84	6	5,1E-03	0,7	2,2	0	-1,03	2,00
A2ANA0	Sec23b	Protein transport protein SEC23 (Fragment)	31,4	6,07	6	5,1E-03	0,2	1,7	0,4	-1,58	-0,67
Q8CGP4	H2ac1	Histone H2A	14	11,21	6	5,2E-03	51,7	36,4	53,4	0,35	
Q61316	Hspa4	Heat shock 70 kDa protein 4	94,1	5,24	6	5,2E-03	2	2	0,6		1,08
Q922F4	Tubb6	Tubulin beta-6 chain	50,1	4,89	6	5,4E-03	30,4	37,1	26	-0,20	0,16
Q61599	Arhgdib	Rho GDP-dissociation inhibitor 2	22,8	5,11	6	5,5E-03	1	1,5	3,4	-0,40	-1,09
Q4VAA2	Cdv3	Protein CDV3	29,7	6,1	6	5,5E-03	1,2	0	0,3	2,00	1,20
G3UWN5	Apoe	Apolipoprotein E (Fragment)	26,4	6,15	6	5,7E-03	1,5	0	1,6	2,00	
Q921I1	Tf	Serotransferrin	76,7	7,18	6	5,7E-03	11,2	7,2	14,6	0,43	-0,26
Q61247	Serpinf2	Alpha-2-antiplasmin	54,9	6,3	6	5,8E-03	1,2	0,3	0	1,20	2,00
P62267	Rps23	40S ribosomal protein S23	15,8	10,49	6	6,0E-03	0	1,2	0	-2,00	
A0A0N4SV00	Cct7	T-complex protein 1 subunit eta	55	7,83	6	6,1E-03	2,2	1	0	0,75	2,00
D3Z7J8	Ccdc61	Centrosomal protein CCDC61 (Fragment)	20,6	5,59	6	6,2E-03	0,6	1,7	6	-0,96	-1,64
Q61635	Ifi47	GTP-binding protein	46,8	6,74	6	6,3E-03	0	0,2	1,2	-2,00	-2,00
E9PXX7	Txndc5	Thioredoxin domain-containing protein 5	38,5	5,39	5	6,6E-03	1,5	4,3	7,2	-0,97	-1,31
P14211	Calr	Calreticulin	48	4,49	5	6,6E-03	0	1,8	0,4	-2,00	-2,00
Q9QXS1	Plec	Plectin	533,9	5,96	5	7,3E-03	73,7	48,2	18,5	0,42	1,20
Q62009	Postn	Periostin	93,1	7,53	5	7,4E-03	6,4	9,1	15,9	-0,35	-0,85
P62827	Ran	GTP-binding nuclear protein Ran	24,4	7,49	5	7,4E-03	0,2	2,5	0	-1,70	2,00
Q9Z2X1	Hnrnpf	Heterogeneous nuclear ribonucleoprotein F	45,7	5,49	5	7,5E-03	4,4	6,5	2,3	-0,39	0,63
P28653	Bgn	Biglycan	41,6	7,27	5	7,7E-03	0	2,7	4,5	-2,00	-2,00
E9PWQ3	Col6a3	Collagen, type VI, alpha 3	353,7	6,93	5	7,8E-03	12,9	57,9	80,2	-1,27	-1,45
P07356	Anxa2	Annexin A2	38,7	7,69	5	7,9E-03	38,4	34,7	18,4		0,70
Q9EQ06	Hsd17b11	Estradiol 17-beta-dehydrogenase 11	32,9	8,66	5	8,0E-03	0	0	1,4		-2,00
E9Q5F6	Ubc	Polyubiquitin-C (Fragment)	22,6	7,4	5	8,3E-03	8,5	4,3	5,4	0,66	0,45
P05784	Krt18	Keratin, type I cytoskeletal 18	47,5	5,33	5	8,4E-03	53,5	26,4	15,7	0,68	1,09
A2BE93	Set	Protein SET (Fragment)	24,9	5,55	5	8,4E-03	2,2	2,1	0,5		1,26
P08207	S100a10	Protein S100-A10	11,2	6,77	5	8,7E-03	2,4	0,2	1,1	1,69	0,74
P12970	Rpl7a	60S ribosomal protein L7a	30	10,56	5	8,9E-03	4,4	3,1	1	0,35	1,26
P62320	Snrpd3	Small nuclear ribonucleoprotein Sm D3	13,9	10,32	5	9,0E-03	1,8	4	1,8	-0,76	
A0A0A6YXW6	Igha	Immunoglobulin heavy constant alpha (Fragment)	42	4,94	5	9,2E-03	1,3	1,2	6,3		-1,32
Q9Z1Q9	Vars1	Valine--tRNA ligase	140,1	7,77	5	9,4E-03	8,7	0	4	2,00	0,74
Q02788	Col6a2	Collagen alpha-2(VI) chain	110,3	6,42	5	9,4E-03	0,2	5,9	6,6	-1,87	-1,88
P42208	Septin2	Septin-2	41,5	6,55	5	9,5E-03	0,7	3,2	0,7	-1,28	
B2RX14	Tut4	Terminal uridylyltransferase 4	184,5	8,19	5	9,5E-03	0	0,5	0	-2,00	
A0A1W2P7Q6	Xpot	Exportin-T	109,7	5,31	5	9,5E-03	0	0,5	0	-2,00	
P47753	Capza1	F-actin-capping protein subunit alpha-1	32,9	5,55	5	9,6E-03	1,5	2,3	3,1	-0,42	-0,70
Q9DCV7	Krt7	Keratin, type II cytoskeletal 7	50,7	5,87	5	9,7E-03	0,5	0	0	2,00	2,00
P21981	Tgm2	Protein-glutamine gamma-glutamyltransferase 2	77	5,1	5	9,9E-03	5,2	2,1	4,3	0,85	0,19
P62137	Ppp1ca	Serine/threonine-protein phosphatase PP1-alpha catalytic subunit	37,5	6,33	5	1,0E-02	0,5	1,5	0	-1,00	2,00
O70435	Psma3	Proteasome subunit alpha type-3	28,4	5,44	5	1,0E-02	0	0	1,1		-2,00
Q07076	Anxa7	Annexin A7	49,9	6,18	5	1,0E-02	0,5	0	0	2,00	2,00
Q587J6	L1td1	LINE-1 type transposase domain-containing protein 1	88,1	5,45	5	1,0E-02	0,5	0	0	2,00	2,00
P97449	Anpep	Aminopeptidase N	109,6	5,9	5	1,0E-02	0	0	0,6		-2,00
Q8CGK3	Lonp1	Lon protease homolog, mitochondrial	105,8	6,57	5	1,0E-02	0,2	1,2	0	-1,43	2,00
O35658	C1qbp	Complement component 1 Q subcomponent-binding protein, mitochondrial	31	4,92	5	1,0E-02	0,2	0,5	0,2	-0,86	
P29351	Ptpn6	Tyrosine-protein phosphatase non-receptor type 6	67,5	7,81	5	1,1E-02	0	1	4,4	-2,00	-2,00
P25911	Lyn	Tyrosine-protein kinase Lyn	58,8	7,15	5	1,1E-02	0	0	1,3		-2,00
P09405	Ncl	Nucleolin	76,7	4,75	5	1,1E-02	12,5	14,9	5,6	-0,18	0,76
O35129	Phb2	Prohibitin-2	33,3	9,83	5	1,1E-02	8,3	6,1	3,4	0,31	0,84
A0A087WS56	Fn1	Fibronectin	249,4	5,82	5	1,1E-02	55,5	25,1	20,9	0,75	0,91
Q922B2	Dars1	Aspartate--tRNA ligase, cytoplasmic	57,1	6,49	5	1,1E-02	1,9	0,2	0	1,62	2,00
P97429	Anxa4	Annexin A4	35,9	5,57	5	1,1E-02	11	6,6	5,2	0,50	0,72
Q9JM76	Arpc3	Actin-related protein 2/3 complex subunit 3	20,5	8,59	5	1,1E-02	1,5	2,1	3,8	-0,33	-0,87
E9Q4F4	Snrpe	Small nuclear ribonucleoprotein E	10,9	8,48	5	1,1E-02	1,5	2,8	1,7	-0,60	
P08030	Aprt	Adenine phosphoribosyltransferase	19,7	6,79	5	1,2E-02	10,6	10,6	4,6		0,79
A0A1B0GSG5	Rnh1	Ribonuclease inhibitor	53,9	5,01	5	1,2E-02	2,8	1,7	0,4	0,49	1,50
Q60847	Col12a1	Collagen alpha-1(XII) chain	340	5,64	5	1,2E-02	0,4	7,1	7,7	-1,79	-1,80
P57759	Erp29	Endoplasmic reticulum resident protein 29	28,8	6,15	5	1,2E-02	0,2	0	1,4	2,00	-1,50
E9QNN1	Dhx9	DEAH box protein 9	149,6	6,83	5	1,2E-02	0,9	2,3	0	-0,88	2,00
Q9DC61	Pmpca	Mitochondrial-processing peptidase subunit alpha	58,2	6,83	5	1,3E-02	1,4	0	0,2	2,00	1,50
Q61990	Pcbp2	Poly(rC)-binding protein 2	38,2	7,77	5	1,3E-02	2,1	1,5	0,2	0,33	1,65
Q8BTM8	Flna	Filamin-A	281	6,04	5	1,3E-02	17,8	16	9,7		0,59
P01592	Jchain	Immunoglobulin J chain	18	4,89	5	1,3E-02	0	0	1		-2,00
Q99JR5	Tinagl1	Tubulointerstitial nephritis antigen-like	52,6	6,77	5	1,3E-02	0	1,2	0	-2,00	
P62908	Rps3	40S ribosomal protein S3	26,7	9,66	5	1,3E-02	8,7	9,4	2,3		1,16
P63325	Rps10	40S ribosomal protein S10	18,9	10,15	5	1,3E-02	1,8	4,5	1,6	-0,86	
Q04857	Col6a1	Collagen alpha-1(VI) chain	108,4	5,36	5	1,4E-02	2,4	13,6	14	-1,40	-1,41
A0A1C7CYU3	Nucb1	Nucleobindin-1	53	5,07	5	1,4E-02	0	1	1,5	-2,00	-2,00
Q8VCW8	Acsf2	Medium-chain acyl-CoA ligase ACSF2, mitochondrial	67,9	8,18	5	1,4E-02	0	0	1		-2,00
P46467	Vps4b	Vacuolar protein sorting-associated protein 4B	49,4	7,11	5	1,4E-02	0	0	1		-2,00
P84244	H3-3a	Histone H3.3	15,3	11,27	5	1,4E-02	22,3	8,7	18,6	0,88	0,18
O55222	Ilk	Integrin-linked protein kinase	51,3	8,07	5	1,4E-02	0,9	0,7	2,3	0,25	-0,88
P56480	Atp5f1b	ATP synthase subunit beta, mitochondrial	56,3	5,34	5	1,4E-02	43,6	49,4	51,4		-0,16
Q04447	Ckb	Creatine kinase B-type	42,7	5,67	5	1,4E-02	0	0,5	6,8	-2,00	-2,00
P17427	Ap2a2	AP-2 complex subunit alpha-2	104	6,93	4	1,4E-02	0	2	1,1	-2,00	-2,00
A8DUK4	Hbb-bs	Beta-globin	15,7	7,69	4	1,5E-02	113,9	53,3	30,2	0,72	1,16
P21279	Gnaq	Guanine nucleotide-binding protein G(q) subunit alpha	42,1	5,68	4	1,5E-02	0	0,3	1,4	-2,00	-2,00
P70670	Naca	Nascent polypeptide-associated complex subunit alpha, muscle-specific form	220,4	9,35	4	1,5E-02	1,6	2,7	0	-0,51	2,00
P36371	Tap2	Antigen peptide transporter 2	77,4	7,24	4	1,5E-02	0,6	0,7	0,4	-0,15	0,40
Q8CIE6	Copa	Coatomer subunit alpha	138,3	7,65	4	1,6E-02	0	0,2	0	-2,00	
P06800	Ptprc	Receptor-type tyrosine-protein phosphatase C	144,7	5,94	4	1,7E-02	0	0,5	1,6	-2,00	-2,00
E9Q5M6	Cfap44	Cilia- and flagella-associated protein 44	211,4	5,53	4	1,7E-02	0	0,7	0,2	-2,00	-2,00
P08113	Hsp90b1	Endoplasmin	92,4	4,82	4	1,7E-02	8,4	9,3	16,8		-0,67
O70172	Pip4k2a	Phosphatidylinositol 5-phosphate 4-kinase type-2 alpha	46,1	6,99	4	1,7E-02	0	0	1,2		-2,00
Q61830	Mrc1	Macrophage mannose receptor 1	164,9	6,83	4	1,7E-02	0	2,5	0,4	-2,00	-2,00
P00493	Hprt1	Hypoxanthine-guanine phosphoribosyltransferase	24,6	6,68	4	1,8E-02	0,3	0,2	1,3	0,40	-1,25
A0A0G2JG10	Dhx15	Pre-mRNA-splicing factor ATP-dependent RNA helicase DHX15	68,5	6,8	4	1,8E-02	2,6	2,8	1,3		0,67
A2BGG7	Ybx1	Y-box-binding protein 1 (Fragment)	24,7	10,1	4	1,8E-02	4,4	2,8	0,9	0,44	1,32
Q61753	Phgdh	D-3-phosphoglycerate dehydrogenase	56,5	6,54	4	1,8E-02	7	3,6	2,3	0,64	1,01
P11679	Krt8	Keratin, type II cytoskeletal 8	54,5	5,82	4	1,8E-02	44,3	29,7	11,2	0,39	1,19
P42932	Cct8	T-complex protein 1 subunit theta	59,5	5,62	4	1,9E-02	8,5	5,6	3,9	0,41	0,74
P48678	Lmna	Prelamin-A/C	74,2	6,98	4	1,9E-02	19,9	13,4	6,6	0,39	1,00
P14824	Anxa6	Annexin A6	75,8	5,5	4	1,9E-02	4	5,5	10,8	-0,32	-0,92
P26041	Msn	Moesin	67,7	6,6	4	1,9E-02	3,5	11,2	16,7	-1,05	-1,31
H7BX99	F2	Prothrombin	70,2	6,43	4	1,9E-02	0,7	2,3	0,5	-1,07	0,33
Q60973	Rbbp7	Histone-binding protein RBBP7	47,8	5,05	4	2,0E-02	0	0,7	0	-2,00	
A0A0G2JGD2	S100a4	Protein S100-A4 (Fragment)	9,1	5,21	4	2,0E-02	2,1	2,8	0,4	-0,29	1,36
G5E8F1	Itgam	Integrin alpha-M	127,5	7,25	4	2,0E-02	0,4	1,7	5,6	-1,24	-1,73
Q60668	Hnrnpd	Heterogeneous nuclear ribonucleoprotein D0	38,3	7,81	4	2,0E-02	3	3,8	1,3	-0,24	0,79
P62821	Rab1A	Ras-related protein Rab-1A	22,7	6,21	4	2,0E-02	0,2	1,7	0,9	-1,58	-1,27
Q76MZ3	Ppp2r1a	Serine/threonine-protein phosphatase 2A 65 kDa regulatory subunit A alpha isoform	65,3	5,11	4	2,0E-02	1,4	3,7	0,7	-0,90	0,67
Q8R180	Ero1a	ERO1-like protein alpha	54,1	6,54	4	2,1E-02	5	4,1	0,9	0,20	1,39
A6ZI46	Aldoart1	Fructose-bisphosphate aldolase	45,3	7,05	4	2,1E-02	6,2	0	1,9	2,00	1,06
Q05144	Rac2	Ras-related C3 botulinum toxin substrate 2	21,4	7,61	4	2,1E-02	0	1,1	2,3	-2,00	-2,00
P08074	Cbr2	Carbonyl reductase [NADPH] 2	25,9	9,01	4	2,1E-02	0	3,4	0	-2,00	
A0A452J8A5	Eci1	Enoyl-CoA delta isomerase 1, mitochondrial	32	8,98	4	2,1E-02	0,7	1,5	2	-0,73	-0,96
Q6P069	Sri	Sorcin	21,6	5,59	4	2,1E-02	1	0	0	2,00	2,00
A0A286YDA2	Nolc1	Nucleolar and coiled-body phosphoprotein 1	73,4	9,35	4	2,2E-02	0,9	0	0	2,00	2,00
A0A1C7CYV0	Pls3	Plastin-3 (Fragment)	70,6	5,62	4	2,2E-02	1,2	1,2	5		-1,23
A2AFQ2	Hsd17b10	3-hydroxyacyl-CoA dehydrogenase type-2	28,4	8,76	4	2,2E-02	2,5	0	1,6	2,00	0,44
P16015	Ca3	Carbonic anhydrase 3	29,3	7,37	4	2,2E-02	0	3,4	11,4	-2,00	-2,00
A0A087WNX7	Srcap	Snf2-related CREBBP activator protein	333,4	5,57	4	2,2E-02	0	0,7	0,2	-2,00	-2,00
P08228	Sod1	Superoxide dismutase [Cu-Zn]	15,9	6,51	4	2,2E-02	5,4	3,3	5,6	0,48	
P62242	Rps8	40S ribosomal protein S8	24,2	10,32	4	2,2E-02	2,6	2,5	0		2,00
Q9JKR6	Hyou1	Hypoxia up-regulated protein 1	111,1	5,19	4	2,3E-02	0,5	3,5	2,2	-1,50	-1,26
Q02013	Aqp1	Aquaporin-1	28,8	7,43	4	2,3E-02	1	0	0	2,00	2,00
Q8BWT1	Acaa2	3-ketoacyl-CoA thiolase, mitochondrial	41,8	8,09	4	2,3E-02	0	0,7	1,8	-2,00	-2,00
Q3UA72	Arpc5	Actin-related protein 2/3 complex subunit 5	9,7	5,19	4	2,4E-02	0,2	0	0,8	2,00	-1,20
O55143	Atp2a2	Sarcoplasmic/endoplasmic reticulum calcium ATPase 2	114,8	5,34	4	2,4E-02	0,2	3,1	0	-1,76	2,00
A0A1B0GS70	Psma1	Proteasome subunit alpha type-1	26,5	6,54	4	2,4E-02	0,7	1,8	1	-0,88	-0,35
Q8K1B8	Fermt3	Fermitin family homolog 3	75,6	7,05	4	2,4E-02	0	0,2	2	-2,00	-2,00
Q99JY0	Hadhb	Trifunctional enzyme subunit beta, mitochondrial	51,4	9,38	4	2,4E-02	0	1	2,5	-2,00	-2,00
F8WIV2	Serpinb6a	Serine (or cysteine) peptidase inhibitor, clade B, member 6a	44,7	6,38	4	2,4E-02	2,9	1	0,3	0,97	1,63
P62082	Rps7	40S ribosomal protein S7	22,1	10,1	4	2,5E-02	6,2	9,5	5,1	-0,42	0,19
F8VQJ3	Lamc1	Laminin subunit gamma-1	177,1	5,19	4	2,5E-02	0	0,7	1,8	-2,00	-2,00
Q9WUM4	Coro1c	Coronin-1C	53,1	7,08	4	2,5E-02	0,7	1,4	0	-0,67	2,00
P27005	S100a8	Protein S100-A8	10,3	5,68	4	2,5E-02	3	1	5,2	1,00	-0,54
A0A1B0GSK5	Rcn3	Reticulocalbin-3 (Fragment)	21,7	4,7	4	2,5E-02	0	0	2,8		-2,00
Q9D0D2	Col9a1	Col9a1 protein	64,7	8,69	4	2,6E-02	0	1	0	-2,00	
O70456	Sfn	14-3-3 protein sigma	27,7	4,78	4	2,6E-02	2,1	6,7	2	-1,05	
P49945	Ftl2	Ferritin light chain 2	20,8	6,89	4	2,6E-02	1,9	6,5	3,1	-1,10	-0,48
P26645	Marcks	Myristoylated alanine-rich C-kinase substrate	29,6	4,34	4	2,6E-02	0,8	0	0	2,00	2,00
P62307	Snrpf	Small nuclear ribonucleoprotein F	9,7	4,67	4	2,6E-02	1,2	0	0	2,00	2,00
Q9EQK5	Mvp	Major vault protein	96,8	5,64	4	2,6E-02	2,7	5,3	2,7	-0,65	
Q61598	Gdi2	Rab GDP dissociation inhibitor beta	50,5	6,25	4	2,6E-02	5,4	9,1	10,8	-0,51	-0,67
P38647	Hspa9	Stress-70 protein, mitochondrial	73,4	6,07	4	2,6E-02	8,2	9,4	4,6		0,56
P41241	Csk	Tyrosine-protein kinase CSK	50,7	7,06	4	2,6E-02	0	0,5	1,9	-2,00	-2,00
P62751	Rpl23a	60S ribosomal protein L23a	17,7	10,45	4	2,7E-02	2	2	0,9		0,76
O54734	Ddost	Dolichyl-diphosphooligosaccharide--protein glycosyltransferase 48 kDa subunit	49	5,83	4	2,7E-02	3,1	1,7	3	0,58	
Q569Z5	Ddx46	Probable ATP-dependent RNA helicase DDX46	117,4	9,26	4	2,7E-02	0	1	0	-2,00	
Q9WTK8	Spo11	Meiotic recombination protein SPO11	44,5	8,59	4	2,7E-02	0,7	0	0	2,00	2,00
Q9Z0E6	Gbp2	Guanylate-binding protein 2	66,7	5,71	4	2,7E-02	0,4	1,3	2,8	-1,06	-1,50
Q7TMM9	Tubb2a	Tubulin beta-2A chain	49,9	4,89	4	2,7E-02	48	58,1	48,9	-0,19	
P61750	Arf4	ADP-ribosylation factor 4	20,4	7,14	4	2,8E-02	0	2,2	0,9	-2,00	-2,00
P04117	Fabp4	Fatty acid-binding protein, adipocyte	14,6	8,4	4	2,8E-02	0	0,7	8,3	-2,00	-2,00
Q3UV11	Krt6b	Keratin, type II cytoskeletal 6B	59,5	8,15	4	2,8E-02	0,7	5,1	0,9	-1,52	-0,25
O88569	Hnrnpa2b1	Heterogeneous nuclear ribonucleoproteins A2/B1	37,4	8,95	4	2,9E-02	6,4	8,6	3,7	-0,29	0,53
E9Q7G0	Numa1	Nuclear mitotic apparatus protein 1	235,5	5,87	4	2,9E-02	0	0	1,1		-2,00
Q99LC5	Etfa	Electron transfer flavoprotein subunit alpha, mitochondrial	35	8,38	4	2,9E-02	0	0	0,8		-2,00
Q68FD5	Cltc	Clathrin heavy chain 1	191,4	5,69	4	2,9E-02	13,9	22,1	23,8	-0,46	-0,53
Q03265	Atp5f1a	ATP synthase subunit alpha, mitochondrial	59,7	9,19	4	2,9E-02	28	29,4	34,4		-0,21
Q9D0F9	Pgm1	Phosphoglucomutase-1	63,7	6,57	4	2,9E-02	1,9	0	1,1	2,00	0,53
Q9JJI8	Rpl38	60S ribosomal protein L38	8,2	10,1	4	3,0E-02	0	1,2	0	-2,00	
Q0P5V2	Sobp	Sine oculis-binding protein homolog	91,7	7,97	4	3,0E-02	0	1,2	0	-2,00	
P51885	Lum	Lumican	38,2	6,43	4	3,1E-02	0	6,6	10,8	-2,00	-2,00
Q80UG5	Septin9	Septin-9	65,5	8,9	4	3,1E-02	1,6	1	0	0,46	2,00
P99027	Rplp2	60S acidic ribosomal protein P2	11,6	4,54	4	3,1E-02	3	2	1,5	0,40	0,67
A0A494B908	Gstp1	GST class-pi (Fragment)	18	5,29	4	3,1E-02	0,7	0	0,2	2,00	1,11
E9Q616	Ahnak	AHNAK nucleoprotein (desmoyokin)	603,9	6,3	4	3,2E-02	9,3	4,3	4,7	0,74	0,66
P61979	Hnrnpk	Heterogeneous nuclear ribonucleoprotein K	50,9	5,54	4	3,2E-02	10,6	10,9	4,2		0,86
P11087	Col1a1	Collagen alpha-1(I) chain	137,9	5,85	4	3,2E-02	3,9	10,4	17,7	-0,91	-1,28
P47738	Aldh2	Aldehyde dehydrogenase, mitochondrial	56,5	7,62	4	3,3E-02	1,2	3,8	8,3	-1,04	-1,49
Q9CR57	Rpl14	60S ribosomal protein L14	23,5	11,02	4	3,3E-02	2	1	0,5	0,67	1,20
A0A0R3P9C8	Ndufa9	NADH dehydrogenase [ubiquinone] 1 alpha subcomplex subunit 9, mitochondrial	42,1	9,09	4	3,3E-02	0	0,9	0	-2,00	
Q3TQP6	Me1	Malic enzyme	61,4	6,48	4	3,3E-02	0	0	4,9		-2,00
O08749	Dld	Dihydrolipoyl dehydrogenase, mitochondrial	54,2	7,9	4	3,3E-02	0,6	0,7	2,6	-0,15	-1,25
P04370	Mbp	Myelin basic protein	27,2	9,58	4	3,3E-02	0	0,7	1,6	-2,00	-2,00
G8JL42	Gtdc1	Glycosyltransferase-like domain-containing protein 1	44,1	7,69	4	3,4E-02	0	0	0,9		-2,00
Q7TPV4	Mybbp1a	Myb-binding protein 1A	151,9	8,95	4	3,4E-02	1,9	0,2	0	1,62	2,00
P29788	Vtn	Vitronectin	54,8	5,88	4	3,4E-02	12,5	3,9	3,5	1,05	1,13
Q91VB8	Hba-a1	Alpha globin 1	15,1	8,22	3	3,4E-02	76,6	25,9	35,2	0,99	0,74
Q7M6Y3	Picalm	Phosphatidylinositol-binding clathrin assembly protein	71,5	7,91	3	3,5E-02	0,5	2,5	3,1	-1,33	-1,44
P02089	Hbb-b2	Hemoglobin subunit beta-2	15,9	8,05	3	3,5E-02	35,2	16	7,7	0,75	1,28
P07758	Serpina1a	Alpha-1-antitrypsin 1-1	46	5,72	3	3,5E-02	5,5	4,2	6,2	0,27	
A0A0N4SVM0	Capza2	F-actin-capping protein subunit alpha (Fragment)	19,5	5,41	3	3,5E-02	1,8	2,6	4,2	-0,36	-0,80
O35381	Anp32a	Acidic leucine-rich nuclear phosphoprotein 32 family member A	28,5	4,07	3	3,5E-02	0	0	1		-2,00
Q9QXK3	Copg2	Coatomer subunit gamma-2	97,6	5,8	3	3,6E-02	0	1,3	0,9	-2,00	-2,00
P21550	Eno3	Beta-enolase	47	7,18	3	3,6E-02	8,6	5,2	7,1	0,49	0,19
Q05816	Fabp5	Fatty acid-binding protein 5	15,1	6,54	3	3,6E-02	0	0	1,2		-2,00
P06728	Apoa4	Apolipoprotein A-IV	45	5,47	3	3,6E-02	0,3	1,5	0,4	-1,33	-0,29
Q9JKF1	Iqgap1	Ras GTPase-activating-like protein IQGAP1	188,6	6,48	3	3,7E-02	10	8,6	13,4	0,15	-0,29
Q6TL19	Gucy2g	Guanylate cyclase 2G	122,5	6,39	3	3,7E-02	0,2	0,2	1,4		-1,50
P17225	Ptbp1	Polypyrimidine tract-binding protein 1	56,4	8,34	3	3,7E-02	3,2	6,3	4,2	-0,65	-0,27
Q9CVB6	Arpc2	Actin-related protein 2/3 complex subunit 2	34,3	7,36	3	3,7E-02	0	0,2	1,3	-2,00	-2,00
P17156	Hspa2	Heat shock-related 70 kDa protein 2	69,6	5,67	3	3,7E-02	6	17,9	5,1	-1,00	0,16
Q6ZWZ4	Rpl36	60S ribosomal protein L36	12,2	11,59	3	3,8E-02	1,8	1,3	0	0,32	2,00
Q9D1G1	Rab1b	Ras-related protein Rab-1B	22,2	5,73	3	3,8E-02	0	0	1		-2,00
A0A0A6YVX9	Igsf8	Immunoglobulin superfamily member 8 (Fragment)	11,5	8,7	3	3,8E-02	0	0	0,5		-2,00
Q9JLI0	Akr1c12	Aldo-keto reductase a	37	6,64	3	3,8E-02	0,9	1,8	0	-0,67	2,00
Q9WV54	Asah1	Acid ceramidase	44,6	8,46	3	3,8E-02	0	0	1		-2,00
P63017	Hspa8	Heat shock cognate 71 kDa protein	70,8	5,52	3	3,8E-02	40,8	41,2	29,8		0,31
Q9D0J8	Ptms	Parathymosin	11,4	4,22	3	3,9E-02	1,2	0,3	0	1,20	2,00
Q8R5J9	Arl6ip5	PRA1 family protein 3	21,5	9,61	3	3,9E-02	2,6	1,8	0,4	0,36	1,47
P60867	Rps20	40S ribosomal protein S20	13,4	9,94	3	4,0E-02	2,7	3	0,8		1,09
P35821	Ptpn1	Tyrosine-protein phosphatase non-receptor type 1	49,6	6,16	3	4,0E-02	0	0	0,9		-2,00
P14152	Mdh1	Malate dehydrogenase, cytoplasmic	36,5	6,58	3	4,0E-02	0,3	0,3	1,7		-1,40
A0A0G2JFT9	Prkacb	cAMP-dependent protein kinase catalytic subunit beta (Fragment)	12,7	9,17	3	4,0E-02	0	1,5	1,3	-2,00	-2,00
P15864	H1-2	Histone H1.2	21,3	11	3	4,0E-02	8,3	4,1	3,3	0,68	0,86
P16627	Hspa1l	Heat shock 70 kDa protein 1-like	70,6	6,24	3	4,0E-02	4,8	0	4,8	2,00	
Q01149	Col1a2	Collagen alpha-2(I) chain	129,5	9,19	3	4,1E-02	0,8	6,3	9,7	-1,55	-1,70
Q99P72	Rtn4	Reticulon-4	126,5	4,54	3	4,1E-02	5,7	2,8	4	0,68	0,35
P46412	Gpx3	Glutathione peroxidase 3	25,4	8,22	3	4,1E-02	0	1,7	1,9	-2,00	-2,00
Q91V41	Rab14	Ras-related protein Rab-14	23,9	6,21	3	4,1E-02	0	1	0,5	-2,00	-2,00
Q00623	Apoa1	Apolipoprotein A-I	30,6	5,73	3	4,1E-02	4,1	2,5	2,3	0,48	0,56
Q3TEA8	Hp1bp3	Heterochromatin protein 1-binding protein 3	60,8	9,7	3	4,3E-02	0	0	0,6		-2,00
E9Q8P6	Unc93b1	Protein unc-93 homolog B1	47,8	7,68	3	4,4E-02	0	0,3	1	-2,00	-2,00
P70691	Ugt1a2	UDP-glucuronosyltransferase 1-2	60,2	8,05	3	4,4E-02	1	0	1,6	2,00	-0,46
P50580	Pa2g4	Proliferation-associated protein 2G4	43,7	6,86	3	4,5E-02	0,8	0,3	0,2	0,91	1,20
Q99MR6	Srrt	Serrate RNA effector molecule homolog	100,4	9,38	3	4,5E-02	1	0,2	0	1,33	2,00
P68510	Ywhah	14-3-3 protein eta	28,2	4,89	3	4,5E-02	9,5	7	8,5	0,30	
P09055	Itgb1	Integrin beta-1	88,2	5,94	3	4,5E-02	3,5	2,8	1,2	0,22	0,98
Q9DBC7	Prkar1a	cAMP-dependent protein kinase type I-alpha regulatory subunit	43,2	5,35	3	4,5E-02	0	0,5	1,1	-2,00	-2,00
P82198	Tgfbi	Transforming growth factor-beta-induced protein ig-h3	74,6	7,06	3	4,6E-02	0	0,9	2,9	-2,00	-2,00
Q8C845	Efhd2	EF-hand domain-containing protein D2	26,8	5,14	3	4,7E-02	0,6	1,5	3,2	-0,86	-1,37
P80314	Cct2	T-complex protein 1 subunit beta	57,4	6,4	3	4,8E-02	11,7	12,9	6,7		0,54
Q8C605	Pfkp	ATP-dependent 6-phosphofructokinase	85,5	6,89	3	4,8E-02	0	0,8	0	-2,00	
A0A0R4J0W6	Lrrc40	Leucine-rich repeat-containing protein 40	68	6,84	3	4,9E-02	0	0,7	0	-2,00	
E9PV24	Fga	Fibrinogen alpha chain	87,4	6,11	3	4,9E-02	22,3	13,5	8,7	0,49	0,88
Q3TDN2	Faf2	FAS-associated factor 2	52,4	5,47	3	5,0E-02	1,1	0,2	0	1,38	2,00

Data file S5. Protein hubs selected by Betweenness and Centroid centralities by processing protein-protein interaction (PPI) networks reconstructed by A) Hubs in CTR, B) Hubs in SFNs-OVA, SFNs-CpG and SFNs-OVA-CpG, C) Hubs in SFNs-OVA and SFNs-OVA-CpG, D) Hubs in SFNs-CpG and SFNs-OVA-CpG.

A)

	Betweenness				Centroid				Av.PSMs				LDA	
Gene Name	CTR	SFNs-OVA	SFNs-CpG	SFNs-OVA-CpG	CTR	SFNs-OVA	SFNs-CpG	SFNs-OVA-CpG	CTR	SFNs-OVA	SFNs-CpG	SFNs-OVA-CpG	F Ratio	Prob>F
Akt1	12602				-269				0,2	0,0	0,0	0,0		
Pik3r2	11732				-470				0,1	0,0	0,0	0,0		
Ubxn7	11481				-460				0,2	0,0	0,0	0,0		
Lipc	7749				-384				0,2	0,0	0,0	0,0		
Mapk10	7349				-507				0,2	0,0	0,0	0,0		
Map3k3	7058				-528				0,2	0,0	0,0	0,0		
Lamc2	5401				-424				0,1	0,0	0,0	0,0		
Cdh3	3980				-586				0,2	0,0	0,0	0,0		
Tmed10	3707				-637				0,2	0,0	0,0	0,0		
Thop1	2615				-602				0,8	0,0	0,0	0,0	4,1	2,0E-02
Spta1	2548				-583				0,4	0,0	0,0	0,0		
Gspt1	2252				-429				0,4	0,0	0,0	0,0		

B)

	Betweenness				Centroid				Av.PSMs				LDA	
Gene Name	CTR	SFNs-OVA	SFNs-CpG	SFNs-OVA-CpG	CTR	SFNs-OVA	SFNs-CpG	SFNs-OVA-CpG	CTR	SFNs-OVA	SFNs-CpG	SFNs-OVA-CpG	F Ratio	Prob>F
Itgb2		23896	33042	15114		-252	-274	-313	0,0	0,2	1,0	0,9		
Fau		13210	10568	11027		-269	-253	-297	0,0	1,0	0,8	0,8		
Srsf1		9636	9829	6749		-386	-389	-455	0,0	0,3	2,2	2,2	7,8	1,2E-03
Rab8b		6992	10154	12918		-407	-432	-426	0,0	0,2	0,5	0,2		
Calr		6588	9943	9114		-502	-434	-509	0,0	0,3	1,0	0,6		
Rab5c		5959	4700	11772		-511	-547	-513	0,0	0,1	0,3	0,5		
Eef1b2		5883	3448	6019		-434	-497	-532	0,0	0,1	0,2	0,7		
Fkbp1a		5242	5155	7405		-569	-538	-608	0,0	0,3	0,5	0,4		
Eif2s1		4172	5370	3470		-406	-456	-437	0,0	0,3	1,3	1,9	7,7	1,3E-03
Dlst		2772	4429	3073		-647	-579	-693	0,0	0,1	0,3	0,3		
Ube2l3	2015	2395	3703	3294	-655	-703	-598	-686	0,5	1,7	1,0	1,1		

C)

	Betweenness				Centroid				Av.PSMs				LDA	
Gene Name	CTR	SFNs-OVA	SFNs-CpG	SFNs-OVA-CpG	CTR	SFNs-OVA	SFNs-CpG	SFNs-OVA-CpG	CTR	SFNs-OVA	SFNs-CpG	SFNs-OVA-CpG	F Ratio	Prob>F
Prkacb		51208		34091		-293		-302	0,0	0,1	0,0	0,5		
Nedd8		7840		5451		-497		-474	0,0	0,1	0,0	0,3		
Pik3r1		7182		14950		-366		-412	0,0	0,1	0,0	0,2		
Pik3cd		6530		8912		-439		-461	0,0	0,1	0,0	0,3		
Rock2		5534		4018		-362		-370	0,0	0,3	0,0	0,2		
Ctnna1		4499		11688		-468		-483	0,0	0,3	0,0	0,2		
Eif4e		3568		5394		-455		-429	0,0	0,3	0,0	0,2		
Acly		2754	1026	3090		-696	-732	-741	0,0	0,4	1,4	0,5		
Fmr1		2594		3167		-425		-456	0,0	0,4	0,0	0,2		

D)

	Betweenness				Centroid				Av.PSMs				LDA	
Gene Name	CTR	SFNs-OVA	SFNs-CpG	SFNs-OVA-CpG	CTR	SFNs-OVA	SFNs-CpG	SFNs-OVA-CpG	CTR	SFNs-OVA	SFNs-CpG	SFNs-OVA-CpG	F Ratio	Prob>F
Ruvbl1			8990	6113			-539	-513	0,0	0,0	0,3	0,3		
Cndp2			6253	5560			-651	-657	0,0	0,0	0,2	0,3		
G6pdx			6083	5488			-538	-628	0,0	0,0	0,9	1,4	4,0	2,2E-02
Capn1			5546	7453			-526	-570	0,0	0,0	0,7	0,3		
Dnm1l	1237	1519	4429	4216	-696	-746	-640	-703	2,0	0,3	0,5	1,0		
Hk1			4264	4290			-700	-726	0,0	0,0	0,5	0,6		
Ppp2cb			3864	6221			-534	-574	0,0	0,0	1,5	1,6	6,8	2,4E-03
B2m			3847	5663			-555	-586	0,0	0,0	0,8	0,3		
Prkar1a			3776	3621			-635	-510	0,0	0,0	0,3	0,3		
Capzb			3102	5551			-581	-592	0,0	0,0	0,3	0,3		

Data file S6. Protein hubs selected by Betweenness and Centroid centralities by processing protein-protein i for MB49 bladder cancer models. A) Hubs in CTR, B) Hubs in SFNs-OVA and SFNs-CpG, C) Hubs in SFNs-OVA, D) Hubs in

A)

	Betweenness			Centroid			Av.PSMs			LDA	
Gene Name	CTR	SFNs-OVA	SFNs-CpG	CTR	SFNs-OVA	SFNs-CpG	CTR	SFNs-OVA	SFNs-CpG	F Ratio	Prob>F
Hmga2	111707			18			0,50	0,00	0,00		
Rab12	20057			-418			0,17	0,00	0,00		
Prkcb	18983			-302			0,19	0,00	0,00		
Bag3	12000			-414			0,15	0,00	0,00		
Rb1	9883			-332			0,15	0,00	0,00		
Smad2	9603			-439			0,15	0,00	0,00		
Apob	9178			-410			0,17	0,00	0,00		
Rock1	6764			-567			0,15	0,00	0,00		
Pias3	6684			-736			0,19	0,00	0,00		
Rabgef1	6620			-726			0,19	0,00	0,00		
Ccnh	6330			-756			0,19	0,00	0,00		
Prkcq	5662			-509			0,17	0,00	0,00		
Kdr	5509			-383			0,19	0,00	0,00		
Gaa	5430			-718			0,19	0,00	0,00		
Tlr4	5390			-598			0,15	0,00	0,00		
Syk	5246			-677			0,56	0,00	0,00		
Aldh7a1	4868			-693			0,15	0,00	0,00		
Anxa1	4565	1284	1055	-739	-909	-781	24,46	22,15	16,81		
Copb2	4128	786		-667	-836		0,56	0,84	0,00		
Sf3b1	4075			-490			0,15	0,00	0,00		
Slf1	4049			-719			0,17	0,00	0,00		
Eif2a	4024			-466			0,45	0,00	0,00		
Derl1	3581	2324		-671	-874		0,56	0,16	0,00		
Rpl10a	3547			-395			0,15	0,00	0,00		
Pdia6	3531	824	197	-747	-846	-734	8,28	10,13	10,40		
Tep1	3345			-655			0,15	0,00	0,00		
Stat3	2875			-642			0,15	0,00	0,00		
Sar1b	2866			-728			0,60	0,00	0,00		
Myo6	2797			-484			0,15	0,00	0,00		

B)

	Betweenness			Centroid			Av.PSMs			LDA	
Gene Name	CTR	SFNs-OVA	SFNs-CpG	CTR	SFNs-OVA	SFNs-CpG	CTR	SFNs-OVA	SFNs-CpG	F Ratio	Prob>F
Prkacb		51120	46999		-213	-306	0,00	1,50	1,26	3,3	4,0E-02
Rac2		15334	16542		-312	-313	0,00	1,14	2,28	4,1	2,1E-02
Ptpn6		9382	6040		-439	-487	0,00	0,98	4,36	4,9	1,1E-02
Kat2a		7134	6998		-452	-482	0,00	0,17	0,21		
Calr		7080	10145		-531	-477	0,00	1,81	0,36	5,5	6,6E-03
Dnm2		6921	3550		-519	-479	0,00	0,82	0,69		
Rab8b		6197	10095		-452	-410	0,00	0,85	1,63		
Eef1b2		5738	3665		-619	-537	0,00	0,17	0,18		
Clta		5537	3278		-471	-466	0,00	0,65	0,42		
Csk		4912	5001		-463	-414	0,00	0,49	1,86	3,8	2,6E-02
Tardbp		3979	4553		-621	-653	0,00	0,82	0,17		
Sec22b		3721	4098		-761	-639	0,00	0,33	0,97		
Ckb		3546	4362		-531	-456	0,00	0,51	6,83	4,5	1,4E-02
Ddb1		3410	2774		-394	-534	0,00	0,17	0,17		
Cryab		3170	2496		-516	-469	0,00	0,68	0,17		
Lrp1		2947	2611		-663	-586	0,00	0,82	0,24		

C)

	Betweenness			Centroid			Av.PSMs			LDA	
Gene Name	CTR	SFNs-OVA	SFNs-CpG	CTR	SFNs-OVA	SFNs-CpG	CTR	SFNs-OVA	SFNs-CpG	F Ratio	Prob>F
Tia1		67385			-123		0,00	0,16	0,00		
Nfkb1		12600			-288		0,00	0,16	0,00		
Speg		10822			-668		0,00	0,16	0,00		
Ssrp1		3973	1112		-777	-742	0,00	1,50	0,24	8,8	6,4E-04
Copa		3536			-642		0,00	0,16	0,00	4,4	1,6E-02

D)

	Betweenness			Centroid			Av.PSMs			LDA	
Gene Name	CTR	SFNs-OVA	SFNs-CpG	CTR	SFNs-OVA	SFNs-CpG	CTR	SFNs-OVA	SFNs-CpG	F Ratio	Prob>F
Polr2a			15905			-396	0,00	0,00	0,37		
Me1			4901			-592	0,00	0,00	4,94	3,5	3,3E-02
Fabp5			4424			-557	0,00	0,00	1,21	3,4	3,6E-02

Supplemental material

MATERIALS AND METHODS

Preparation of injectable formulations of SFNs

Bombyx mori cocoons (kindly donated by Nembri Industrie Tessili S.r.l., Capriolo, BS, Italy) were cut into fine pieces and degummed in a Na_2CO_3 aqueous solution (0.02 M) at 100 °C for 30 minutes; the degummed silk fibroin (SF) fibres were washed in distilled water and dried at room temperature. Then, SF was solubilized in an aqueous LiBr (9.3 M) solution at 60°C for 4 hrs; the obtained solution was dialyzed against distilled water for 72 hrs at room temperature using tubes of dialysis-regenerated cellulose (Spectrum Laboratories, Milan, Italy) with a 3-5 kDa Molecular Weight Cut-Off (MWCO). The SF final concentration (9.16% w/v) was determined by freeze-drying at a pressure of 8 x 10^{-1} mbar and a temperature of -50 °C for 72 hrs (Modulyo® Edwards Freeze dryer, Kingston, NY, USA).

For SFNs preparation, SF (1.5% w/v) was added dropwise to acetone; for SFNs-OVA, a solution of SF (1% w/v) and OVA (Merck, Darmstadt, Germany) (0.5% w/v) was prepared and then added dropwise to acetone; for SFNs-CpG, a solution of SF (1.5% w/v) and CpG (TIB Molbiol, Genoa, Italy) (0.1% w/v) was prepared and then added dropwise to acetone. The fibroin/acetone volume ratio was 1:5 in all cases. Next, all the nanoparticle suspensions were dialyzed against deionized water, obtained from a Milli-Q® Direct Water Purification System (Millipore, Milan, Italy), for 72 hrs at room temperature using tubes of dialysis-regenerated cellulose (12 kDa MWCO). Then, SFNs were centrifuged at 10000 rpm for 5 min and washed with water three times to remove any residual unloaded OVA or CpG. Finally, nanoparticles were re-suspended in deionized water; mannitol was added at the concentration of 0.5% w/v as a cryoprotectant and to reduce the formation of aggregates. The final mixture was aliquoted into vials before freeze-drying at a pressure of 8 x 10-1 mbar and a temperature of -50 °C for 72 hrs (Modulyo® Edwards Freeze dryer, Kingston, NY, USA). Final formulations were stored at 4°C until use (maximum of three months). In addition, a

physical mixture of SFNs-OVA and SFNs-CpG was prepared by mixing the freeze-dried formulations of SFNs-OVA and SFNs-CpG in a 1:1 ratio.

Characterization of SFNs injectable formulations

Loading of ovalbumin (OVA) in SFNs-OVA was analyzed as follows. Briefly, 5 µL of the solution was analyzed in a liquid chromatographer (Agilent HPLC series 1100 system, Santa Clara, CA, USA) using a TSK-gel SuperSW 2000 column (4.6 × 300 mm) and a mobile phase composed of 0.1 M Na_2SO_4 and 0.05% NaN_3 in 0.1 M phosphate buffer, pH 6.7. Flow rate and temperature were fixed at 0.35 mL/min and 25 °C, respectively. Three batches for each formulation were considered, and each sample was analyzed in triplicate. After calibration (5 points, 3 replicates, 0.1-1 mg/mL), the encapsulation efficiency % (EE) was calculated as:

$$EE = (\text{total amount of OVA} - \text{unbounded OVA})/\text{total amount of OVA} \times 100$$

The OVA loading % was calculated as:

$$\text{Loading \%} = (\text{total amount of OVA} - \text{unbounded OVA})/\text{weight of SFNs.}$$

The dimensional distribution of SFNs was analyzed using NanoSight NS300 equipment (Malvern Panalytical, Grovewood Rd, WR14 1XZ, Great Malvern, Worcestershire, UK). The nanoparticle formulations were dispersed in water, vortexed for 30 s, sonicated for 30 min and filtered by a 0.45 µm filter before the analysis. Five measurements of 90 s each were performed for each sample. Data were analyzed with the NTA software 3.0.

The dimensional distribution of SFNs was analyzed using NanoSight NS300 equipment (Malvern Panalytical, Grovewood Rd, WR14 1XZ, Great Malvern, Worcestershire, UK). The nanoparticle formulations were dispersed in water, vortexed for 30 s, sonicated for 30 min and filtered by a 0.45 µm filter before the analysis. Five measurements of 90 s each were performed for each sample. Data were analyzed with the NTA software 3.0.The analyses of the mean size, polydispersity index (PDI) and zeta potential of SFNs were analyzed by Zetasizer Nano Zs (Malvern Panalytical, Grovewood

Rd, WR14 1XZ, Great Malvern, Worcestershire, UK) performed as follows. First, aqueous suspensions (1 mg/ml) of all SNFs were prepared and allowed to equilibrate overnight at 25°C with gentle stirring. Then the nanoparticle dispersions were filtered with a 0.45 μm filter and analyzed. The measurements were performed in triplicate for each sample. Next, to measure the Z-potential, all SFNs were suspended (1 mg/ml) in KCl 1 mM, allowed to equilibrate overnight at room temperature with gentle stirring, and analyzed.

Thermal analysis of SFNs was performed as follows. Mid-IR (650–4000 cm^{-1}) spectra were recorded on powder samples using a Bruker Equinox 55 spectrometer equipped with a pyroelectric detector (DTGS type) with a resolution of 4 cm^{-1}. Temperature and enthalpy values were measured by differential scanning calorimetry (DSC) by a NEXTA DSC (Hitachi, Europark Fichtenhain A12, 47807 Krefeld, Germany) equipped with a DSC821e module and an intracooler device for sub-ambient temperature analysis (Julabo FT 900). Samples in the range 1–3 mg were weighed (Mettler M3 Microbalance) and placed in sealed aluminium pans with pierced lids (β = 10 K min^{-1}, nitrogen atmosphere (flow rate 50 mL min^{-1}), −10/400 °C temperature range). The instrument was preventively calibrated with indium as a standard reference. Measurements were carried out at least in triplicate. A Mettler STARe thermogravimetric analysis (TGA) system (Perkin Elmer Pyris 1, Wellesley, Minneapolis, MN, USA) with simultaneous DSC (TGA/DSC1) was used to measure mass losses upon heating 2–3 mg samples in alumina crucibles with lids (β = 10 K min^{-1}, nitrogen atmosphere (flow rate 50 mL min^{-1}), 30/400 °C temperature range). Calibration procedure and triplicate measurements were applied, as for DSC above.

After allowing the samples to rebalance at room temperature, residual humidity was determined by Coulometric Titrator HI904 (Hanna Instruments). The titration was performed twice for each vial (n=3 vials for each formulation). The osmolarity was measured using a micro osmometer (Precision System Inc., Natick, MA) after reconstitution of 10 mg of lyophilized sample in 2 ml saline (0.9% w/v NaCl in deionized water) at 37°C. The pH of the reconstituted product was measured by a pH meter (Mettler-Toledo, US).

Analysis of SFNs internalization by cancer cells

For this experiment, SFNs loaded with curcumin were used. Briefly, SF aqueous solution was diluted (1.5% w/v) and added dropwise to the acetone containing 0.08 mg/ml of curcumin. After dialysis (12 kDa MWCO), SFN-CUR suspension was freeze-dried at 8×10^{-1} mbar and −50° C.

Curcumin-SFNs were incubated with the following mouse or human cancer cell lines: a) MB49 (murine bladder cancer); b) LLC1 (mouse Lewis lung carcinoma); c) B16/F10 (murine melanoma); d) U-87 (human glioblastoma); e) DLD-1 (human colon adenocarcinoma); f) KPC (human pancreatic ductal adenocarcinoma); g) LNCap.FGC (human prostate adenocarcinoma); h) 5637 (human bladder carcinoma). All cancer cell lines were purchased from ATCC except for the MB49 cell line (Sigma-Aldrich, Milan, Italy) and KPC cell line (Ximbio, London, UK).

Cancer cell lines (25000 cells/well in 24-well plates) were grown adherently in the presence of culture medium, constituted by RPMI culture medium (Gibco-ThermoFisher Scientific, Waltham, Massachusetts, US) added with 10% Fetal Bovine Serum (FBS) and 1% Penicillin, Streptomycin, Amphotericin B Mixture (Lonza, Basel, Switzerland), at 37°C in 5% CO_2. SFNs loaded with either curcumin or OVA were added to the cultures at a concentration of 200 μg/ml for 1, 2, 4 and 24 hours. Cancer cells cultured alone or in the presence of empty SFNs were the negative control of the experiments. After the incubation, the cancer cells were harvested by trypsinization (Trypsin-EDTA, Euroclone Milan, Italy) for 5 min at 37°C and 5% CO_2, washed and re-suspended in 200 μl of fresh culture medium. Vital 7- AAD dye (0.25 μg/sample) (Becton Dickinson, BD, Franklin Lakes, New Jersey, US) was added to each sample to identify the dead cells by cytofluorimetric analyses. The cell suspension was analyzed by a FACS Canto II flow cytometry (BD) equipped with three lasers (488 nm, 640 nm, 405 nm) using FACS DIVA software v6 (BD). This analysis benefited from the different light excitation and emission frequencies of fibroin and curcumin: in particular, 515 nm (excitation) and 585 nm (emission) for fibroin, 488 nm (excitation) and 525 nm

(emission) for curcumin. Hence, the analyses were conducted using a violet light-emitting laser for the fibroin and a green light-emitting laser for the curcumin.

Ex vivo internalization of SFNs loaded with curcumin by excised tumors was analyzed by confocal microscopy. First, C57BL/6J mice were challenged with MB49 bladder cancer cells as described below. When tumors reached 1 cm^3 dimension, mice were sacrificed, and the tumor was excised, minced and passed through a cell strainer (40 μm) to obtain a homogenous cell suspension. Then, tumor cells were re-suspended in culture medium and co-incubated, or not, with SFNs at a concentration of 200 μg/ml for 1, 4 and 24 hrs. Then, the internalization of curcumin-loaded SFNs by tumor cells was analyzed by confocal microscopy. In particular, the plasma membrane of cells treated with curcumin-loaded SFNs was labelled with Alexa594-conjugated wheat germ agglutinin (ThermoFisher Scientific, Waltham, Massachusetts, US) following the manufacturer's instruction and optic sections were acquired by using an Olympus FV500 confocal microscope (Olympus Corporation). The green signal (curcumin), the red signal (Alexa594), and the bright field were imaged using a sequential acquisition mode.

Ex vivo internalization of SFNs loaded with OVA by excised tumors was analyzed as follows. First, C57BL/6J/6 mice were challenged with B16/F10 melanoma cells as described below (section Mice). Then, when tumors reached 1 cm^3 dimension, mice were sacrificed, and the tumor was excised, minced and passed through a cell strainer (40 μm) to obtain a homogenous cell suspension. Then, tumor cells were re-suspended in culture medium and co-incubated, or not, with OVA-loaded SFNs at a concentration of 200 μg/ml for 4 hrs. Then, the internalization of OVA-loaded SFNs by tumor cells was analyzed by flow cytometry as described below.

In vivo internalization of SFNs loaded with OVA was also analyzed. In brief, C57BL/6Jmice were challenged with B16/F10 melanoma cells, as described below. When tumors reached 0.5 cm^3 dimension, SFNs loaded with OVA (200 μg per mouse) were injected subcutaneously into the peri-tumoral area. Mice were sacrificed after 4 hrs from SFNs injection. A control mouse challenged with B16/F10 melanoma cells was sacrificed as control. Intracellular staining for OVA was

performed. To this aim, tumors were collected, minced and passed through a cell strainer (40 µm) to obtain a homogenous cell suspension. Cells (106) were stained with LIVE/DEAD™ Fixable Aqua Dead Cell Stain Kit (Thermo Fisher Scientific, Waltham, MA, US) to identify the dead cells by cytofluorimetric analyses and then incubated with a PerCP-Cyanine 5.5 mouse anti-mouse CD45.2 antibody (BD) for 15 min at RT. Then they were fixed and permeabilized by BD Cytofix Cytoperm (BD) and incubated with a FITC rabbit anti-OVA antibody (Abcam, Cambridge, UK). Cells were then analyzed by an LSR Fortessa X20 flow cytometer (BD).

Analysis of SFNs internalization by DCs

Splenic DCs were magnetically separated from C57BL/6J spleen cells using Pan Dendritic Cell Isolation Kit (Miltenyi Biotec, Bergisch Gladbach, Germany) according to manufacturer instructions. In brief, the C57BL/6J spleen was collected, minced and passed through a cell strainer (40 µm) to obtain a homogenous cell suspension. DCs were isolated by depletion of non-target cells (negative selection) performed through immune-magnetic separation on LS columns (Miltenyi Biotec). DCs were then seeded at $5x10^5$ cells/well in 24-well plates in the presence of culture medium at 37°C in 5% CO2. SFNs loaded with curcumin (25 µg/ml) were added to the culture for 4 and 24 hours. DCs were stained with Fixable Viability Stain 780 (BD) and anti-mouse PE-Cy7-labelled anti-CD11c antibody (BD catalog no. 558079) at the end of incubation.

Concerning intratumoral DCs, in vivo internalization of SFNs-OVA was analyzed by flow cytometry. C57BL/6J mice were challenged with B16/F10 melanoma cells as described below. When tumors reached 0.5 cm^3 dimension, SFNs loaded with OVA (200 µg per mouse) were injected subcutaneously into the peri-tumoral area. Mice were sacrificed after 4 hrs from SFNs injection. A control mouse challenged with B16/F10 melanoma cells was sacrificed as control. Intracellular staining for OVA was performed. To this aim, tumors were collected, minced, and passed through a cell strainer (40 µm) to obtain a homogenous cell suspension. Cells derived from tumors (10^6) were stained with LIVE/DEAD™ Fixable Aqua Dead Cell Stain Kit (Thermo Fisher

Scientific, Waltham, MA, US) to identify the dead cells by cytofluorimetric analyses and then incubated with a PerCP-Cyanine 5.5 anti-mouse CD45.2 (BD catalog no. 561096), Phycoerythrin (PE) rat anti-mouse MHC-II (IA/IE) (Thermo-Fisher Scientific catalog no 12-5321-82) and PE-Cyanine 5.5 Armenian hamster anti-mouse CD11c (Thermo-Fisher Scientific catalog no 35-0114-82) antibodies for 15 min at RT then fixed and permeabilized by BD Cytofix Cytoperm (BD), and incubated with a Fluorescein Isothiocyanate (FITC) rabbit anti-OVA antibody (Abcam, Cambridge, UK catalog no. ab85584). Cells were then analyzed by an LSR Fortessa X20 flow cytometer (BD).

ADAS generation

Adipose tissue was derived from liposuction waste from a healthy donor after obtaining the informed consent. Briefly, the sample was digested with an enzymatic solution (collagenase type I 0.1% in PBS) at 37°C for 1 h before centrifugation at 1200 rpm for 5 min at RT. The pelleted stromal vascular fraction (SVF), containing the mesenchymal stromal cells, was suspended in alpha-MEM supplemented with 10% FCS to block the residual collagenase activity. The pellet was suspended in an amount of medium corresponding to the initial lipo-aspirate volume and divided into 100-mm diameter Petri dishes (2 ml cell suspension/dish).

To the first confluence the cells were plated for the analysis of the nanoparticle's toxicity by thiazolyl blue (MTT; Sigma) assay.

MTT assay

Cells ($3x10^3$/well) were plated in wells of a 96-well plate and incubated with SFNs (200 μg/ml) for 1, 4 and 24 hours at 37°C. At each considered time, culture medium was removed and replaced with 0.5 ml of serum-free medium and 25 ml of 3-(4,5-dimethylthiazol-2-yl)-2,5-diphenyltetrazolium bromide (stock solution, 5 mg/ml). After 3 hour incubation in the dark, the medium was removed, and the converted dye was solubilized with absolute ethanol. Absorbance of converted dye was measured at a wavelength of 570 nm with background subtraction at 670 nm. Percent cell viability

was calculated as follows: 100 × mean (of triplicates) optical density of SFNs treated samples/mean optical density of untreated controls.

Sample preparation for Liquid Chromatography with tandem mass spectrometry (LC-MS/MS) analysis

Paraffin-embedded tissue sections from B16/F10 melanoma and MB49 bladder carcinoma mouse models were deparaffinized in hexane using three solvent changes. Each embedded biopsy was cut to obtain 10 µm sections from the same block. Slices were transferred into a 5 ml collection tube and added to hexane (Sigma-Aldrich Inc., St Louis, MO, USA). The samples were gently vortexed and placed on a rotary shaker for 10 minutes at room temperature. The samples were then centrifuged at 4800 rpm for 15 minutes at 20°C. Supernatants were discarded, and pellets underwent two additional hexane washes. Finally, the pellets were dried under a gentle nitrogen flow and stored at -20°C.

Dewaxed tissues were solubilized in RapigestTM SF reagent (Waters Co, Milford, MA, USA) at the final concentration of 0.5% (w/v) and then incubated under stirring 100°C for 20 minutes and subsequently at 80°C for 2 hrs. Protein concentration was assayed using the SPNTM Protein Assay kit (G-Biosciences, Maryland Heights, MO, USA). From each sample, 50 µg ± 0.5 µg of proteins were digested by adding Sequencing Grade Modified Trypsin (Promega, Madison, WI, USA) at an enzyme/substrate ratio of 1:50 (w/w) and incubating them overnight at 37°C; an additional aliquot of Trypsin was added (enzyme/substrate ratio of 1:100 w/w) in the morning and the digestion continued for 4 hrs. The enzymatic reaction was chemically stopped with the addition of 0.5% TFA (Sigma-Aldrich Inc., St. Louis, MO, USA), and a subsequent incubation at 37°C for 45 minutes completed the acidic hydrolysis of RapiGest. The water-immiscible degradation products were removed by centrifuging at 13,000 × g for 10 min. Finally, the tryptic digested mixtures were desalted using PepCleanTMC18 spin column (Thermo Fisher Scientific, Waltham, MA, USA),

concentrated in a SpeedVac (Savant Instruments, Farmingdale, NY, USA) at 60 °C and re-suspended in 0.1% formic acid (Sigma-Aldrich Inc., St. Louis, MO, USA) at a concentration of 0.2 µg/µL.

LC-MS/MS analysis

Trypsin-digested mixtures were analyzed using a platform consisting of a nano-liquid chromatographic system, the Eksigent nanoLC-Ultra 2D System (Eksigent, AB SCIEX Dublin, CA, USA), configured in trap-elute mode coupled with a high-resolution mass spectrometer. For each experimental condition, three biological replicates were analyzed in twice technical replicates for a total of 48 LC-MS/MS runs. Briefly, samples were first loaded on the nanoLC trap (200 µm x 500 µm ChromXP C18, 3 µm, 120 Å) and washed with the loading pump running in isocratic mode with 0.1% formic acid in water for 10 min at a flow rate of 3 µL/min. The automatic switching of the nanoLC ten-port valve then eluted the trapped mixture on a nano-reversed phase column (75 µm x 15 cm 3C18-CL, 3 µm, 120 Å), through a 150 min gradient of eluent B (eluent A, 0.1% formic acid in water; eluent B, 0.1% formic acid in acetonitrile), at a flow rate of 300 nL/min. Specifically, the gradient was: from 5–10% B in 3min, 10–40% B in 130 min, 40–95% B in 10 min and holding at 95% B for 10 min. Mass spectra were acquired using an LTQ-Orbitrap XL-ETD mass spectrometer (Thermo Fisher Scientific, San José, CA, USA), equipped with a nanospray ionization source (Thermo Fisher). The spray capillary voltage was set at 1.7 kV, and the ion transfer capillary temperature was held at 220 °C. Full mass spectra were recorded in positive ion mode over a 400–1600 m/z range and with a resolution setting of 30000 FWHM and scan rate of 2 spectra per second, followed by five low-resolution MS/MS events, sequentially generated in a data-dependent manner on the top five most intense ions selected from the full MS spectrum (at 35% collision energy), using the dynamic exclusion of 0.5 min for MS/MS analysis. Mass spectrometer scan functions and high-performance liquid chromatography solvent gradients were controlled by the Xcalibur data system version 1.4 (Thermo Fisher Scientific).

235

236 **RESULTS**

237 The DSC thermal analysis supported the spectroscopic data. The nanoparticles showed a typical
238 profile of an amorphous compound with an endothermic effect around 270°C, associated with a loss
239 of mass in the thermo-gravimetric curve, linked to sample decomposition (data not shown). The
240 residual humidity never exceeded 3%, indicating an effective lyophilization of the product that
241 preserves its stability and effectiveness. Further analyses were performed to check the suitability of
242 each formulation for in vivo administration. First, four vials were randomly selected for each
243 formulation, and quality control was performed by visual inspection of the cake's appearance. A
244 solid and porous cake was formed, free of defects following the aqueous solvent's evaporation
245 during lyophilization. The cake dissolved rapidly by adding saline solution (0.9% w/v NaCl in
246 water), generating a nanoparticle suspension that looked clear and free of subvisible particles. For
247 each formulation, the osmolarity value was always within the range required for injectable
248 formulations (250-350 mOsm/Kg) and, in particular, always between 320 and 350 mOsm/Kg.
249 Moreover, the measured pH value was always in the range of 7.2 to 7.6.
250 SFNs-CUR had the same characteristics (morphology, particle size and size distribution, zeta
251 potential, physical-chemical properties) as SFNs, SFNs-OVA and SFNs-CpG.

252

253

SUPPLEMENTAL FIGURES

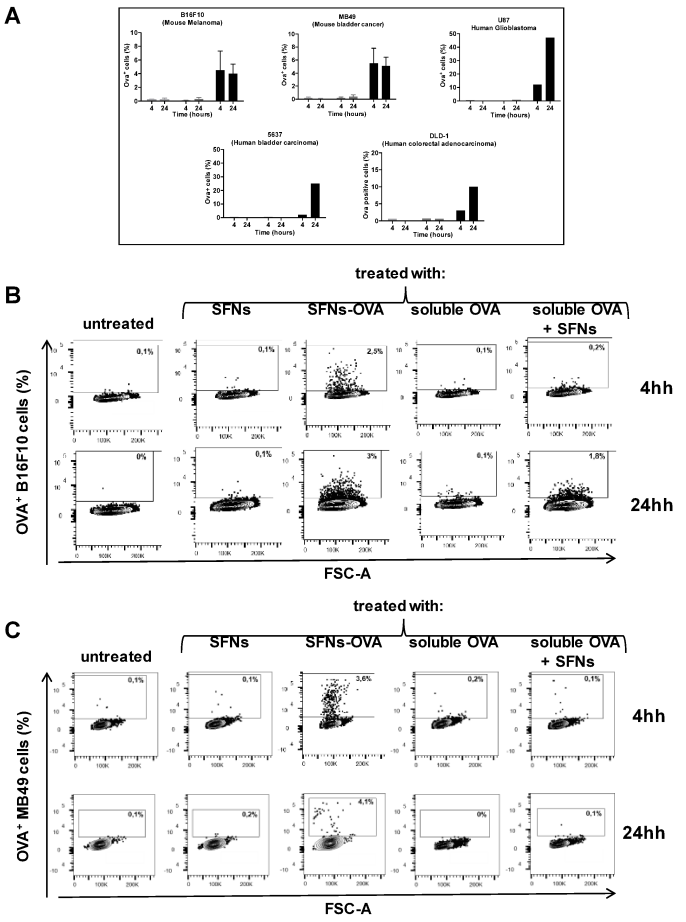

Figure S1. Analysis of nanoparticle internalization. (A) Analysis of SFNs-OVA internalization by different cancer cell lines: the different mouse or human cancer cell lines were incubated for 4 and 24 hours, alone (light grey bars) or in the presence of unloaded SFNs (dark grey bars) or SFNs-OVA (black bars), intracellularly stained with anti-OVA FITC antibody and evaluated by flow cytometry; (B) B16/F10 melanoma cell line was incubated for 4 (upper panels) or 24 (lower panels) hours alone or with either SFNs, SFNs-OVA, soluble OVA, soluble OVA mixed with unloaded SFNs, then fixed and permeabilized before incubation with an anti-OVA FITC labelled mAb and the following cytometric analysis; (C) MB49 bladder cancer cell line was incubated for 4 (upper panels) or 24 (lower panels) hours alone or with either SFNs, SFNs-OVA, soluble OVA, soluble OVA mixed with unloaded SFNs, then fixed and permeabilized before incubation with an anti-OVA FITC labelled mAb and the following cytometric analysis.

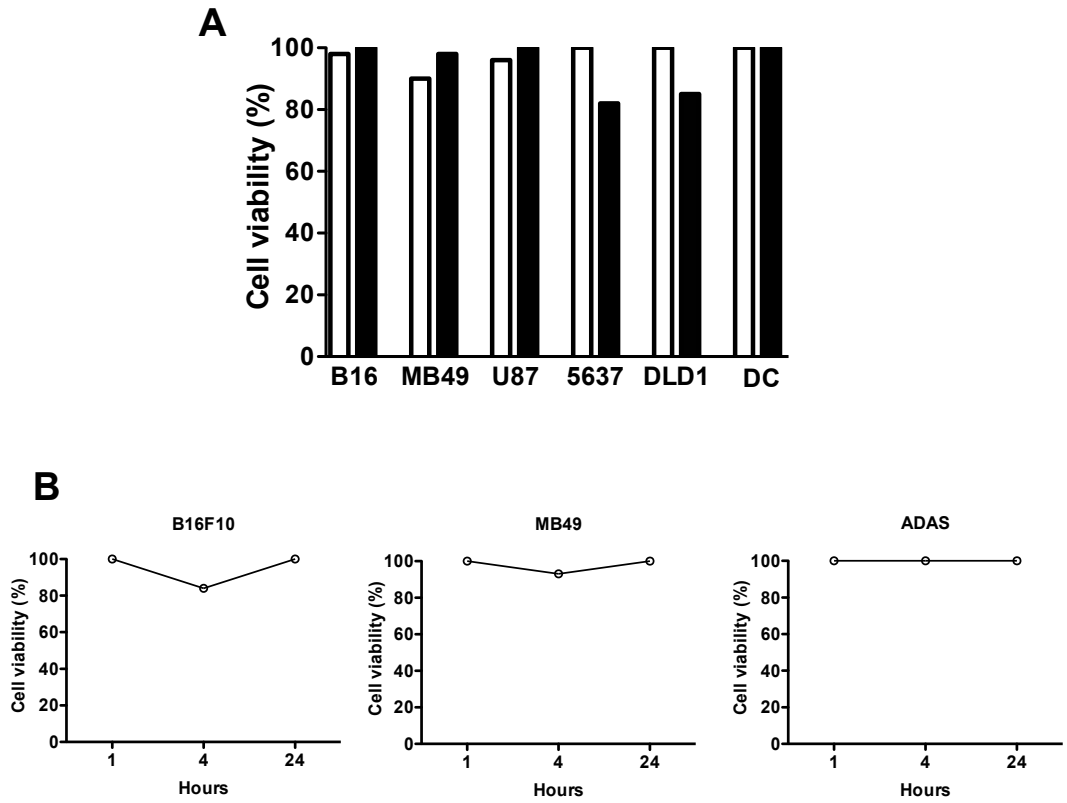

Figure S2. Viability of different cancer and healthy cell types after SFNs internalization. (A) Cancer cells (25000 cells/well in 24-well plates) or splenic DCs ($5x10^5$ cells/well in 24-well plates) were incubated in the presence or not of SFNs-OVA at a concentration of 200 μg/ml for 4 (white bars) and 24 (black bars) hours; Then the cells were stained with LIVE/DEAD™ Fixable Aqua Dead Cell Stain Kit (Thermo Fisher Scientific, Waltham, MA, US) to identify the dead cells by cytofluorimetric analyses. Data are expessed as 100 x viability of untreated cells /viability of treated cells. (B) MTT viability analysis on B16/F10 and MB49 cancer cell lines and on Adipose Adult Stromal Cells (ADAS) from an healthy donor after 1, 4 or 24 hour incubation alone or in the presence of SFNs at a concentration of 200 μg/ml. Percent cell viability was calculated as follows: 100 × mean (of triplicates) optical density of SFNs treated samples/mean optical density of untreated controls.

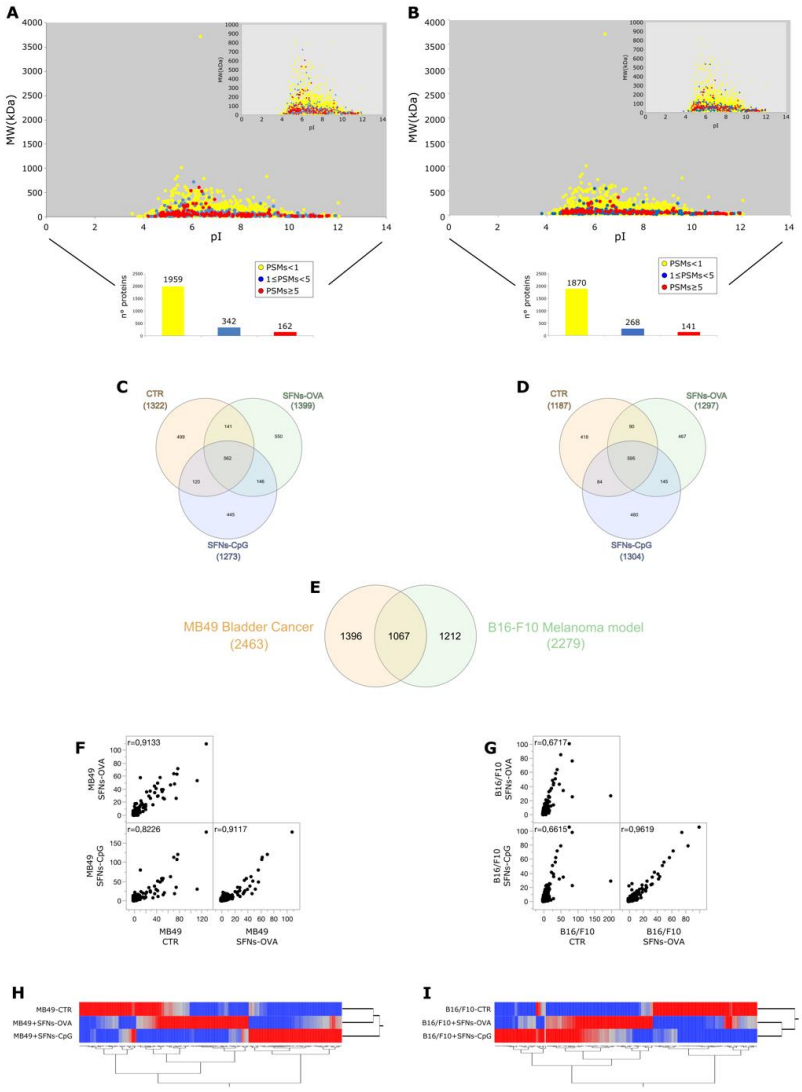

Figure S3. nLC-hrMS/MS analysis results. Proteins identified in MB49 bladder cancer (A) and B16/F10 melanoma (B) model plotted by their pI and MW; color codes indicate proteins identified using average Peptide spectrum matches (PSMs)<1 (yellow), average 1≤average PSMs<5 (blue), average PSMs≥5 (red). Venn diagrams of proteins identified in MB49 bladder cancer (C) and B16/F10 melanoma (D) model. E) Venn diagram among proteins identified in MB49 bladder cancer and B16/F10 melanoma model. *Spearman*'s correlation among profiles of differentially

287 expressed proteins (DEPs) in MB49 bladder cancer (F) and B16/F10 melanoma (G) models.
288 Hierarchical clustering from DEPs in MB49 bladder cancer (H) and B16/F10 melanoma (I) model.
289

290

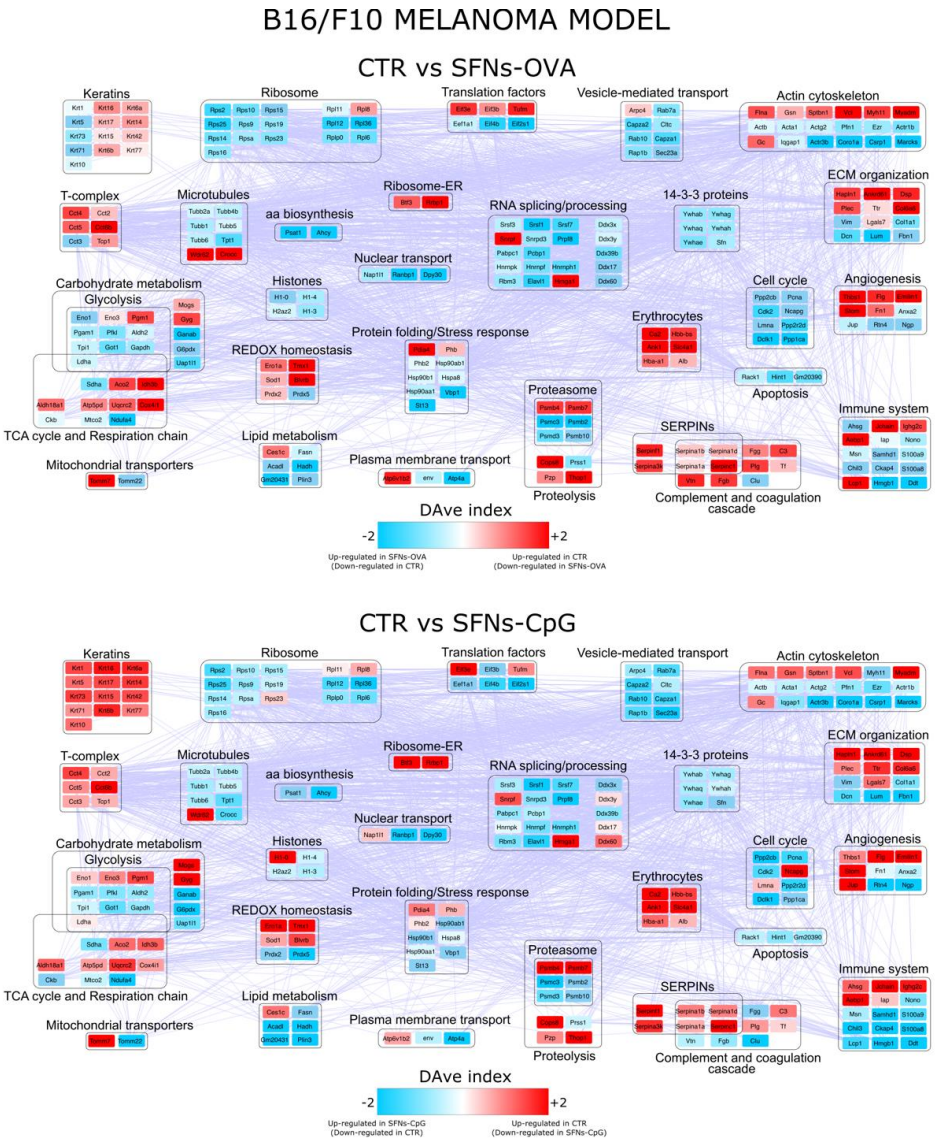

291

292 **Figure S4**. Protein-protein interaction network model reconstructed by Cytoscape's STRING App
293 starting from proteins differentially expressed in B16/F10 melanoma model untreated (CTR) and
294 treated with SFNs-OVA or SFNs-CpG. Proteins were grouped in functional modules. Red color
295 code (positive DAve values) indicates proteins up-regulated in CTR (vs SFNs-OVA or/and vs
296 SFNs-CpG), while the blue color code (negative DAve values) indicates proteins up-regulated in
297 SFNs-OVA or/and SFNs-CpG (vs CTR).

298

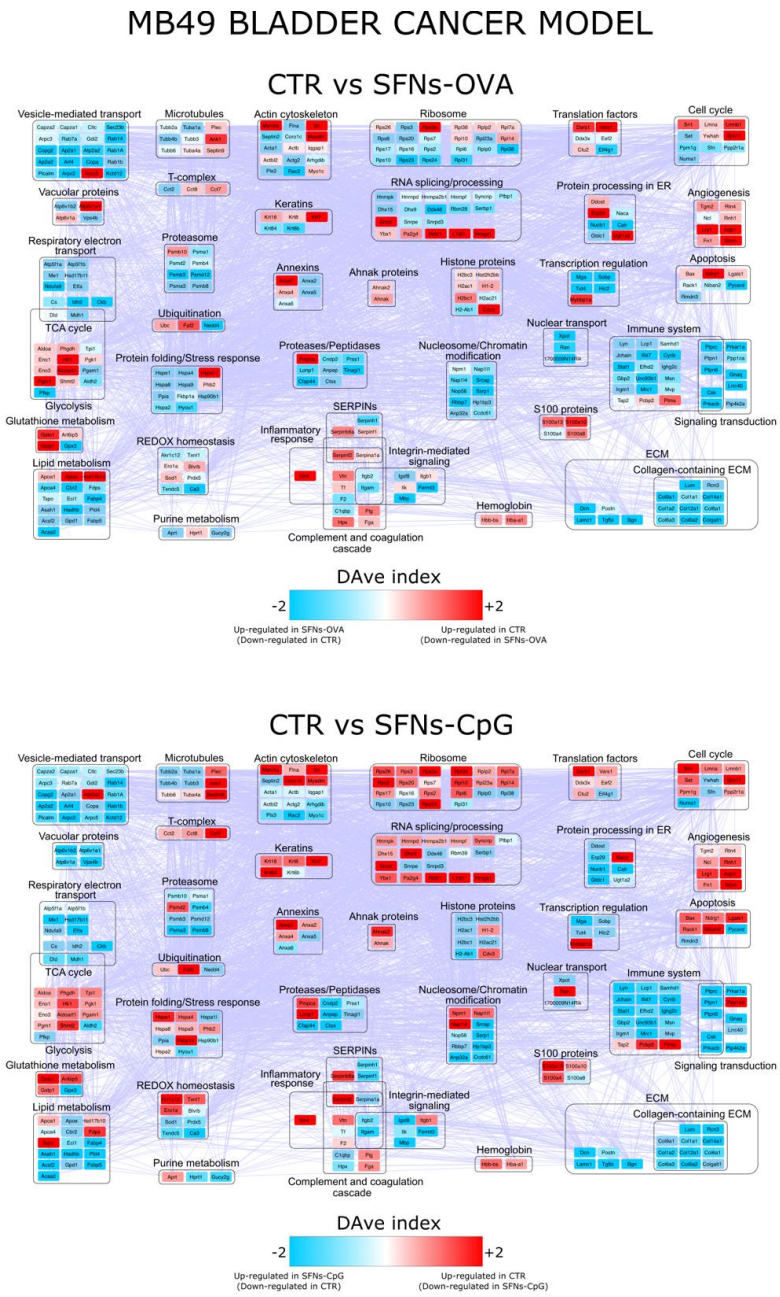

Figure S5. Protein-protein interaction network model reconstructed by Cytoscape's STRING App starting from proteins differentially expressed in MB49 bladder cancer model untreated (CTR) and treated with SFNs-OVA or SFNs-CpG. Proteins were grouped in functional modules. Red color code (positive DAve values) indicates proteins up-regulated in CTR (*vs* SFNs-OVA or/and *vs* SFNs-CpG), while the blue color code (negative DAve values) indicates proteins up-regulated in SFNs-OVA or/and SFNs-CpG (*vs* CTR).

306

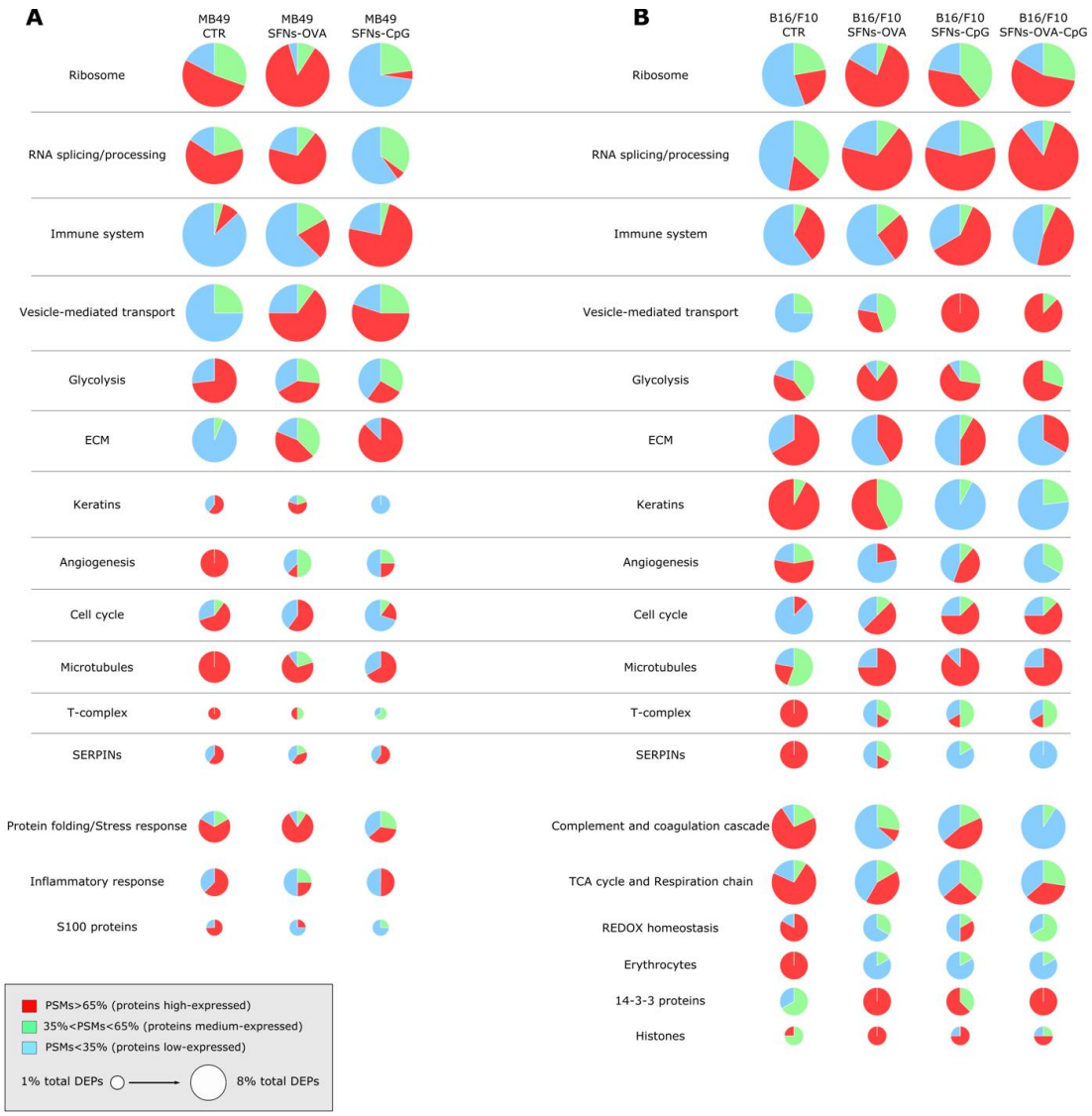

307

308 **Figure S6.** Pie charts showing the functional modules (Biological processes, Molecular function
309 and Protein families) mostly affected by SFNs treatments in MB49 bladder cancer (A) and B16/F10
310 melanoma (B) models. Red, green and blue color codes indicate the percentage of proteins with
311 high-, medium- and low expression, respectively, based on a PSMs-based label-free quantification.
312 The pie chart size is proportional to the number of DEPs per module.

313

314

315

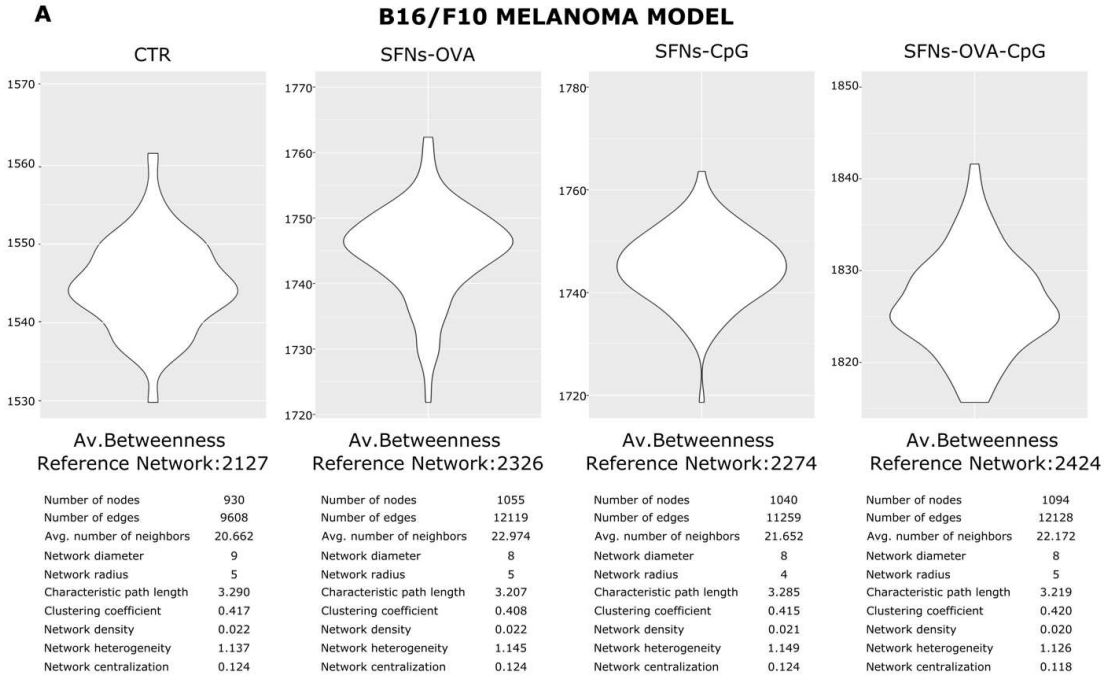
A
B16/F10 MELANOMA MODEL
CTR
SFNs-OVA
SFNs-CpG
SFNs-OVA-CpG
Av.Betweenness
Reference Network:2127
Av.Betweenness
Reference Network:2326
Av.Betweenness
Reference Network:2274
Av.Betweenness
Reference Network:2424
Number of nodes 930
Number of edges 9608
Avg. number of neighbors 20.662
Network diameter 9
Network radius 5
Characteristic path length 3.290
Clustering coefficient 0.417
Network density 0.022
Network heterogeneity 1.137
Network centralization 0.124
Number of nodes 1055
Number of edges 12119
Avg. number of neighbors 22.974
Network diameter 8
Network radius 5
Characteristic path length 3.207
Clustering coefficient 0.408
Network density 0.022
Network heterogeneity 1.145
Network centralization 0.124
Number of nodes 1040
Number of edges 11259
Avg. number of neighbors 21.652
Network diameter 8
Network radius 4
Characteristic path length 3.285
Clustering coefficient 0.415
Network density 0.021
Network heterogeneity 1.149
Network centralization 0.124
Number of nodes 1094
Number of edges 12128
Avg. number of neighbors 22.172
Network diameter 8
Network radius 5
Characteristic path length 3.219
Clustering coefficient 0.420
Network density 0.020
Network heterogeneity 1.126
Network centralization 0.118
B
MB49 BLADDER CANCER MODEL
CTR
SFNs-OVA
SFNs-CpG
Av.Betweenness
Reference Network:2458
Av.Betweenness
Reference Network:2532
Av.Betweenness
Reference Network:2415
Number of nodes 1065
Number of edges 10231
Avg. number of neighbors 19.213
Network diameter 8
Network radius 5
Characteristic path length 3.311
Clustering coefficient 0.390
Network density 0.018
Network heterogeneity 1.177
Network centralization 0.115
Number of nodes 1148
Number of edges 11242
Avg. number of neighbors 19.585
Network diameter 8
Network radius 4
Characteristic path length 3.208
Clustering coefficient 0.390
Network density 0.017
Network heterogeneity 1.107
Network centralization 0.111
Number of nodes 1023
Number of edges 9003
Avg. number of neighbors 17.601
Network diameter 10
Network radius 5
Characteristic path length 3.364
Clustering coefficient 0.409
Network density 0.017
Network heterogeneity 1.054
Network centralization 0.105

316
317

318 **Figure S7**. Violin plots reporting the average betweenness calculated in random network models
319 reconstructed from protein identified in B16/F10 melanoma (A) and MB49 bladder cancer (B)
320 models; the average betweenness in reference networks is shown. The topological parameters
321 calculated by Cytoscape's Network Analyzer App are reported for both models and each
322 reconstructed network.
323
324